CHARACTERIZATION AND CRYSTALLIZATION OF TRANSLOCATOR PROTEIN 18 kDa (TSPO) FROM *RHODOBACTER SPHAEROIDES*

By

Fei Li

A DISSERTATION

Submitted to
Michigan State University
in partial fulfillment of the requirements
for the degree of

Biochemistry and Molecular Biology--Doctor of Philosophy

2014

CHARACTERIZATION AND CRYSTALLIZATION OF TRANSLOCATOR PROTEIN 18 kDa (TSPO) FROM *RHODOBACTER SPHAEROIDES*

By

Fei Li

Translocator protein 18 kDa (TSPO), previously known as the peripheral benzodiazepine receptor (PBR), is a mitochondrial outer membrane protein that is a continuing research focus due to its importance in cholesterol and porphyrin transport and apoptotic signaling. Dysfunction of TSPO has been shown to relate to various diseases, including metastatic cancer, inflammation, Alzheimer, and Parkinson disease. Functions of TSPO have been investigated but the molecular details remain an enigma, due in part to two major bottlenecks: 1) the lack of atomic resolution structural information; and 2) conflicting data from both *in vivo* and *in vitro* characterization.

The *Rhodobacter sphaeroides* homolog of TSPO (*Rs*TSPO) was discovered as an oxygen sensor regulating photosynthesis and respiration in this bacterium and shares 34 % sequence identity with the human protein. In addition, the knock-out phenotype of *R. sphaeroides* can be functionally complemented by the rat homolog, confirming the use of *Rs*TSPO as a valid model system for the mammalian protein. In this study, we have successfully established an expression, purification, and characterization methodology for the *Rs*TSPO that allowed us to investigate *Rs*TSPO with molecular detail. *R. sphaeroides* is also an highly successful system for producing crystal structures of membrane proteins. A crystallization strategy was established and optimized with *Rs*TSPO that has resulted in the first high resolution crystal structure of a TSPO family protein.

A sensitive tryptophan fluorescence quenching assay was used to characterize the binding of purified *Rs*TSPO with various ligands. Novel ligands of TSPO previously shown to affect

apoptosis were identified and support a role of TSPO in the regulation of the apoptosis pathway. Detailed characterization of ligand binding with *Rs*TSPO and mutants *in vitro* combined with computational modeling of *Rs*TSPO structure and analysis of previous mutagenesis data led to a model of TSPO-ligand interaction.

A cholesterol binding enhancement motif was identified in TSPO that is highly conserved within the mammalian proteins and is able to account for the 1000 fold different binding affinity of *Rs*TSPO compared to the mammalian homologs. This motif is also observed in other membrane proteins interacting with cholesterol, highlighting the potential general importance of this enhancement motif in the regulation of cholesterol binding in mammals. In addition, residues within the same motif were identified by evolutionary covariance analysis as playing a critical role in the stability of TSPO proteins, providing useful information for structural analysis of TSPO.

Extensive screening and optimization of crystallization strategies for *Rs*TSPO were carried out with both the vapor diffusion and the lipidic cubic phase (LCP) methods. Successful crystallization and structure determination of *Rs*TSPO with the LCP method not only provided the long-awaited structural information to facilitate interpretation of biochemical data on TSPO, but it also provides unique and valuable knowledge to guide crystallization of other TSPO family proteins, as well as similar small α helical membrane proteins.

ACKNOWLEDGEMENTS

TABLE OF CONTENTS

LIST OF TABLES

LIST OF FIGURES

KEY TO ABBREVIATIONS

A. U.   asymmetric unit

βME β-mercaptoethanol

BCA   bicinchroninic acid

BSA   bovine serum albumin

CV   column volume

CMC   critical micelle concentration

DDM   dodecyl maltoside

DM   decyl maltoside

EDTA   ethylenediaminetetraacetic acid

FPLC   fast protein liquid chromatography

kD   kilodalton

LCP   lipidic cubic phase

LDAO   lauryl dimethylamine n-oxide

LAPAO   3-dodecylamido-N,N′-dimethylpropyl amine oxide

MAG   monoacylglycerol

MES   2-(n-morpholino)ethanesulfonic acid

MALDI   matrix-assisted laser desorption ionization mass spectrometry

MW   molecular weight

MWCO   molecular weight cut-off

Ni-NTA	nickel-nitrilotriacetic acid
NMR	nuclear magnetic resonance
PCR	polymerase chain reaction
PEG	polyethylene glycol
Rs	*Rhodobacter sphaeroides*
SDS-PAGE	sodium dodecyl sulfate polyacrylamide gel electrophoresis
SeMet	selenomethionyl
TLC	thin layer chromatography
TM	transmembrane
Tris	tris (hydroxymethyl) aminomethane
TSPO	Translocator protein 18 kDa
WT	wild type

CHAPTER 1

An introduction to Translocator Protein 18 kDa (TSPO) and membrane protein crystallography

Background on Translocator Protein 18 kDa (TSPO)

Discovery of the peripheral benzodiazepine receptor (PBR)

The peripheral benzodiazepine receptor (PBR) was first discovered by serendipity in 1977 in an experiment searching for the high affinity binding site for the widely prescribed anxiolytic and sedative hypnotic benzodiazepine drug Diazepam [1]. In addition to its target in the central nervous system (CNS), another nanomolar affinity binding site was also found in a variety of peripheral nervous system (PNS) [2]. Due to its abundance in peripheral tissues as well as to distinguish it from the central benzodiazepine receptor (CBR), which is now known as the ligand gated $GABA_A$ receptor, this peripheral binding protein was named the "peripheral benzodiazepine receptor" (PBR). Later, another class of ligands, represented by the isoquinoline carboxamide PK11195, was discovered to bind to PBR exclusively, with high affinity detected consistently across species while benzodiazepines bind to PBR and CBR with varied affinities. Therefore, PK11195 is now often used as the diagnostic ligand for PBR.

In 2006, PBR was renamed as Translocator Protein 18 kDa (TSPO) [3] to better represent the emerging understanding of a family of highly conserved proteins found in Archaea to plants and humans [4]. TSPO family proteins are integral membrane proteins with 5 predicted transmembrane helices [3]. Functions of TSPO proteins span from regulation of steroid hormone and heme biosynthesis, to regulation of apoptosis and a role in cardiovascular [4] and neurological disease [5]. Over the past 30 years, extensive studies of this developmentally-required protein have been carried out and resulted in significant advances in our knowledge of TSPO. A brief review of the current understanding of the structure and function of TSPO, primarily based on studies from mammalian and *Rhodobacter sphaeroides* systems, is provided here.

Function of TSPO as a mitochondrial transporter

TSPO is located in the outer membrane of mitochondria and highly concentrated at contact sites of the inner and outer mitochondrial membranes [6-8]. It has been purified in a complex with the outer membrane-located voltage dependent anion channel (VDAC) and adenine nucleotide translocator (ANT) in the inner membrane [9], but the significance of these associations remains controversial [10]. Additionally, TSPO is reported to transport cholesterol [11] and porphyrins [12] as endogenous ligands and to do so as part of a transport complex involving proteins from both the inner and outer mitochondrial membranes. Although these functions remain to be fully characterized, extensive investigations have provided considerable understanding of the functions of TSPO under various physiological and pathological conditions.

Function of TSPO in steroidogenic tissues

TSPO is found in almost all tissues examined, among which it is most highly expressed in steroid hormone producing tissues such as adrenal glands and kidney [13]. A major function of TSPO in steroidogenic tissues is proposed to be transporting cholesterol across the mitochondrial membrane to be further converted into steroid hormones [14].

Cholesterol is the sole precursor of steroid hormones and bile salts. Several pathways have been suggested to traffic cholesterol to mitochondria for steroidogenesis [15,16]. The sources of cholesterol in the cell can be divided into *de novo* synthesis in the endoplasmic reticulum (ER) or transfer from external cholesterol sources, such as the cholesterol-containing low density lipoproteins (LDL) or the high density lipoprotein (HDL). Free cholesterol is transported to mitochondria through two distinct pathways: either via a cholesterol binding protein that interacts with mitochondrial outer membrane proteins, such as TSPO, or directly from the ER through membrane fusion. A receiver protein complex containing TSPO located in the outer

mitochondrial membrane (OMM) then transports cholesterol across the mitochondrial membranes to be further processed by the cytochrome P450 cholesterol side chain cleavage enzyme (CYP11A1). The transport complex was proposed to include several proteins related to TSPO, including the steroidogenic acute regulatory (StAR) protein, TSPO-associated protein 7 (PAP7, ACBD3), and protein kinase A regulatory subunit 1a (PKAR1A). However, the details of these interactions are not yet understood.

The first and the rate-limiting step of steroid biosynthesis is also the transport of cholesterol from OMM to the inner mitochondrial membrane (IMM) [17,18]. TSPO has been proposed to be the cholesterol transporter in this critical step [11,19-21], but other proteins are also suggested to play a role in this process. A model of this translocation protein complex has been proposed by Papadopoulos and colleagues [15] (Figure 1.1). Briefly, cholesterol is relayed to TSPO by several proteins and eventually the StAR protein upon hormone stimulation. The mechanism of transport of cholesterol by TSPO is not fully understood. One model proposes that cholesterol is transported through the interface of TSPO and the VDAC [15,22]. The transfer complex is also proposed to contain the ANT in the IMM although the exact function is unknown. Translocated cholesterol is then cleaved and converted into pregnenolone by the CYP11A1 associated with the matrix side of the IMM. Pregnenolone is further used to generate varieties of steroids in downstream pathways.
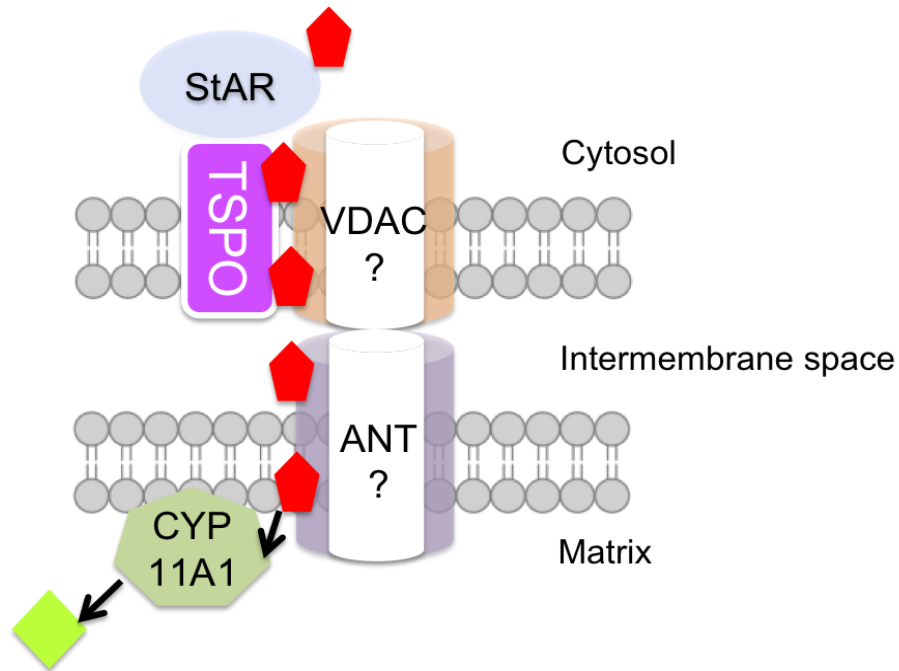
Figure 1.1 Proposed mechanism of cholesterol transport through the cholesterol transporter complex.

Cholesterol is shown as red pentagons while the converted pregnenolone is shown as a green diamond. Proteins involved in this process are shown as cartoons at the proposed location in mitochondria. Figure adapted from Rone *et al.* [15].

Function of TSPO in porphyrin metabolic pathways

In mammals, the biosynthesis of heme and porphyrins starts from the condensation of glycine and succinyl-CoA into δ-aminolevulinic acid (ALA) in mitochondria. ALA is exported to the cytosol and subsequently converted to coproporphyrinogen III after several enzymatic reactions. Coproporphyrinogen III is then transported back into mitochondria to be further converted to various porphyrin molecules including protoporphyrin IX (PpIX) and heme [23] (Figure 1.2). Heme and hemin were originally found to inhibit the binding of PK11195 and Ro5-4864 to TSPO in human blood and several rat organs [8]. Subsequent studies confirmed that TSPO plays a role in the heme biosynthesis pathway [24] and a homolog of TSPO, TSPO from *Rhodobacter sphaeroides* (*Rs*TSPO), was identified to regulate the formation of photosynthetic complexes [25]. Therefore TSPO was proposed to play a role in transporting porphyrin precursors for both respiratory and photosynthetic functions across the membranes as well as regulating the heme biosynthesis pathway [3].

TSPO has been reported to export porphyrins both from *R. sphaeroides* and from mammalian mitochondria [25-27]. In both systems, TSPO is proposed to be part of a stress response mechanism. In mammalian systems, both oxygen and light stress were reported to induce polymerization and activate the transport function of TSPO [28,29] and therefore to reduce the accumulation of porphyrin as well as the generation of reactive oxygen species (ROS) [30]. In the *R. sphaeroides* system, the regulation by TSPO of the export of pigments produced in the heme/bacteriochlorophyll/carotenoid biosynthesis pathways is proposed, thereby controlling expression of related genes and the switch between photosynthesis and respiration upon environmental cues such as light and oxygen stress. However, the exact function of TSPO in relation to porphyrin transport, including both import and export under various stress conditions,

is still not well understood.
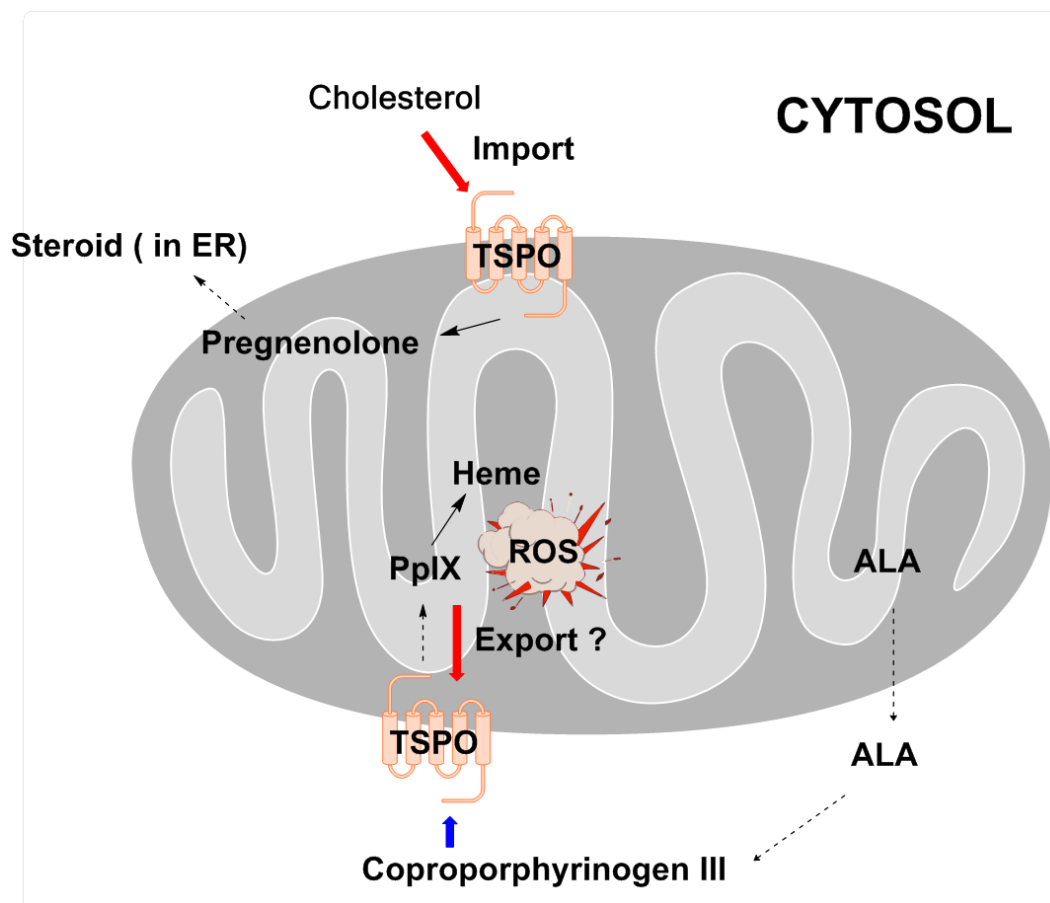
Figure 1.2 Functions of TSPO as a mitochondrial porphyrin and cholesterol transporter.

Cholesterol and porphyrin transport across mitochondrial membranes related to TSPO functions is shown. In the cholesterol transport pathway, cholesterol is imported through the cholesterol transport complex involving TSPO. Pregnenolone is produced by cleavage of the side-chain of cholesterol immediately after transport and is exported to the ER for further processing. In the porphyrin transport pathway, TSPO could potentially act both as the importer and/or exporter of heme precursors or breakdown products, thus playing a role in the regulation of reactive oxygen species (ROS).

TSPO as a regulator of mitochondrial permeability transition pore (MPTP) and mitochondrial homeostasis

Mitochondria play important roles in the proper function of cells, not only by providing most of the energy needed for various biological processes, but also by participating in the execution of the cell by regulating cell death through apoptosis and/or necrosis [31,32]. Apoptosis refers to a process of controlled cell death through the activation of the apoptosis pathway that leads to the recycling of the cell with minimum damage to the tissue. Current understanding of apoptosis puts mitochondria at center stage, although signaling pathways that do not involve mitochondria have also been characterized [33]. The initiation of apoptosis is usually preceded by a loss of the mitochondrial membrane potential ($\Delta\Psi_m$), which is proposed to be regulated by the MPTP, and followed by the release of cytochrome *c* and apoptosis inducing factor (AIF) from the mitochondrial intermembrane space [34]. MPTP is a multi-protein complex formed at the contact sites of the inner and outer mitochondrial membranes. It was originally proposed to be mainly composed of VDAC located in the outer membrane and ANT in the inner membrane [35,36]. However, an important role of ATP synthase has been identified lately [37]; thus, the exact components of MPTP are still under debate. But together with other proteins, TSPO is proposed to regulate the MPTP, since TSPO forms a 70 kDa complex with VDAC and ANT [9] and various TSPO ligands have been shown to regulate apoptosis [38] (Figure 1.3). In addition, it has been suggested that the diverse effects of TSPO ligands on multiple processes are mediated by the fine interplay of TSPO with the MPTP complex and its interacting proteins, through which the homeostasis of the mitochondria is altered, as discussed in a recent issue of Current Molecular Medicine on the broad implications of TSPO in mitochondrial biology [39]. However, it is currently still unclear how MPTP and apoptosis are regulated by TSPO.
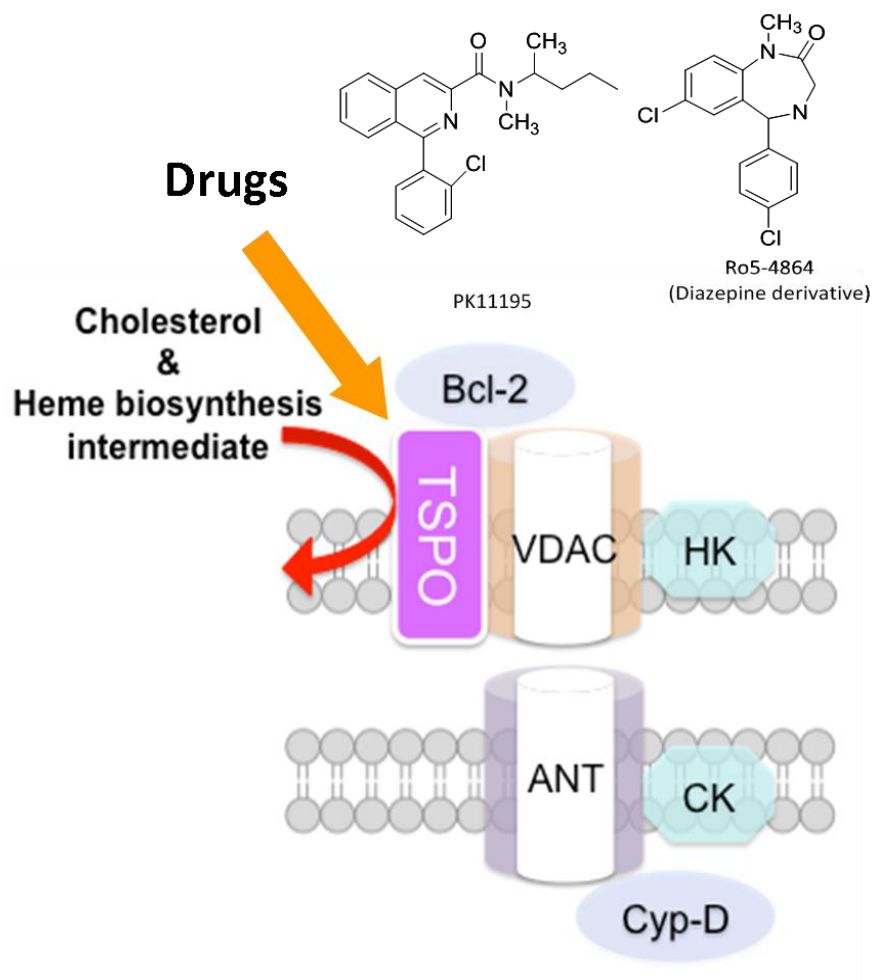
Figure 1. 3 Proposed regulatory effect of TSPO and TSPO ligands on MPTP.

One model of the MPTP complex is shown in the cartoon with VDAC and ANT proposed to be the major structural components of the pore. TSPO as well as other regulatory proteins are associated with VDAC and ANT. TSPO ligands, including diazepines and PK11195, regulate the function of MPTP, as well as the mitochondrial homeostasis, through binding to TSPO and regulating the interaction of TSPO with the MPTP complex. (CK, creatine kinase; HK, hexokinase; CypD, cyclosporine D; Bcl-2: B-cell lymphoma 2)

TSPO in pathological conditions

As mentioned above, TSPO is ubiquitously expressed in all tissues and has been proposed to regulate the homeostasis of the whole cell through the essential MPTP pathway. Abnormal expression and dysfunction of TSPO therefore would potentially cause severe diseases. Indeed, high expression of TSPO is observed in various pathological conditions, including cancer, brain injury, neuronal degeneration, and ischemia-reperfusion injury [13]. Efforts have been made to understand the function of TSPO in disease states, to use TSPO as a diagnostic tool for early identification, and to develop therapeutic treatments targeting TSPO. Although the mechanisms of these diseases, as well as the involvement of TSPO and TSPO ligands during the disease processes, are still not understood, a brief review is provided here to summarize current understanding of the roles TSPO may play in these complex diseases and potential treatments utilizing TSPO ligands.

TSPO in cancer

TSPO is highly expressed in cancerous tissues of the breast, ovary, colon, prostate, and brain [40-45], and TSPO ligands PK11195 and Ro5-4864 have been shown to augment the apoptosis of human tumor cells (MCF-7 [46], C6 glioma cells [47], and human prostate cancer cells [48]) when given along with various chemotherapeutic agents [49]. In addition, the level of TSPO up-regulation is correlated with the aggressiveness of breast cancer [43]. Overexpression of TSPO in MCF-7 cells increased proliferation, whereas silencing of TSPO in MDA-MB-231 cells led to a decrease in proliferation [50]. On the other hand, accumulation of cholesterol has been proposed to be a common phenotype of cancer cells since the original reports of cholesterol crystals observed in solid tumors [51]. Therefore, Batarseh *et al.* [13] proposed that the higher level of TSPO in tumor cells was the driving force for lipid transport to mitochondria and nuclei

and the accumulated cholesterol in the membranes of tumor cells might also influence the degree of membrane fluidity, which in turn plays a role in activation of signaling pathways involved in cancer cell proliferation [52]. Considering the role of TSPO in porphyrin transport, it was also suggested that overexpression of TSPO in cancer cells increased their tolerance to ROS [53,54] and enhanced their metastasis through ROS activated downstream pathways [55].

Taken together, it is reasonable to propose that overexpression of TSPO in cancer cells supports their survival by both increasing the cell viability as well as suppressing cell death [10]. However, controversies still remain in the field and the mechanisms underlying TSPO/mitochondria regulation on cancer metastasis remain unclear.

TSPO in ischemia/reperfusion (I/R) injury

Cardiovascular disease is the leading cause of death in the United States and a serious hazard to public health worldwide. It refers to any disease that affects the cardiovascular system, principally cardiac disease, vascular diseases of the brain and kidney, and peripheral arterial disease [56]. Among all the acute and chronic cardiovascular diseases, ischemic heart disease (IHD), or myocardial ischemia, is the most common cause of death in most western countries and a major cause of hospital admissions. Ischemia refers to a state where the blood supply is restricted, causing a shortage of oxygen and glucose needed for cellular metabolism and resulting in damage or dysfunction of tissue. As a working heart requires a significant amount of nutrients supplied by blood, restriction soon leads to severe consequences including decreases in ATP and pH, increased anaerobic glycolysis, and increases in Na^+ and Ca^{2+} concentrations caused by the inhibition of oxidative phosphorylation. Reperfusion refers to the restoration of blood flow to an organ or tissue after the ischemia. Ischemia/reperfusion injury (I/R injury) is caused by augmented cell death when oxygen (O_2) is reintroduced following

12

ischemia and frequently results in depressed myocardial function. The result may be lethal or cause morbidities that prolong hospitalization and increase costs even after a successful treatment of cardiovascular disease [57].

Induction of the opening of the MPTP is commonly accepted as the cause of cell death during I/R injury, although the mechanism is still not well understood [58-60]. During normal conditions, mitochondria in cardiac tissue mainly rely on the oxidative phosphorylation pathway to generate ATP needed for muscle contraction. This process is highly efficient but also heavily O_2 dependent. Mitochondrial calcium concentrations $[Ca^{2+}]_m$ play a critical role in regulating oxidative phosphorylation during this process. During ischemia, when O_2 supply is limited, mitochondria in the myocytes can no longer produce enough ATP, which leads to a rapid decrease in [ATP] and subsequent loss of [ADP], [AMP] and $[P_i]$. Metabolism will switch to glycolysis, resulting in a decrease in pH and activation of the Na^+/H^+ antiporter that eventually leads to an increase in mitochondrial $[Ca^{2+}]_m$. When O_2 is re-introduced, high levels of ROS are generated when O_2 meets the build up of a reducing in the electron transport chain (ETC) accumulated during ischemia. $[Ca^{2+}]_m$ is further increased as well. The overall effect is a condition that favors opening of the MPTP. When uncontrolled, this massive opening of the MPTP will lead to necrotic cell death.

Regulation of I/R injury by TSPO through MPTP

Much evidence suggests that the MPTP plays a critical role in regulating cell death through apoptosis and/or necrosis. Low level opening of the MPTP facilitates transport of small molecules into the mitochondrial matrix, leading to swollen mitochondrial inner membranes and

broken outer membranes. Release of apoptosis inducing factors, such as cytochrome *c*, from the mitochondrial intermembrane space leads to activation of the apoptosis pathway and controlled cell death through apoptosis. More dramatic opening of the MPTP further leads to complete dissipation of the membrane potential, which impacts the bioenergetics of the cell and leads to cell death through necrosis [61]. Conditions frequently experienced by the heart and brain during reperfusion after a period of ischemia promote the MPTP opening by Ca^{2+} overload (Figure. 1.4). As indicated in Figure 1.3 and Figure 1.4, TSPO ligands have been proposed to reduce I/R injury by inhibiting the MPTP opening and possibly by reducing the production of ROS [62] during reperfusion.

The important role of TSPO in I/R injury is indicated by a variety of studies that show effects of its ligands on the process of cell death through regulation of apoptosis and necrosis. The high affinity TSPO ligands TRO40303, SSR180575 and Ro5-4864 have myocardial protective effects against I/R injury in a mouse model by inhibiting necrosis [63,64] and improve cardiac functional recovery during the post-I/R period [38]. Other drugs, such as the widely used anesthetic Propofol® and related compounds, also show cardio-protection [65] and preliminary data [66] suggest that these effects involve TSPO. A number of proteins including myxoma viral protein M11L and HIV-1 protein Vpr appear to inhibit apoptotic cell death of the host cell through interaction with TSPO [67,68]. It is clear from these many studies that TSPO ligands may have strong regulatory effects on cell death related to I/R injury. In addition, all studies so far regarding the regulatory effects of TSPO ligands on cell death suggest that these effects are mediated through the regulation of the MPTP.
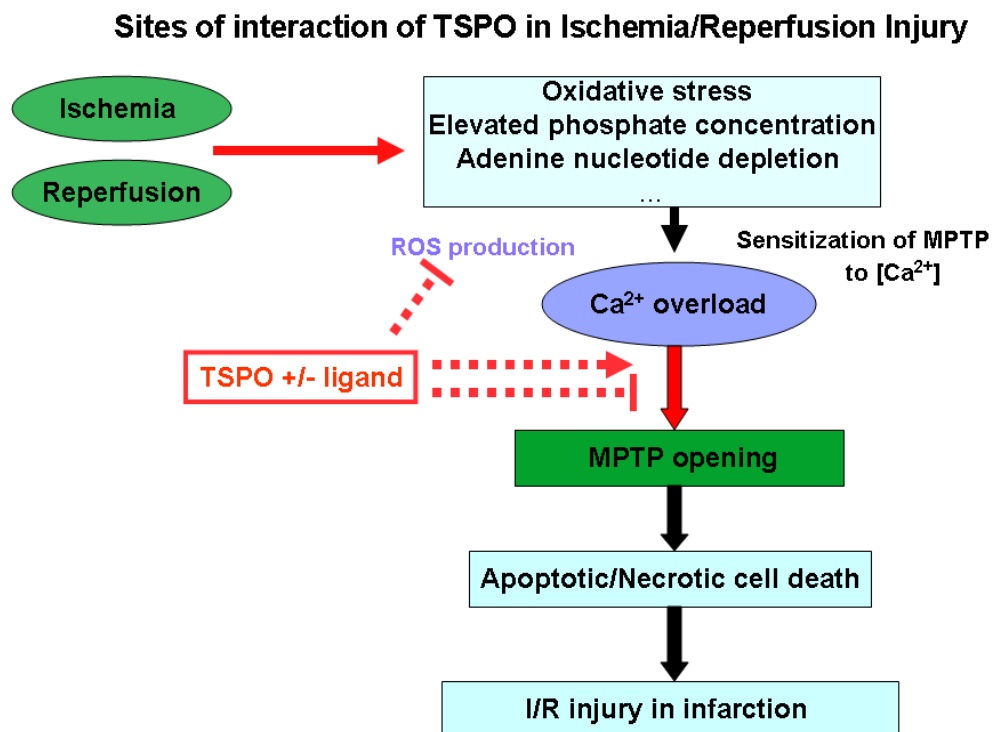
Figure 1.4 Proposed model of interaction of TSPO in the I/R injury process.

MPTP opening is the central regulator of I/R injury. Overexpression of TSPO inhibits the opening of the MPTP by direct interaction with the MPTP complex and/or reducing the ROS level during reperfusion [38]. TSPO ligands demonstrate additional regulation of the MPTP opening [63,64,69], thus I/R injury, through positive/negative regulation of TSPO.

Targeting TSPO in diagnosis and treatment of neural diseases

TSPO expression levels in both CNS and PNS are very low under normal healthy conditions [70]. In the CNS, TSPO is usually expressed in microglia [71], reactive astrocytes [72] and neurons [73], while it has been reported to be expressed in Schwann cells, macrophages and neurons in the PNS [74-76] (Figure 1.5). Interestingly, expression of TSPO is markedly increased under disease conditions [5] including Alzheimer disease [77], Parkinson disease [78,79], Huntington disease [80], stroke [81], brain damage [82], and multiple sclerosis [83]. The up-regulation of TSPO expression mainly occurs in the activated microglia, microphages, and astrocytes [84,85], which represent the site of damage, inflammation and sites of neuronal loss [79,86] that indicate neurodegenerative disease. In addition, the level of TSPO up-regulation is correlated with the severity of the disease [80]. Taken together, expression of TSPO has been used as a sensitive *in vivo* biomarker for diagnosis of various neurological diseases [73,77].
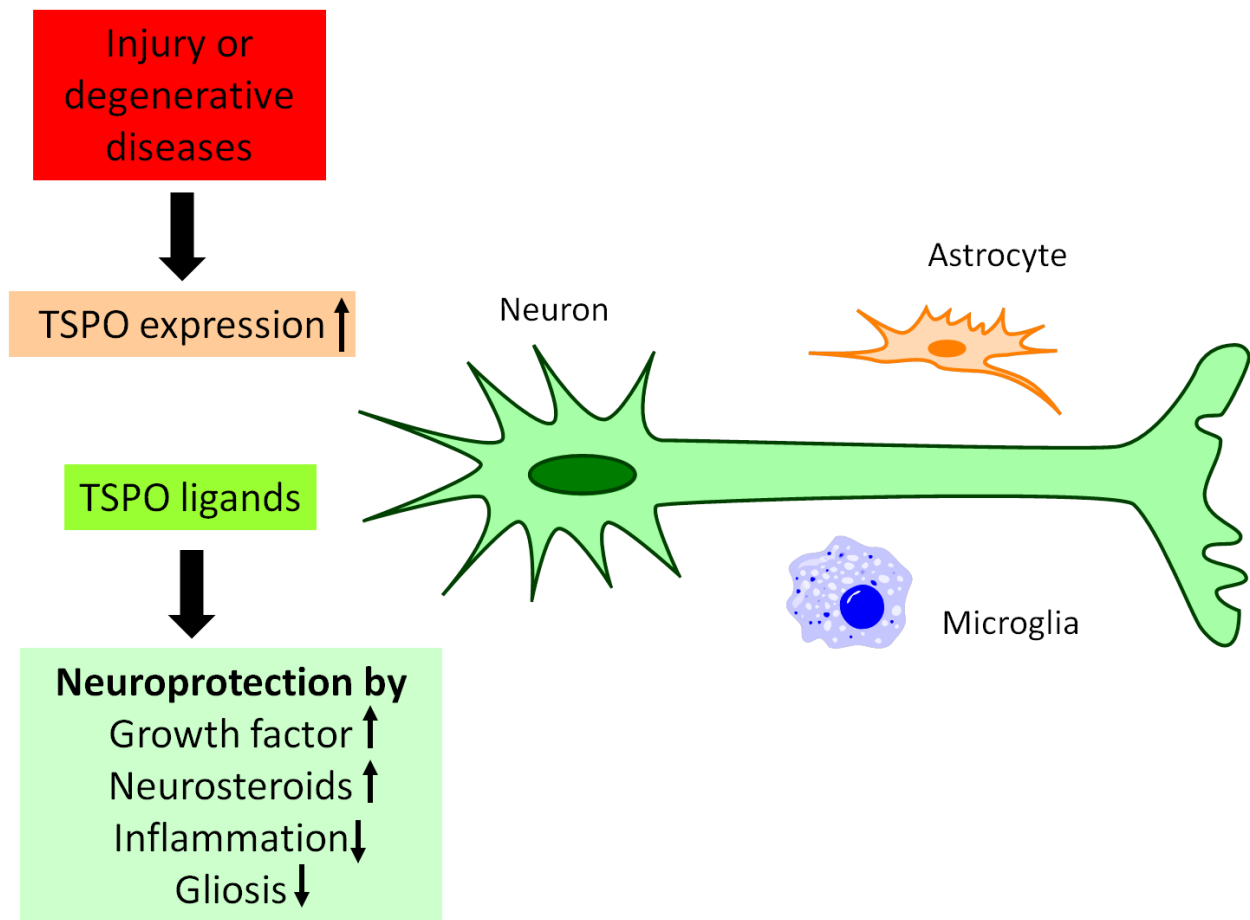
Figure 1.5 Effect of TSPO expression and TSPO ligands.

Injury to brain and peripheral neurons will cause increased expression levels of TSPO in these tissues and the activation of astrocytes and microglia. TSPO ligands were shown to have neuron-protective effects by increasing the expression level of growth factor and neurosteroids, thus reducing inflammation and gliosis. Figure adapted from Rupprecht *et al.* [5].

The mechanism of how TSPO is involved in various neurological diseases and whether the overexpression of TSPO is the cause or the outcome of the pathology are still not well understood. Several possible explanations have been suggested [5,87]. Since the rate-limiting step of steroid biosynthesis, including all neurosteroids, is the transport of cholesterol through TSPO, it was proposed that TSPO regulates the brain function through regulation of neurosteroid production. Papadopoulos *et al.* [88] proposed that cholesterol and steroid levels regulated by TSPO play a role in the degeneration and regeneration of neurons while others also proposed that neurosteroids synthesized downstream of TSPO may act as signaling molecules to other receptors in the brain. For instance, TSPO has been shown to potentiate the $GABA_A$ receptor through up-regulation of allopregnanolone production after inflammation [89,90]. On the other hand, TSPO could also regulate the function and state of the brain through its effects on apoptosis and mitochondrial and whole cell homeostasis *via* regulation of the MPTP. In fact, Jayakumar *et al.* [91] reported that the TSPO ligands PK11195, Ro5-4864, and PpIX stimulated ROS production in the CNS in a MPTP dependent manner. It is also highly possible that the combination and balancing of above mechanisms result in the overall effect of TSPO in neuropathology. Further investigations are certainly needed to better understand how TSPO functions in various neurological diseases.

Application of TSPO ligands in neurological diseases

Although the mechanism of how TSPO functions in the neural systems is still largely unknown, TSPO ligands have played critical roles in facilitating the diagnosis and treatment of various neurological diseases. Due to the highly site specific overexpression of TSPO in areas of brain damage and inflammation, TSPO ligands have been widely used in imaging [92]. Various derivatives of PK11195 were developed to allow better imaging of brain injury as well as to

provide tools for investigating the mechanisms behind these neurological diseases [82,83,92]. For instance, a human single polymorphism mutation with lower affinity to PK11195 derivatives was identified in PET studies [93] and was shown to be related to reduced pregnenolone production [94] and higher incidence of bipolar disorder [95]. Following up on these findings, a cholesterol binding enhancement motif was identified and characterized *in vitro* by mutational analysis of *R*sTSPO. The results of these studies are reported in Chapter 3.

In addition, the therapeutic potential of these compounds has been explored. A number of ligands, including PK11195 [75,96] and Ro5-4864 [97,98], have shown neuroprotective effects [5] and several drugs targeting TSPO are in phase II and phase III clinical trials. Overall, our current knowledge suggests that TSPO plays an important role in maintaining the normal functions of brain and it is very promising to target TSPO for the treatment of various severe neurological diseases.

TSPO *in Rhodobacter sphaeroides*

R. sphaeroides is a metabolically versatile photosynthetic proteobacterium capable of growth under a wide variety of environmental conditions. It is also one of the closest free-living relatives of the mitochondrion [99] and provides a genetically tractable model system for examining proteins in molecular detail as well as their *in vivo* functionality. Importantly, it is a very successful system for expressing and crystallizing membrane proteins. Several homologs of important membrane protein complexes, such as cytochrome *c* oxidase (C*c*O) and the photosynthetic reaction center, have been crystallized from *R. sphaeroides*.

TSPO was independently discovered in *R. sphaeroides* and *R. capsulatus* as the CrtK gene in the carotenoid synthesis operon [100] and was known for its ability to regulate the switch between photosynthesis and respiration in response to oxygen and light conditions [26,27]. It

was subsequently recognized as homologous to the mitochondrial PBR [25,101] and similarly proposed to be involved in the transport of small molecules, such as porphyrin intermediates of the heme and chlorophyll biosynthesis/degradation pathways [26,102].

TSPO in *R. sphaeroides* (*Rs*TSPO) is an 18 kDa transmembrane protein localized to the outer membrane of *R. sphaeroides*. *Rs*TSPO shares a high sequence identity (34 %) with human TSPO (Figure 1.6) and rat TSPO has been shown to substitute for *Rs*TSPO in *R. sphaeroides,* suggesting a further functional link [27]. Along with overall high sequence identity, *Rs*TSPO shares high similarity to the human TSPO in the proposed porphyrin [102] and drug binding sites [103] in the first extra-membrane loop (loop 1), and in the proposed cholesterol binding site, the Cholesterol Recognition/interaction Amino acid Consensus (CRAC) sequence [104]. On the other hand, *Rs*TSPO displays interesting binding behavior compared to its mammalian homologues: mammalian TSPO has been shown to bind to PK11195 and cholesterol at nanomolar affinity and porphyrins at micromolar affinity, but we have shown that *Rs*TSPO binds to all three with micromolar affinity (Chapter 2). The similarities and differences therefore provide us with a unique opportunity to better understand the critical determinants for the ligand binding affinity and the binding mechanism by mutagenesis and systematic analysis in *Rhodobacter*. For example, investigation of the large difference in cholesterol binding affinity between the mammalian and the *Rhodobacter* TSPO discussed in Chapter 3 led to identification of a novel cholesterol binding enhancement motif and better understanding of the molecular determinants of high affinity cholesterol binding.

The bacterial protein *Rs*TSPO is important to study in itself. Given its role in transport of small metabolites in and out of bacteria, understanding of the mechanism of transport by *Rs*TSPO could provide important insights to facilitate the understanding of transport mechanisms

as well as the evolution of transporters. In addition, *R. sphaeroides* provides a potential *in vivo* drug screen assay: a benzodiazepine drug inhibits the color change of *R. sphaeroides* cultures containing the rat version of TSPO during the switch between photosynthesis and respiration [27].

```
                         TM1                              Loop 1
R. sphaeroides   .......... MNMD    4
R. capsulatus    ........... MS     2
Human            .......... MAPP    4
Mouse            .......... MPES    4
Rat              .......... MSQS    4
Bovine           .......... MAPP    4
Zebrafish        ............. M    1
A. thaliana      MDSQDIRYGGDDRDAATTAMAETERKSADDNKGKRDQKRAMAKR   45
S. pombe         ........ MDLNYQVFTSIS   12
B. Subtilis      ........... MK     2
A. fulgidus      ........... MN     2
P. fluorescens   ...............
Drosophila       ......... MADRPCAGN    9
Eubacterium      ......... MKRNNK   6

                         TM1                              Loop 1
R. sphaeroides   WALFLTFLAACGAPATTGALL KPDE...WYDNLNKPWWNPPRWVF   46
R. capsulatus    LTLFAVYFVACACAGATGAIF SPGA...WYDSLKKPSWVPNWLF   44
Human            WVPAMGFTLAPSLGCFVGSRF VHGEGLRWYAGLQKPSWHPPHWVL   49
Mouse            WVPAVGLTLVPSLGGFMGAYF VRGEGLRWYASLQKPSWHPPRWTL   49
Rat              WVPAVGLTLVPSLGGFMGAYF VRGEGLRWYASLQKPSWHPPRWTL   49
Bovine           WVPAVGFTLLPSLGGFLGAQY TRGEGFRWYASLQKPPWHPPRWIL   49
Zebrafish        WIPMLSLTALPHVGGIFGGII TRREVKTWYSTLNKPSWRPPNAAF   46
A. thaliana      GLKSLTVAVAAPVLVTLFATY FLGTSDGYGNRAKSSSWIPPLWLL   90
S. pombe         KNWWSASLVPVACGWFIGNSY KPRKD...YENKKQPKFHPPASAF   54
B. Subtilis      KIVGAIVVFVITYALFSAADY LFPIDQEWYNSLKKPDWTPPGSAI   47
A. fulgidus      ILKLVASILAVLAIGFAGSFF TAQSVQTWYAGVEKPFFTPPNWLF   47
P. fluorescens   MVTFLIFLIACGAAATTGMVF QPGGQ...WYAQLNKPKFTPPNWVF   42
Drosophila       ILRIAGAVILPNLGGIYNGRL TRQHLQSWYANLKFPSFKPPNSVF   54
Eubacterium      WLDLVLYILSAEVIGMSSGLL AGSFN.EFFQKYNKPPLMPPSWVF   50

                         TM2                              TM3
R. sphaeroides   PLAWTSLYFLMSLAAMRVAQLEGS.......GQALAFYAAQLAFNT   85
R. capsulatus    PVAWSTLYILMSISAARVSGLAMENE..LAVLGLAFWAVQIAVNT   87
Human            GPVWGTLYSAMGYGSYLVWKELGGFT.EKAVVPLGLYTGQLALNW   93
Mouse            APIWGTLYSAMGYGSYLVWKELGGFT.EDAMVPLGLYTGQLALNW   93
Rat              APIWGTLYSAMGYGSYIIWKELGGFT.EEAMVPLGLYTGQLALNW   93
Bovine           APIWGTLYSAMGYGSYMIWKELGGFS.KEAVVPLGLYAGQLALNW   93
Zebrafish        PVVWTTLYTGMGYGSYLVWKELGGFT.QDAMVPLGLYGLQLALNW   90
A. thaliana      HTTCLASSGLMGLAAWLVWVDGGFHK..KPNALYLYLAQFLLCL   132
S. pombe         GPAWTLLYLTMGYASHLAYKADPLMITNASRNGSILYIAQLAANF   99
B. Subtilis      GIIWALFLFALISLSAAIVYAAFSFKN..AKSFWFALLINYILNQ   89
A. fulgidus      GPAWTLLYFLIGIVLYIAWEN.GFW.NDSRVKATFFT.QLGLNF   88
P. fluorescens   PVAWTTIYLLLAWVGYRLTMIPGS.....EMVLALWAAQIALNT   81
Drosophila       APMWISLYAGMGYGSYLVWRDGGGFAGEAAKLPLIAYGTQLALNW   99
Eubacterium      PVVWVILYAVMGVSAHLIHYSNAAVS..IKRKLLMVYWVQLIVNF   93

                                      TM4
R. sphaeroides   LWTPVFFGMKRMATALAVMVMWLFVAATMWAFFQLDTWAGVLFV   130
R. capsulatus    LWTPIFFGHRLAGGMLVLVLLWLSVFATCVLFWSVDWLSGLMFV   132
Human            AWPPIFFGARQMGWALVDLLLVSGAAAATTVAWYQVSPLAARLLY   138
Mouse            AWPPIFFGARQMGWALADLLLVSGVATATTLAWHVSPPAARLLY   138
Rat              AWPPIFFGARQMGWALVDLMLVSGVATATTLAWHRVSPPAARLLY   138
Bovine           AWPPLFFGTRQMGWALVDLLLTGGMAAATAMAWHQVSPPAACLLY   138
Zebrafish        AWTPIFFGAHKIQLALIELLLMSGTVAATMVSWYPISRTATLLMV   135
A. thaliana      VWDPVTFRVGSGVAGLAVWLGQSAALFGCYKAFNEISPVAGNLVK   177
S. pombe         AWMPLFYGLAKPKLALADLGILTGLVGWLAKTWWPLAPTASKWLI   144
B. Subtilis      AFSYFQFTQKNLLAASIDCLLVAITAIVLMIIAKKYSRAASYLLL   134
A. fulgidus      LWSILFFGLQNPLAGLVDIIALDIAVILTIVYIYHHS.KASLLLL   132
P. fluorescens   LWTPVFFGAQRIVAAMLILVLLWLVVAVMVLALRLDVITGLILF   126
Drosophila       AWTPIFGQHNIKGGLIDIVALTAAASACGVLFYRVNKTAGLLFV   144
Eubacterium      WSIIFVHFELLWLAAADIVLLLVLIGIMILGFGKVNRIAGDINI   138

                     TM5          CRAC
R. sphaeroides   PYLIWATAATGLNFEAMRLNWNRPEARA............   158
R. capsulatus    PYVIWVTVAGALNFSVWRLNPGEKPITL............   160
Human            PYLAWLAFTTTLNYCVWRDNHGWRGGRRLPE..........   169
Mouse            PYLAWLAFATVLNYYVWRDNSGRRGGSRLPE..........   169
Rat              PYLAWLAFATMLNYYVWRDNSGRRGGSRLTE..........   169
Bovine           PYLAWLAFAATLNYRMWQDNQVRRSGRRLSE..........   169
Zebrafish        PYMAWLCVATSLNYCIWRDNPEPKKED.............   162
A. thaliana      PCLAWAAFVAAVNVKLAVA....................   196
S. pombe         PYLAWLGYAGYLNLGYCLLN...................   164
B. Subtilis      PYFLWSAFATFLSFTIYSMNL...................   155
A. fulgidus      PYLGWILFASALNFAIYLLNA...................   153
P. fluorescens   PYLAWLCVAVALNFSIMRNNRAGYGS..............   152
Drosophila       PYVAWLGFATALNYAIWKLNPEKEQAPKDEEKPSSSHAKSS   185
Eubacterium      PYFLWVAFATYLNVATIFVN...................   158
```

Figure 1.6 Sequence alignment of TSPO proteins.

Figure 1.6 (cont'd)

Shown in the alignment are TSPO proteins from *R. sphaeroides* 2.4.1 (accession number AAF24291) *R. capsulatus* (Z11165), human (CAB55884), mouse (NP_033905), rat (NP_036647), bovine (DAA29060), zebrafish (NP_001006032), *Arabidopsis thaliana* (AAL16286), *Schizosaccharomyces pombe* (CAA22182.2), *Bacillus subtilis* (YP_004204918.1), *Archaeoglobus fulgidus* (NP_070304.1), *Pseudomonas fluorescens* (YP_348542.1), *Drosophila melanogaster* (AAF51482) and *Eubacterium* (EDS01113.1). Conserved amino acids are shown in colors from deep red to yellow. Secondary structure is predicted based on the sequence of *Rs*TSPO by the server Toppred [105]. Transmembrane helices are labeled in blue on top of the sequences. The cholesterol recognition/interaction amino acid consensus (CRAC) is highlighted in a magenta rectangular box with the 3 critical amino acid labeled with cyan triangles. The proposed drug/porphyrin binding loop (loop 1) is highlighted in a purple rectangular box. The human polymorphism residue is labeled with star. This alignment was made using the CLUSTALW server and the picture was created in the Aline program [106].

Protein crystallography

X-ray crystallography is a well established method of determining the arrangement of atoms within a crystal, including for salts, metals, minerals, and semiconductors, as well as for biological molecules. Macromolecular crystallography is a technique using X-rays to study the arrangement of atoms within biological molecules such as proteins, viruses, and nucleic acids. Since the determination of the first crystal structure of myoglobin in the 1950s [107], X-ray crystallography has helped to elucidate the detailed structures of over thousands of proteins, and advanced our understanding of their mechanisms and of numerous processes/diseases. These atomic resolution structures have also served as platforms for the development of many important classes of drugs.

X-rays are suitable for determining the structure of macromolecules because the wavelength of X-rays (~ 1 Å) is similar to the bond length of atoms within the biological macromolecules. Therefore, the diffraction of X-rays by the electrons around the atoms can be used to calculate the position of the atoms and the structure of the protein to high accuracy. Despite the rapid development of various other methods including nuclear magnetic resonance (NMR), electron microscopy (EM), and atomic force microscopy (AFM), X-ray crystallography is still the most powerful method to obtain the three-dimensional structures of macromolecules due to its incomparable high resolution and high accuracy. Recent developments in protein production, purification methods, automation in liquid handling, high energy X-ray sources, and structural genomic pipelines have also sped up and popularized this technique. As a result, the Protein Data Bank (PDB) recently reached the 100,000 structure deposit milestone in May 2014.

Importance of membrane protein structures

It is estimated that more than 30 % of proteins encoded in the human genome are membrane

proteins, including integral membrane proteins as well as peripheral membrane proteins. The importance of membrane proteins cannot be overstated; they mediate the transport of almost everything between and within cells, from nutrients to neuronal signals. Mutations of membrane proteins have been identified in many diseases, including severe diseases such as Alzheimer [108,109] and Huntington diseases [110]. Not surprisingly, more than 50 % of the drugs on the market target membrane proteins [111]. Structures of membrane proteins are critical for understanding the fundamental mechanisms of their functions, as well as for rationally designing drugs targeting membrane proteins for better treatment. However, the structures of membrane proteins are severely underrepresented in the PDB. Compared to the well-established pipeline and high throughput production of structures of soluble proteins, solving the structures of membrane proteins is still a formidable task.

Challenges and advances in membrane protein crystallography

Membrane proteins are notoriously hard to work with for several reasons: 1) they are usually naturally expressed at low levels; 2) they are designed to be surrounded by lipids, which usually are not compatible with the biochemical and biophysical techniques used for characterization; 3) they are often unstable when extracted into solution even with the protection of detergent. However, in order to determine a structure of a membrane protein by X-ray crystallography, milligram quantities of purified, homogenous membrane protein are usually required. Despite the challenges imposed by these requirements, significant advances have been made to facilitate the crystallization and structure determination of membrane proteins in the past few years [112].

Production of membrane proteins

The first bottleneck towards solving a structure of a membrane protein is to obtain the protein of interest in sufficient amount. Historically, most membrane proteins, particularly

eukaryotic membrane proteins, that have been crystallized are from rich natural sources, such as the photosynthetic reaction center from *R. sphaeroides* [113], rhodopsin from the retina [114], and cytochrome *c* oxidase from bovine heart [115]. A membrane protein that is synthesized by ribosomes usually needs to be inserted into the biological membrane with the help of other proteins, such as the translocon, which is often specific for the host organism. In addition, membrane proteins are frequently post-translationally modified within the membrane. As a result, overexpression of membrane proteins in bacterial systems has frequently led to inclusion bodies, incorrect folding, and toxicity to the host cell.

Despite the fact that *Escherichia coli* is still the most popular system for protein expression, several other systems have been developed to facilitate the expression of membrane proteins, especially eukaryotic membrane proteins that are frequently found to be incorrectly folded when expressed in bacteria. Among others, the mammalian expression system [116] and the insect cell expression system [117] are two popular methods. Both systems have the insertion and post-translation modification machinery to facilitate the correct folding and expression of eukaryotic membrane proteins. Increasing numbers of membrane proteins have been successfully expressed from these systems, but incorrect folding and modification have also been reported. For each particular membrane protein, finding the right expression system still requires a significant amount of testing and manipulations.

Purification of membrane proteins

The fundamental difficulty in purifying membrane proteins lies in their hydrophobic nature and their membrane localization. A detergent, an amphiphilic molecule with a hydrophilic head group and a hydrophobic tail, is needed to extract the membrane protein from the natural membrane into solution. However, finding the right detergent for each membrane protein still

relies on trial and error. Even with the right detergent, a membrane protein is usually less stable when it is extracted into solution. Lipid is another key factor that plays an important role in membrane protein purification and crystallization. Experience in this lab as well as others has suggested that natural lipids co-purified with the membrane protein may stabilize the protein and facilitate crystallization. Unfortunately, it is very hard to quantify and control the lipid content in each particular purification. Ligands also play an important role in stabilizing membrane proteins. Recent technical developments, such as the fluorescence-detection size-exclusion chromatography (FSEC) [118] and high throughput thermal stability assays [119] have allowed us to rapidly screen for the construct and ligand to optimize purification of membrane proteins.

Crystallization of membrane proteins

Crystallization itself still poses a significant difficulty towards obtaining a crystal structure of a membrane protein. Over the past decade, major technical developments, including automated liquid handing systems for high throughput crystallization experiments [120], micro-beams at synchrotron X-ray sources to facilitate the data collection on small crystals [121], and new software to process sub-optimal diffraction data collected for membrane protein crystals, have greatly improved our ability to obtain structural information from membrane protein crystals. In addition, major advances have been made in the theories and methods for crystallization of membrane proteins, such as the bicelle [122] and the lipidic cubic phase (LCP) [123] crystallization methods and the understanding of the influence of lipids during the process of crystallization. In this thesis, various methods were investigated for the crystallization of TSPO, providing a case study for evaluating and rationally designing crystallization strategies for difficult membrane proteins. Details of the investigation and the successful optimization of crystallization methods for TSPO from *R. sphaeroides* are discussed in Chapter 4.

Importance of understanding the structure-function relationship of TSPO

As mentioned above, TSPO has been shown to play critical roles in several aspects of human health. Therefore, it has been a long-standing research focus in various fields from basic science to the pharmaceutical industry. Despite years of study and hundreds of ligands developed and investigated in various systems, it is still unclear how exactly TSPO functions in various scenarios, and how its function is regulated by ligands. Additionally, there remain discrepancies and controversies in the literature regarding the binding of TSPO ligands and the physiological significance of their interactions [103,124,125]. For instance, TSPO ligands have been reported to have pro-apoptotic effects in cancer cells [126] but to be anti-apoptotic in cardiac tissue after ischemia and reperfusion injury [63,127,128]. Two major difficulties are significantly hindering our ability to understand the structure-function relationship of TSPO: 1) difficulty related to the interpretation of binding data measured in complex systems such as total membranes or whole cells from different tissues; and 2) the lack of high resolution structures of TSPO to guide the functional studies and rationalize the drug development process.

To address the aforementioned issues, the aims of this study are to characterize the binding properties of various ligands to a homologue of human TSPO, *Rs*TSPO, in its purified state and to obtain high resolution structures of *Rs*TSPO with and without ligand bound. Since *Rs*TSPO is a unique small integral transmembrane protein from the outer mitochondrial membrane, it presents unusual challenges. It has very small cytoplasmic loop regions for mediating crystal contacts and an odd number of α helices, representing a class of membrane proteins that are difficult to crystallize. Therefore, the successful optimization of the purification and crystallization conditions for *Rs*TSPO that is reported here provides valuable knowledge to facilitate the crystallization of similar membrane proteins.

REFERENCES

REFERENCES

1. Braestrup C, Squires RF: **Specific benzodiazepine receptors in rat brain characterized by high-affinity (3H)diazepam binding**. *Proc Natl Acad Sci U S A* 1977, **74**:3805-3809.

2. Verma A, Snyder SH: **Peripheral type benzodiazepine receptors**. *Annu Rev Pharmacol Toxicol* 1989, **29**:307-322.

3. Papadopoulos V, Baraldi M, Guilarte TR, Knudsen TB, Lacapère JJ, Lindemann P, Norenberg MD, Nutt D, Weizman A, Zhang MR, *et al.*: **Translocator protein (18kDa): new nomenclature for the peripheral-type benzodiazepine receptor based on its structure and molecular function**. *Trends Pharmacol Sci* 2006, **27**:402-409.

4. Fan J, Lindemann P, Feuilloley MG, Papadopoulos V: **Structural and functional evolution of the translocator protein (18 kDa)**. *Curr Mol Med* 2012, **12**:369-386.

5. Rupprecht R, Papadopoulos V, Rammes G, Baghai TC, Fan J, Akula N, Groyer G, Adams D, Schumacher M: **Translocator protein (18 kDa) (TSPO) as a therapeutic target for neurological and psychiatric disorders**. *Nat Rev Drug Discov* 2010, **9**:971-988.

6. Woods MJ, Zisterer DM, Williams DC: **Two cellular and subcellular locations for the peripheral-type benzodiazepine receptor in rat liver**. *Biochem Pharmacol* 1996, **51**:1283-1292.

7. Anholt RR, Pedersen PL, De Souza EB, Snyder SH: **The peripheral-type benzodiazepine receptor. Localization to the mitochondrial outer membrane**. *J Biol Chem* 1986, **261**:576-583.

8. Snyder SH, Verma A, Trifiletti RR: **The peripheral-type benzodiazepine receptor: a protein of mitochondrial outer membranes utilizing porphyrins as endogenous ligands**. *FASEB J* 1987, **1**:282-288.

9. McEnery MW, Snowman AM, Trifiletti RR, Snyder SH: **Isolation of the mitochondrial benzodiazepine receptor: association with the voltage-dependent anion channel and the adenine nucleotide carrier**. *Proc Natl Acad Sci U S A* 1992, **89**:3170-3174.

10. Veenman L, Papadopoulos V, Gavish M: **Channel-like functions of the 18-kDa translocator protein (TSPO): regulation of apoptosis and steroidogenesis as part of the host-defense response**. *Curr Pharm Des* 2007, **13**:2385-2405.

11. Krueger KE, Papadopoulos V: **Peripheral-type benzodiazepine receptors mediate translocation of cholesterol from outer to inner mitochondrial membranes in adrenocortical cells**. *J Biol Chem* 1990, **265**:15015-15022.

12. Verma A, Nye JS, Snyder SH: **Porphyrins are endogenous ligands for the mitochondrial (peripheral-type) benzodiazepine receptor**. *Proc Natl Acad Sci U S A* 1987,

84:2256-2260.

13. Batarseh A, Papadopoulos V: **Regulation of translocator protein 18 kDa (TSPO) expression in health and disease states**. *Mol Cell Endocrinol* 2010, **327**:1-12.

14. Lacapère JJ, Papadopoulos V: **Peripheral-type benzodiazepine receptor: structure and function of a cholesterol-binding protein in steroid and bile acid biosynthesis**. *Steroids* 2003, **68**:569-585.

15. Rone MB, Fan J, Papadopoulos V: **Cholesterol transport in steroid biosynthesis: role of protein-protein interactions and implications in disease states**. *Biochim Biophys Acta* 2009, **1791**:646-658.

16. Miller WL: **Steroid hormone synthesis in mitochondria**. *Mol Cell Endocrinol* 2013, **379**:62-73.

17. Simpson ER, Waterman MR: **Regulation by ACTH of steroid hormone biosynthesis in the adrenal cortex**. *Can J Biochem Cell Biol* 1983, **61**:692-707.

18. Jefcoate C: **High-flux mitochondrial cholesterol trafficking, a specialized function of the adrenal cortex**. *J Clin Invest* 2002, **110**:881-890.

19. Mukhin AG, Papadopoulos V, Costa E, Krueger KE: **Mitochondrial benzodiazepine receptors regulate steroid biosynthesis**. *Proc Natl Acad Sci U S A* 1989, **86**:9813-9816.

20. Barnea ER, Fares F, Gavish M: **Modulatory action of benzodiazepines on human term placental steroidogenesis in vitro**. *Mol Cell Endocrinol* 1989, **64**:155-159.

21. Papadopoulos V, Mukhin AG, Costa E, Krueger KE: **The peripheral-type benzodiazepine receptor is functionally linked to Leydig cell steroidogenesis**. *J Biol Chem* 1990, **265**:3772-3779.

22. Rone MB, Liu J, Blonder J, Ye X, Veenstra TD, Young JC, Papadopoulos V: **Targeting and insertion of the cholesterol-binding translocator protein into the outer mitochondrial membrane**. *Biochemistry* 2009, **48**:6909-6920.

23. Ajioka RS, Phillips JD, Kushner JP: **Biosynthesis of heme in mammals**. *Biochim Biophys Acta* 2006, **1763**:723-736.

24. Taketani S, Kohno H, Okuda M, Furukawa T, Tokunaga R: **Induction of peripheral-type benzodiazepine receptors during differentiation of mouse erythroleukemia cells. A possible involvement of these receptors in heme biosynthesis**. *J Biol Chem* 1994, **269**:7527-7531.

25. Yeliseev AA, Kaplan S: **A sensory transducer homologous to the mammalian peripheral-type benzodiazepine receptor regulates photosynthetic membrane complex formation in *Rhodobacter sphaeroides* 2.4.1**. *J Biol Chem* 1995, **270**:21167-21175.

26. Yeliseev AA, Kaplan S: **A novel mechanism for the regulation of photosynthesis gene expression by the TspO outer membrane protein of *Rhodobacter sphaeroides* 2.4.1**. *J Biol Chem* 1999, **274**:21234-21243.

27. Yeliseev AA, Krueger KE, Kaplan S: **A mammalian mitochondrial drug receptor functions as a bacterial "oxygen" sensor**. *Proc Natl Acad Sci U S A* 1997, **94**:5101-5106.

28. Delavoie F, Li H, Hardwick M, Robert JC, Giatzakis C, Péranzi G, Yao ZX, Maccario J, Lacapère JJ, Papadopoulos V: **In vivo and in vitro peripheral-type benzodiazepine receptor polymerization: functional significance in drug ligand and cholesterol binding**. *Biochemistry* 2003, **42**:4506-4519.

29. Wendler G, Lindemann P, Lacapère JJ, Papadopoulos V: **Protoporphyrin IX binding and transport by recombinant mouse PBR**. *Biochem Biophys Res Commun* 2003, **311**:847-852.

30. Zeno S, Veenman L, Katz Y, Bode J, Gavish M, Zaaroor M: **The 18 kDa mitochondrial translocator protein (TSPO) prevents accumulation of protoporphyrin IX. Involvement of reactive oxygen species (ROS)**. *Curr Mol Med* 2012, **12**:494-501.

31. Kroemer G, Dallaporta B, Resche-Rigon M: **The mitochondrial death/life regulator in apoptosis and necrosis**. *Annu Rev Physiol* 1998, **60**:619-642.

32. Tait SW, Green DR: **Mitochondria and cell death: outer membrane permeabilization and beyond**. *Nat Rev Mol Cell Biol* 2010, **11**:621-632.

33. Wajant H: **The Fas signaling pathway: more than a paradigm**. *Science* 2002, **296**:1635-1636.

34. Jiang X, Wang X: **Cytochrome C-mediated apoptosis**. *Annu Rev Biochem* 2004, **73**:87-106.

35. Crompton M: **The mitochondrial permeability transition pore and its role in cell death**. *Biochem J* 1999, **341 (Pt 2)**:233-249.

36. Leung AW, Halestrap AP: **Recent progress in elucidating the molecular mechanism of the mitochondrial permeability transition pore**. *Biochim Biophys Acta* 2008, **1777**:946-952.

37. Giorgio V, von Stockum S, Antoniel M, Fabbro A, Fogolari F, Forte M, Glick GD, Petronilli V, Zoratti M, Szabó I, *et al.*: **Dimers of mitochondrial ATP synthase form the permeability transition pore**. *Proc Natl Acad Sci U S A* 2013.

38. Xiao JJ, Liang DD, Zhang H, Liu Y, Li FJ, Chen YH: **4 '-Chlorodiazepam, a translocator protein (18 kDa) antagonist, improves cardiac functional recovery during postischemia reperfusion in rats**. *Exp Biol Med* 2010, **235**:478-486.

39. Gatliff J, Campanella M: **The 18 kDa translocator protein (TSPO): a new perspective in

mitochondrial biology. *Curr Mol Med* 2012, **12**:356-368.

40. Batarseh A, Li J, Papadopoulos V: **Protein kinase C epsilon regulation of translocator protein (18 kDa) Tspo gene expression is mediated through a MAPK pathway targeting STAT3 and c-Jun transcription factors**. *Biochemistry* 2010, **49**:4766-4778.

41. Katz Y, Eitan A, Amiri Z, Gavish M: **Dramatic increase in peripheral benzodiazepine binding sites in human colonic adenocarcinoma as compared to normal colon**. *Eur J Pharmacol* 1988, **148**:483-484.

42. Katz Y, Ben-Baruch G, Kloog Y, Menczer J, Gavish M: **Increased density of peripheral benzodiazepine-binding sites in ovarian carcinomas as compared with benign ovarian tumours and normal ovaries**. *Clin Sci (Lond)* 1990, **78**:155-158.

43. Hardwick M, Fertikh D, Culty M, Li H, Vidic B, Papadopoulos V: **Peripheral-type benzodiazepine receptor (PBR) in human breast cancer: correlation of breast cancer cell aggressive phenotype with PBR expression, nuclear localization, and PBR-mediated cell proliferation and nuclear transport of cholesterol**. *Cancer Res* 1999, **59**:831-842.

44. Brown RC, Degenhardt B, Kotoula M, Papadopoulous V: **Location-dependent role of the human glioma cell peripheral-type benzodiazepine receptor in proliferation and steroid biosynthesis**. *Cancer Lett* 2000, **156**:125-132.

45. Corsi L, Geminiani E, Avallone R, Baraldi M: **Nuclear location-dependent role of peripheral benzodiazepine receptor (PBR) in hepatic tumoral cell lines proliferation**. *Life Sci* 2005, **76**:2523-2533.

46. Carmel I, Fares FA, Leschiner S, Scherubl H, Weisinger G, Gavish M: **Peripheral-type benzodiazepine receptors in the regulation of proliferation of MCF-7 human breast carcinoma cell line**. *Biochem Pharmacol* 1999, **58**:273-278.

47. Rechichi M, Salvetti A, Chelli B, Costa B, Da Pozzo E, Spinetti F, Lena A, Evangelista M, Rainaldi G, Martini C, *et al.*: **TSPO over-expression increases motility, transmigration and proliferation properties of C6 rat glioma cells**. *Biochim Biophys Acta* 2008, **1782**:118-125.

48. Fafalios A, Akhavan A, Parwani AV, Bies RR, McHugh KJ, Pflug BR: **Translocator protein blockade reduces prostate tumor growth**. *Clin Cancer Res* 2009, **15**:6177-6184.

49. Sutter AP, Maaser K, Grabowski P, Bradacs G, Vormbrock K, Hopfner M, Krahn A, Heine B, Stein H, Somasundaram R, *et al.*: **Peripheral benzodiazepine receptor ligands induce apoptosis and cell cycle arrest in human hepatocellular carcinoma cells and enhance chemosensitivity to paclitaxel, docetaxel, doxorubicin and the Bcl-2 inhibitor HA14-1**. *J Hepatol* 2004, **41**:799-807.

50. Li W, Hardwick MJ, Rosenthal D, Culty M, Papadopoulos V: **Peripheral-type benzodiazepine receptor overexpression and knockdown in human breast cancer**

cells indicate its prominent role in tumor cell proliferation. *Biochem Pharmacol* 2007, **73**:491-503.

51. White C: **On the occurrence of crystals in tumours.** *J Pathol Bacteriol* 1909, **13**:3-10.

52. Singleton PA, Bourguignon LY: **CD44 interaction with ankyrin and IP3 receptor in lipid rafts promotes hyaluronan-mediated Ca2+ signaling leading to nitric oxide production and endothelial cell adhesion and proliferation**. *Exp Cell Res* 2004, **295**:102-118.

53. Trachootham D, Alexandre J, Huang P: **Targeting cancer cells by ROS-mediated mechanisms: a radical therapeutic approach?** *Nat Rev Drug Discov* 2009, **8**:579-591.

54. Kumar B, Koul S, Khandrika L, Meacham RB, Koul HK: **Oxidative stress is inherent in prostate cancer cells and is required for aggressive phenotype**. *Cancer Res* 2008, **68**:1777-1785.

55. Wu WS: **The signaling mechanism of ROS in tumor progression**. *Cancer Metastasis Rev* 2006, **25**:695-705.

56. Fuster V, Kelly B, Vedanthan R: **Global Cardiovascular Health**. *J Am Coll Cardio* 2011, **58**:1208-1210.

57. Orhan G, Yapici N, Yuksel M, Sargin M, Senay S, Yalcin AS, Aykac Z, Aka SA: **Effects of N-acetylcysteine on myocardial ischemia-reperfusion injury in bypass surgery**. *Heart and Vessels* 2006, **21**:42-47.

58. Halestrap AP: **The mitochondrial permeability transition: its molecular mechanism and role in reperfusion injury**. *Biochem Soc Symp* 1999, **66**:181-203.

59. Halestrap AP, Pasdois P: **The role of the mitochondrial permeability transition pore in heart disease**. *Biochim Biophys Acta* 2009, **1787**:1402-1415.

60. Halestrap AP: **A pore way to die: the role of mitochondria in reperfusion injury and cardioprotection**. *Biochem Soc Trans* 2010, **38**:841-860.

61. Kroemer G: **Introduction: mitochondrial control of apoptosis**. *Biochimie* 2002, **84**:103-104.

62. Sileikyte J, Petronilli V, Zulian A, Dabbeni-Sala F, Tognon G, Nikolov P, Bernardi P, Ricchelli F: **Regulation of the inner membrane mitochondrial permeability transition by the outer membrane translocator protein (peripheral benzodiazepine receptor)**. *J Biol Chem* **286**:1046-1053.

63. Obame FN, Zini R, Souktani R, Berdeaux A, Morin D: **Peripheral benzodiazepine receptor-induced myocardial protection is mediated by inhibition of mitochondrial membrane permeabilization**. *J Pharmacol Exp Ther* 2007, **323**:336-345.

64. Schaller S, Paradis S, Ngoh GA, Assaly R, Buisson B, Drouot C, Ostuni MA, Lacapere JJ, Bassissi F, Bordet T, *et al.*: **TRO40303, a new cardioprotective compound, inhibits mitochondrial permeability transition**. *J Pharmacol Exp Ther* **333**:696-706.

65. Roy N, Friehs I, Cowan DB, Zurakowski D, McGowan FX, del Nido PJ: **Dopamine induces postischemic cardiomyocyte apoptosis in vivo: an effect ameliorated by propofol**. *Ann Thorac Surg* 2006, **82**:2192-2199.

66. Garib V, Lang K, Niggemann B, Zanker KS, Brandt L, Dittmar T: **Propofol-induced calcium signalling and actin reorganization within breast carcinoma cells**. *Eur J Anaesthesiol* 2005, **22**:609-615.

67. Castedo M, Perfettini JL, Kroemer G: **Mitochondrial apoptosis and the peripheral benzodiazepine receptor: a novel target for viral and pharmacological manipulation**. *J Exp Med* 2002, **196**:1121-1125.

68. Everett H, Barry M, Sun X, Lee SF, Frantz C, Berthiaume LG, McFadden G, Bleackley RC: **The myxoma poxvirus protein, M11L, prevents apoptosis by direct interaction with the mitochondrial permeability transition pore**. *J Exp Med* 2002, **196**:1127-1139.

69. Halestrap AP, Clarke SJ, Javadov SA: **Mitochondrial permeability transition pore opening during myocardial reperfusion - a target for cardioprotection**. *Cardiovascular Research* 2004, **61**:372-385.

70. Cosenza-Nashat M, Zhao ML, Suh HS, Morgan J, Natividad R, Morgello S, Lee SC: **Expression of the translocator protein of 18 kDa by microglia, macrophages and astrocytes based on immunohistochemical localization in abnormal human brain**. *Neuropathol Appl Neurobiol* 2009, **35**:306-328.

71. Gavish M, Bachman I, Shoukrun R, Katz Y, Veenman L, Weisinger G, Weizman A: **Enigma of the peripheral benzodiazepine receptor**. *Pharmacol Rev* 1999, **51**:629-650.

72. Maeda J, Higuchi M, Inaji M, Ji B, Haneda E, Okauchi T, Zhang MR, Suzuki K, Suhara T: **Phase-dependent roles of reactive microglia and astrocytes in nervous system injury as delineated by imaging of peripheral benzodiazepine receptor**. *Brain Res* 2007, **1157**:100-111.

73. Chen MK, Guilarte TR: **Translocator protein 18 kDa (TSPO): molecular sensor of brain injury and repair**. *Pharmacol Ther* 2008, **118**:1-17.

74. Karchewski LA, Bloechlinger S, Woolf CJ: **Axonal injury-dependent induction of the peripheral benzodiazepine receptor in small-diameter adult rat primary sensory neurons**. *Eur J Neurosci* 2004, **20**:671-683.

75. Mills CD, Bitler JL, Woolf CJ: **Role of the peripheral benzodiazepine receptor in sensory neuron regeneration**. *Mol Cell Neurosci* 2005, **30**:228-237.

76. Lacor P, Gandolfo P, Tonon MC, Brault E, Dalibert I, Schumacher M, Benavides J, Ferzaz B:

Regulation of the expression of peripheral benzodiazepine receptors and their endogenous ligands during rat sciatic nerve degeneration and regeneration: a role for PBR in neurosteroidogenesis. *Brain Res* 1999, **815**:70-80.

77. Ji B, Maeda J, Sawada M, Ono M, Okauchi T, Inaji M, Zhang MR, Suzuki K, Ando K, Staufenbiel M, *et al.*: **Imaging of peripheral benzodiazepine receptor expression as biomarkers of detrimental versus beneficial glial responses in mouse models of Alzheimer's and other CNS pathologies**. *J Neurosci* 2008, **28**:12255-12267.

78. Gerhard A, Pavese N, Hotton G, Turkheimer F, Es M, Hammers A, Eggert K, Oertel W, Banati RB, Brooks DJ: **In vivo imaging of microglial activation with [11C](R)-PK11195 PET in idiopathic Parkinson's disease**. *Neurobiol Dis* 2006, **21**:404-412.

79. Ouchi Y, Yoshikawa E, Sekine Y, Futatsubashi M, Kanno T, Ogusu T, Torizuka T: **Microglial activation and dopamine terminal loss in early Parkinson's disease**. *Ann Neurol* 2005, **57**:168-175.

80. Pavese N, Gerhard A, Tai YF, Ho AK, Turkheimer F, Barker RA, Brooks DJ, Piccini P: **Microglial activation correlates with severity in Huntington disease: a clinical and PET study**. *Neurology* 2006, **66**:1638-1643.

81. Gerhard A, Schwarz J, Myers R, Wise R, Banati RB: **Evolution of microglial activation in patients after ischemic stroke: a [11C](R)-PK11195 PET study**. *Neuroimage* 2005, **24**:591-595.

82. Venneti S, Wagner AK, Wang G, Slagel SL, Chen X, Lopresti BJ, Mathis CA, Wiley CA: **The high affinity peripheral benzodiazepine receptor ligand DAA1106 binds specifically to microglia in a rat model of traumatic brain injury: implications for PET imaging**. *Exp Neurol* 2007, **207**:118-127.

83. Versijpt J, Debruyne JC, Van Laere KJ, De Vos F, Keppens J, Strijckmans K, Achten E, Slegers G, Dierckx RA, Korf J, *et al.*: **Microglial imaging with positron emission tomography and atrophy measurements with magnetic resonance imaging in multiple sclerosis: a correlative study**. *Mult Scler* 2005, **11**:127-134.

84. Vowinckel E, Reutens D, Becher B, Verge G, Evans A, Owens T, Antel JP: **PK11195 binding to the peripheral benzodiazepine receptor as a marker of microglia activation in multiple sclerosis and experimental autoimmune encephalomyelitis**. *J Neurosci Res* 1997, **50**:345-353.

85. Bird JL, Izquierdo-Garcia D, Davies JR, Rudd JH, Probst KC, Figg N, Clark JC, Weissberg PL, Davenport AP, Warburton EA: **Evaluation of translocator protein quantification as a tool for characterising macrophage burden in human carotid atherosclerosis**. *Atherosclerosis* 2010, **210**:388-391.

86. Yasuno F, Ota M, Kosaka J, Ito H, Higuchi M, Doronbekov TK, Nozaki S, Fujimura Y, Koeda M, Asada T, *et al.*: **Increased binding of peripheral benzodiazepine receptor in**

Alzheimer's disease measured by positron emission tomography with [11C]DAA1106. *Biol Psychiatry* 2008, **64**:835-841.

87. Papadopoulos V, Lecanu L: **Translocator protein (18 kDa) TSPO: an emerging therapeutic target in neurotrauma**. *Exp Neurol* 2009, **219**:53-57.

88. Papadopoulos V, Lecanu L, Brown RC, Han Z, Yao ZX: **Peripheral-type benzodiazepine receptor in neurosteroid biosynthesis, neuropathology and neurological disorders**. *Neuroscience* 2006, **138**:749-756.

89. Poisbeau P, Patte-Mensah C, Keller AF, Barrot M, Breton JD, Luis-Delgado OE, Freund-Mercier MJ, Mensah-Nyagan AG, Schlichter R: **Inflammatory pain upregulates spinal inhibition via endogenous neurosteroid production**. *J Neurosci* 2005, **25**:11768-11776.

90. Inquimbert P, Rodeau JL, Schlichter R: **Regional differences in the decay kinetics of GABA(A) receptor-mediated miniature IPSCs in the dorsal horn of the rat spinal cord are determined by mitochondrial transport of cholesterol**. *J Neurosci* 2008, **28**:3427-3437.

91. Jayakumar AR, Panickar KS, Norenberg MD: **Effects on free radical generation by ligands of the peripheral benzodiazepine receptor in cultured neural cells**. *J Neurochem* 2002, **83**:1226-1234.

92. Chauveau F, Boutin H, Van Camp N, Dollé F, Tavitian B: **Nuclear imaging of neuroinflammation: a comprehensive review of [11C]PK11195 challengers**. *Eur J Nucl Med Mol Imaging* 2008, **35**:2304-2319.

93. Owen DR, Yeo AJ, Gunn RN, Song K, Wadsworth G, Lewis A, Rhodes C, Pulford DJ, Bennacef I, Parker CA, *et al.*: **An 18-kDa translocator protein (TSPO) polymorphism explains differences in binding affinity of the PET radioligand PBR28**. *J Cereb Blood Flow Metab* 2012, **32**:1-5.

94. Costa B, Pini S, Martini C, Abelli M, Gabelloni P, Landi S, Muti M, Gesi C, Lari L, Cardini A, et al.: **Ala147Thr substitution in translocator protein is associated with adult separation anxiety in patients with depression**. *Psychiatr Genet* 2009, **19**:110-111.

95. Colasanti A, Owen DR, Grozeva D, Rabiner EA, Matthews PM, Craddock N, Young AH: **Bipolar Disorder is associated with the rs6971 polymorphism in the gene encoding 18 kDa Translocator Protein (TSPO)**. *Psychoneuroendocrinology* 2013, **38**:2826-2829.

96. Ryu JK, Choi HB, McLarnon JG: **Peripheral benzodiazepine receptor ligand PK11195 reduces microglial activation and neuronal death in quinolinic acid-injected rat striatum**. *Neurobiol Dis* 2005, **20**:550-561.

97. Veiga S, Azcoitia I, Garcia-Segura LM: **Ro5-4864, a peripheral benzodiazepine receptor ligand, reduces reactive gliosis and protects hippocampal hilar neurons from kainic acid excitotoxicity**. *J Neurosci Res* 2005, **80**:129-137.

98. Parker MA, Bazan HE, Marcheselli V, Rodriguez de Turco EB, Bazan NG: **Platelet-activating factor induces permeability transition and cytochrome c release in isolated brain mitochondria**. *J Neurosci Res* 2002, **69**:39-50.

99. Bui ET, Bradley PJ, Johnson PJ: **A common evolutionary origin for mitochondria and hydrogenosomes**. *Proc Natl Acad Sci U S A* 1996, **93**:9651-9656.

100. Armstrong GA, Alberti M, Leach F, Hearst JE: **Nucleotide-sequence, organization, and nature of the protein products of the carotenoid biosynthesis gene-cluster of *Rhodobacter capsulatus***. *Mol Gen Gen* 1989, **216**.

101. Baker ME, Fanestil DD: **Mammalian peripheral-type benzodiazepine receptor is homologous to CrtK protein of *Rhodobacter capsulatus*, a photosynthetic bacterium**. *Cell* 1991, **65**:721-722.

102. Yeliseev AA, Kaplan S: **TspO of *Rhodobacter sphaeroides*. A structural and functional model for the mammalian peripheral benzodiazepine receptor**. *J Biol Chem* 2000, **275**:5657-5667.

103. Scarf AM, Auman KM, Kassiou M: **Is there any correlation between binding and functional effects at the translocator protein (TSPO) (18 kDa)?** *Curr Mol Med* 2012, **12**:387-397.

104. Li H, Yao Z, Degenhardt B, Teper G, Papadopoulos V: **Cholesterol binding at the cholesterol recognition/ interaction amino acid consensus (CRAC) of the peripheral-type benzodiazepine receptor and inhibition of steroidogenesis by an HIV TAT-CRAC peptide**. *Proc Natl Acad Sci U S A* 2001, **98**:1267-1272.

105. Cserzö M, Wallin E, Simon I, von Heijne G, Elofsson A: **Prediction of transmembrane alpha-helices in prokaryotic membrane proteins: the dense alignment surface method**. *Protein Eng* 1997, **10**:673-676.

106. Bond CS, Schüttelkopf AW: **ALINE: a WYSIWYG protein-sequence alignment editor for publication-quality alignments**. *Acta Crystallogr D Biol Crystallogr* 2009, **65**:510-512.

107. Kendrew JC, Dickerson RE, Strandberg BE, Hart RG, Davies DR, Phillips DC, Shore VC: **Structure of myoglobin: A three-dimensional Fourier synthesis at 2 A. resolution**. *Nature* 1960, **185**:422-427.

108. Yan R, Bienkowski MJ, Shuck ME, Miao H, Tory MC, Pauley AM, Brashier JR, Stratman NC, Mathews WR, Buhl AE, *et al.*: **Membrane-anchored aspartyl protease with Alzheimer's disease beta-secretase activity**. *Nature* 1999, **402**:533-537.

109. Li J, Xu M, Zhou H, Ma J, Potter H: **Alzheimer presenilins in the nuclear membrane, interphase kinetochores, and centrosomes suggest a role in chromosome segregation**. *Cell* 1997, **90**:917-927.

110. Butterfield DA, Oeswein JQ, Markesbery WR: **Electron spin resonance study of membrane protein alterations in erythrocytes in Huntington's disease**. *Nature* 1977, **267**:453-455.

111. Yildirim MA, Goh KI, Cusick ME, Barabási AL, Vidal M: **Drug-target network**. *Nat Biotechnol* 2007, **25**:1119-1126.

112. Stroud RM: **New tools in membrane protein determination**. *F1000 Biol Rep* 2011, **3**:8.

113. Allen JP, Feher G, Yeates TO, Komiya H, Rees DC: **Structure of the reaction center from *Rhodobacter sphaeroides* R-26: the cofactors**. *Proc Natl Acad Sci U S A* 1987, **84**:5730-5734.

114. Palczewski K, Kumasaka T, Hori T, Behnke CA, Motoshima H, Fox BA, Le Trong I, Teller DC, Okada T, Stenkamp RE, *et al.*: **Crystal structure of rhodopsin: A G protein-coupled receptor**. *Science* 2000, **289**:739-745.

115. Tsukihara T, Aoyama H, Yamashita E, Tomizaki T, Yamaguchi H, Shinzawa-Itoh K, Nakashima R, Yaono R, Yoshikawa S: **The whole structure of the 13-subunit oxidized cytochrome *c* oxidase at 2.8 A**. *Science* 1996, **272**:1136-1144.

116. Chaudhary S, Pak JE, Gruswitz F, Sharma V, Stroud RM: **Overexpressing human membrane proteins in stably transfected and clonal human embryonic kidney 293S cells**. *Nat Protoc* 2012, **7**:453-466.

117. Kost TA, Condreay JP, Jarvis DL: **Baculovirus as versatile vectors for protein expression in insect and mammalian cells**. *Nat Biotechnol* 2005, **23**:567-575.

118. Kawate T, Gouaux E: **Fluorescence-detection size-exclusion chromatography for precrystallization screening of integral membrane proteins**. *Structure* 2006, **14**:673-681.

119. Alexandrov AI, Mileni M, Chien EY, Hanson MA, Stevens RC: **Microscale fluorescent thermal stability assay for membrane proteins**. *Structure* 2008, **16**:351-359.

120. Cherezov V, Peddi A, Muthusubramaniam L, Zheng YF, Caffrey M: **A robotic system for crystallizing membrane and soluble proteins in lipidic mesophases**. *Acta Crystallogr D Biol Crystallogr* 2004, **60**:1795-1807.

121. Fischetti RF, Xu S, Yoder DW, Becker M, Nagarajan V, Sanishvili R, Hilgart MC, Stepanov S, Makarov O, Smith JL: **Mini-beam collimator enables microcrystallography experiments on standard beamlines**. *J Synchrotron Radiat* 2009, **16**:217-225.

122. Faham S, Bowie JU: **Bicelle crystallization: a new method for crystallizing membrane proteins yields a monomeric bacteriorhodopsin structure**. *J Mol Biol* 2002, **316**:1-6.

123. Caffrey M, Cherezov V: **Crystallizing membrane proteins using lipidic mesophases**. *Nature Protocols* 2009, **4**:706-731.

124. Scarf AM, Luus C, Da Pozzo E, Selleri S, Guarino C, Martini C, Ittner LM, Kassiou M: **Evidence for complex binding profiles and species differences at the translocator protein (TSPO) (18 kDa)**. *Curr Mol Med* 2012, **12**:488-493.

125. Gonzalez-Polo RA, Carvalho G, Braun T, Decaudin D, Fabre C, Larochette N, Perfettini JL, Djavaheri-Mergny M, Youlyouz-Marfak I, Codogno P, *et al.*: **PK11195 potently sensitizes to apoptosis induction independently from the peripheral benzodiazepin receptor**. *Oncogene* 2005, **24**:7503-7513.

126. Decaudin D, Castedo M, Nemati F, Beurdeley-Thomas A, De Pinieux G, Caron A, Pouillart P, Wijdenes J, Rouillard D, Kroemer G, *et al.*: **Peripheral benzodiazepine receptor ligands reverse apoptosis resistance of cancer cells in vitro and in vivo**. *Cancer Res* 2002, **62**:1388-1393.

127. Xiao J, Liang D, Zhang H, Liu Y, Li F, Chen YH: **4'-Chlorodiazepam, a translocator protein (18 kDa) antagonist, improves cardiac functional recovery during postischemia reperfusion in rats**. *Exp Biol Med (Maywood)* 2010, **235**:478-486.

128. Schaller S, Paradis S, Ngoh GA, Assaly R, Buisson B, Drouot C, Ostuni MA, Lacapere JJ, Bassissi F, Bordet T, *et al.*: **TRO40303, a new cardioprotective compound, inhibits mitochondrial permeability transition**. *J Pharmacol Exp Ther* 2010, **333**:696-706.

CHAPTER 2

Characterization and modeling of the oligomeric state and ligand binding behavior of purified Translocator Protein 18 kDa (TSPO) from *Rhodobacter sphaeroides*

INTRODUCTION

Translocator Protein 18 kDa (TSPO) was originally discovered as a secondary binding site for the widely prescribed anti-anxiety drugs, benzodiazepines, in the mitochondria of rat kidney [1]. For this reason, it became known as the peripheral-type benzodiazepine receptor (PBR). In 2006, it was renamed as Translocator Protein 18 kDa (TSPO) [2] to better represent the emerging understanding of a family of highly conserved integral membrane proteins (Figure 1.6) found in Archaea through to plants and human, with a broad spectrum of functions including steroid and porphyrin transport and regulation of apoptosis, inflammation, metastatic cancer and cardiovascular diseases [3,4].

In mammalian cells, TSPO is primarily located in the outer mitochondrial membrane and concentrated at the outer/inner membrane contact sites [5]. It is expressed in all organs examined so far and at particularly high levels in steroid hormone producing tissues, such as adrenal glands and kidney. Knock-out of TSPO is developmentally lethal in the mouse [6]. The major function of TSPO has been proposed to be transporting small molecules, including cholesterol and heme biosynthesis intermediates, into or out of mitochondria to be further metabolized [7-10]. In addition, TSPO has been found to be highly expressed in areas of brain injury and inflammation [11], and aggressive cancers [12,13], as well as brains of Alzheimer and Huntington disease patients [14]. In these situations, TSPO has been proposed to be involved in the regulation of the mitochondrial permeability transition pore (MPTP) [15,16], thus exerting its effects on cellular homeostasis (see reviews in *Current Molecular Medicine* [17,18]). TSPO ligands, including benzodiazepines and more specific compounds represented by the diagnostic ligand PK11195, have been shown to attenuate cancer cell proliferation [13], to have neuro-protective effects [19], and to inhibit the MPTP [20]. The interaction of TSPO with ligands continues to be a strong research focus aimed at the development of drugs targeting TSPO for imaging and treatment of

diverse disease states.

Mitochondria play important roles in the normal function of cells and also in regulating cell death through apoptosis and/or necrosis [21,22]. The initiation of apoptosis is usually preceded by a loss of the mitochondrial membrane potential ($\Delta\Psi_m$), which is proposed to be regulated by the MPTP [23], a multi-protein complex whose structural components are still not established. Together with other proteins, TSPO has been implicated as a regulator of the MPTP, having been isolated originally in a complex with the voltage dependent anion channel (VDAC) and the adenine nucleotide translocator (ANT) [24]. Both VDAC and ANT are candidate components of the MPTP [15,25], but other possibilities remain [26]. Various TSPO ligands have been shown to regulate apoptosis [27]; however, it is currently still unclear how MPTP or apoptosis is regulated by TSPO.

In the purple non-sulfur bacteria that are suggested as ancestors of mitochondria [28], TSPO was discovered in the carotenoid gene cluster as CrtK [29], first in *Rhodobacter capsulatus* [29], and subsequently in *R. sphaeroides* (*Rs*TSPO) [30]. Initially designated as the tryptophan-rich sensory protein (TspO), the bacterial protein was recognized as homologous to the mitochondrial PBR [30,31]. In *Rhodobacter* it is located in the outer membrane and involved in regulating photosynthetic gene expression in response to oxygen and light conditions [32,33]. Similar to its mammalian ortholog, *Rs*TSPO is proposed to be involved in the transport of small molecules such as porphyrin intermediates of the heme and chlorophyll biosynthesis/degradation pathways [33,34]. *Rs*TSPO shares considerable sequence homology with human TSPO (*Hs*TSPO) (Figure 1.6) and rat TSPO has been shown to substitute for *Rs*TSPO in *R. sphaeroides,* suggesting a functional link [32]. Along with overall significant sequence identity (30 %), *Rs*TSPO shares noteworthy sequence similarity to the *Hs*TSPO in the first extra-membrane loop

(loop 1) which is proposed to participate in porphyrin [34] and drug binding [35], as well as in the cholesterol binding site located at the Cholesterol Recognition/interaction Amino acid Consensus (CRAC) sequence at the C-terminus, including the end of trans-membrane helix V [36].

Although *R. sphaeroides* does not make cholesterol, it does produce a related class of steroid-like molecules, hopanoids [37], which may account for why the proposed critical residues for cholesterol binding are well conserved between mammalian and *Rs*TSPO. However, the sequences before and after the CRAC region vary. A recent paper reported that the human single polymorphism A147T immediately preceding the CRAC sequence in helix V resulted in 2 orders of magnitude reduction in affinity for a PK11195 analog used for PET imaging [38]. This finding highlights the adjacent variable region (residue 144-146 in the human sequence) that could play a role in differences in ligand binding between *Rhodobacter* and human TSPO. In addition, loop 1, implicated in drug and porphyrin binding by mutations in both *Rhodobacter* [34] and mammalian [35] TSPO, is highly variable in the initial one third, while the rest is conserved. Differences in this region may also play a role in the significantly higher affinity of PK11195 reported for human [39] and for rat TSPO expressed in *R. sphaeroides* compared to the endogenous *Rs*TSPO [32]. In addition, the mutation W38C in this loop 1 region was observed to influence dimerization and stability of *Rs*TSPO, suggesting a complex role in protein structure [34]. With respect to cholesterol binding, information on the binding behavior of *Rs*TSPO is still not available and the possibility of direct or allosteric competition between PK11195, cholesterol and porphyrin has been suggested [40] but not established.

There remain discrepancies and controversies in the literature regarding the binding of TSPO ligands and the physiological significance of their interactions [35,41,42]. For instance,

TSPO ligands have been reported to have pro-apoptotic effects in cancer cells [43] but to be anti-apoptotic in cardiac tissue after ischemia and reperfusion injury [20,44,45]. A major difficulty comes from the interpretation of binding data measured in complex systems such as total membranes or whole cells from different tissues where other proteins may affect the interaction. To clarify some of these issues, we have expressed and purified to homogeneity the *Rs*TSPO wild-type and the reported dimer-stabilizing mutant W38C [34]. We describe studies of their oligomerization state as well as their binding to ligands, including cholesterol, porphyrin, the diagnostic drug PK11195, and a series of compounds with reported apoptosis-influencing properties. Using a sensitive tryptophan fluorescence quenching assay, our results show that these ligands have direct interactions with *Rs*TSPO at micro-molar affinity. We provide an atomic-detail model of the *Rs*TSPO dimer, based on a 10 Å resolution cryo-EM density map [46] and using EM-Fold [47], and discuss the relationship between ligand interactions in the context of the dimer model. Some novel ligands characterized in this study provide candidates for the optimization of crystallization of TSPO.

MATERIALS AND METHODS

Materials

Chemicals were purchased from Sigma-Aldrich (St. Louis, MO). Dodecyl maltoside (DDM), decyl maltoside (DM) and n-dodecylphosphocholine (Fos-Choline-12) (Anagrade) were purchased from Anatrace (Maumee, OH). The *Rs*TSPO expression plasmid was a gift from Dr. Samuel Kaplan from the University of Texas and the codon-optimized HsTSPO was synthesized by DNA 2.0 [®]. Pfu Turbo [®] polymerase was purchased from Agilent technologies (Santa Clara, CA). Restriction enzymes and T4 ligase were purchased from New England Biolabs (Ipswich, MA).

Cloning

The coding sequence of *Rs*TSPO was sub-cloned into the pUC12 vector for mutagenesis. The W38C mutant of *Rs*TSPO was made by QuikChange Mutagenesis[©] (Stratagene). Fusion protein constructs were made by the splicing-by-overlapping-extension method [48]. Constructs were confirmed by sequencing and ligated into the PRK415 expression vector with KpnI and HindIII restriction sites or the pJ411 (DNA 2.0 [®]) expression vector with NdeI and EcoRI restriction sites. The human TSPO gene was codon optimized for *E. coli* expression and purchased from DNA 2.0 [®] in the pJ411 vector. Expression vectors containing the desired TSPO coding sequence were confirmed by sequencing and introduced into the *E. coli* expression strain BL21 λDE3.

Protein expression and purification

The transformed bacteria were cultured at 30 °C in 100 mL LB medium containing appropriate antibiotics overnight. Fifteen mL of the overnight culture were then transferred into 1 L of auto-induction media (ZYM-5025) [49] containing glycerol, glucose and lactose and the appropriate antibiotics. Cultures were grown at 30 °C for *Rs*TSPO, *Rs*TSPOW38C and fusion proteins and decreased to 12 °C for *Hs*TSPO to reduce the inclusion bodies and GroEL. Cells were harvested when the OD_{600} reached above 4.0. Harvested cells were resuspended in lysis buffer (50 mM KH_2PO4 pH 6.5, 1 mM EDTA) supplemented with Roche [®] protease inhibitor cocktail and were lysed through two passes at 20,000 p.s.i in a French press homogenizer. Broken cells were centrifuged at 200 x g for 5 mins, 10,000 x g for 30 mins, and 150,000 x g for 90 mins at 4 °C to isolate the membranes. Isolated membranes were resuspended with buffer A (50 mM Tris-HCl, pH 8, 150 mM NaCl, 10% glycerol) and quick frozen with liquid nitrogen and stored at -70 °C before purification.

Membranes were thawed on ice, resuspended to 10 mg/ml total protein in buffer A, solubilized by adding 1 % DDM, 1 mM PMSF and Roche ® protease inhibitor cocktail (no EDTA) and stirred at 4 °C for 1 hr. Solubilized membranes were centrifuged at 150,000 x g for 30 mins to remove the unsolubilized fraction. The supernatant was loaded on a 10 mL Ni-NTA (Qiagen) gravity column pre-equilibrated with buffer A. After extensive washing with buffer A supplemented with 0.2 % DM and 50 mM imidazole, fractions containing the desired protein were eluted using buffer A supplemented with 0.2 % DM and 300 mM imidazole over two column volumes. Fractions containing the desired protein were pooled, concentrated with a 50 kDa cutoff Amicon filter (Millipore), washed once with buffer A supplemented with 0.2 % DM, and diluted to 10 mL. Trypsin was added at 0.2 mg per 1 mg of *Rs*TSPO10ht and the protein solution was incubated at 4 °C overnight. Trypsin treated *Rs*TSPO10ht was concentrated to 250 µL with a 30 kDa cutoff Amicon filter and loaded onto a Superose® 12 300/10 gel filtration column (GE Life Sciences) pre-equilibrated with buffer B (50 mM Tris-HCl, pH 8.0, 150 mM NaCl, 0.2 % DM, 2 mM β-mercaptoethanol [βME]) and run at 0.3 mL/min. The homogeneous peak fractions of *Rs*TSPO were pooled and the concentration of the protein was determined by UV absorbance at 280 nm. The purity of the protein was estimated on SDS-PAGE stained with Coomassie blue. The average yield of wild-type *Rs*TSPO was 5 mg per L of culture. *Rs*TSPO was also solublized and purified in Fos-Choline-12 (2 % and 0.2 %) using the same buffer conditions but omitting the SEC step. This version of the enzyme was used for comparative binding experiments (Figure 2.8).

Codon optimized *Hs*TSPO was expressed at good levels in *E. coli* and was purified in the same way as *Rs*TSPO. However, the *E. coli* chaperone protein GroEL was found to co-purify with *Hs*TSPO as a persistent contaminant. As shown in Figure 2.3, a reasonably pure *Hs*TSPO

monomer with a trace of dimer was present in the sample, but with a significant amount of GroEL co-purified (Figure 2.3). The fortuitous absence of tryptophan in GroEL, combined with the unusually high tryptophan content of TSPO (13 out of 169 amino acids), made it possible to carry out some ligand binding studies with the human protein based on fluorescence quenching, but not to characterize its oligomeric state.

Light scattering measurements of oligomeric state of purified *Rs*TSPO

A static light scattering method combined with UV absorption and refractive index measurement was used to investigate the oligomeric state of the purified *Rs*TSPO [50]. Four uL of a 30 mg/mL purified *Rs*TSPO sample was loaded on a Superdex® 200 300/10 column coupled with the triple detector array (Malvern) and run in buffer B at 0.3 mL/min at 4 °C. Purified ovalbumin and pure DM were run in the same buffer under the same conditions. Data analysis was done in OmniSEC® software to calculate the molecular weight of the protein-detergent complex and fraction of protein by comparing the light scattering, which represents the size of the protein-detergent complex, and the amount of proteins in the complex as measured by UV_{280} ($\varepsilon = 71960$ M^{-1} cm^{-1}).

Tryptophan fluorescence quenching binding assay

A tryptophan fluorescence quenching assay was used to study the binding properties of TSPO by utilizing the intrinsic tryptophan fluorescence [46]. For the *Rs*TSPO and *Rs*TSPOW38C, 2.5 μM purified protein was titrated with increasing amounts of ligand in the desired concentration range at room temperature. Each titration point was monitored by a spectral scan from 290 nm to 400 nm (excitation at 285 nm) on a PTI QuantaMaster™ spectrofluorimeter. Control experiments were performed to evaluate the absorption/emission of ligands as well as buffers and solvents. Due to the slight shift of the tryptophan fluorescence

peak during the experiment caused by differential quenching of buried tryptophans *vs* solvent exposed ones, the area under each emission spectrum was integrated to account for all tryptophans and a percentage quenching ratio for each concentration was calculated. The binding curve was obtained by plotting the percentage quenching f_{Quen} against total ligand concentration $[L_t]$ in Origin $^{©}$. Equation (1) was derived based on a single binding site per monomer assumption, taking into consideration ligand depletion. $[L_t]$ is the total ligand concentration plotted on the binding curves. The calculation of the K_d is corrected by Equation (1) for ligand depletion which occurs at low ligand concentrations due the relatively high protein/ligand ratio.

$$f_{Quen} = Offs + F\max \frac{(f[Pt]+[Lt]+Kd - \sqrt{f([Pt]+[Lt]+Kd)^2 - 4f[Pt][Lt]}}{2f[Pt]} \tag{1}$$

$$F_{\max} = \frac{F_i - F_f}{F_i} \tag{2}$$

f_{Quen} represents the calculated percentage quenching at each concentration, F_{max} is the maximum amplitude of fluorescence quenching, which equals the difference between the initial and final fluorescence signals divided by the initial fluorescence, $[L_t]$ is the total ligand concentration, $[P_t]$ is the total concentration of purified *Rs*TSPO protein (fixed at 2.5 µM in the experiment and during the fitting procedure) and K_d is the apparent dissociation constant. *Offs* (offset) allows a fit unconstrained to go through zero, while *f* is a parameter to account for the effective fraction of protein involved in binding. *Offs* and *f* help to optimize the fitting by accounting for binding modes involving different numbers of sites. For partially purified *Hs*TSPO with a total protein concentration at 2.5 µM, the binding curve was obtained the same way as for *Rs*TSPO but the apparent dissociation constant K_{app} was estimated as the concentration of the half-max quenching, since it is assumed that nonspecific binding to

contaminating GroEL may give a K_{app} that is larger than the actual value. These HsTSPO experiments were done with a mutant, C153E, that removed the possible complication of the extra cysteine in the human protein and which showed no difference in terms of expression, purification or reported function. All ligands are dissolved in DMSO as a stock solution and diluted with DMSO or buffer for measurement except for cholesterol and PpIX, which were dissolved in pure ethanol or 0.15 M NaCl, respectively. Control quenching curves with solvent alone were carried out. One representative binding curve is shown in each figure while the K_d is reported as the average of 3 replicate measurements fitted with Equation (1).

Modeling of the RsTSPO dimer

The experimental EM density map from the EM database (ID: EMDB-1698) was processed in Chimera [51] to match published helix placement in a RsTSPO dimer density. Final models were generated using a modified protocol from Lindert *et al*. [47] Twenty thousand decoys were generated using a simultaneously combined BCL::EM-Fold and the membrane protein protocol in BCL::MP-fold [52]. Briefly, the trans-membrane helices were first assembled into the density rods as a monomer. The models were evaluated by their agreement with the density map as well as a knowledge-based potential. The models were then clustered combining all models with the same arrangement of trans-membrane helices (topology). The best scoring 150 topologies were then symmetrized and subjected to another round of EM-fold refinement against the density map. The full-atom models were generated using Rosetta [53,54]; out of the 150 refined topological fold from previous step, 75 best scoring folds were used to generate 2000 all-atom models per fold. Then, within each topology, the models are clustered with respect to loop conformation. For the best scoring 20 loop conformations from each of the 75 topologies, three rounds of iterative loop modeling, side chain repacking, and relaxation were conducted

using the density map as a restraint in Rosetta [47,54]. Twenty-five models were created in each iteration and the top-scoring models were moved forward to the next iteration. The final models were ranked by the Rosetta full atom energy score [53-55]. All figures were generated in Pymol v1.3. The simulation did not test topologies that include domain swaps.

RESULTS

*Rs*TSPO forms a dimer *in vitro*

      *Rs*TSPO was successfully purified to homogeneity by nickel affinity followed by size exclusion chromatography (SEC) (Figures 2.1, 2.2A). The molecular weight of purified *Rs*TSPO with a 10 histidine tag was determined to be 19371.76 ± 1.77 Da (17910.26 Da for un-tagged *Rs*TSPO) by mass spectrometry, correlating well with the calculated molecular weight from the amino acid sequence (19347.58 Da). The SEC running profile in 0.2 % DM showed a peak that suggested a dimer form based on elution profile and molecular weight standards. To obtain a more accurate estimate of the size of *Rs*TSPO, we characterized the purified *Rs*TSPO in solution by using a combination of light scattering, UV and refractive index measurements. A representative run of the $UV_{280\,nm}$, refractive index and light scattering measurements is shown in Figure 2.1A and a representative SDS-PAGE is shown in Figure 2.1B. The molecular weight of the *Rs*TSPO-detergent complex was determined to be ~100 kDa from the scattering peak, with a protein fraction of ~36 % from comparison of scattering and 280 nm absorption; therefore, the molecular weight of *Rs*TSPO protein in the complex was calculated to be 37 kDa, indicating a dimer of *Rs*TSPO (given a monomer of 18 kDa) within the protein-detergent complex (Table 2.1). Purified ovalbumin and pure DM were also characterized under the same conditions. Ovalbumin showed a calculated molecular weight of ~44 kDa as a monomer and DM showed a

micelle size of ~37 kDa; both agreed very well with literature values, and are consistent with the

equivalent of approximately 2 micelles of DM in the dimer/detergent complex.
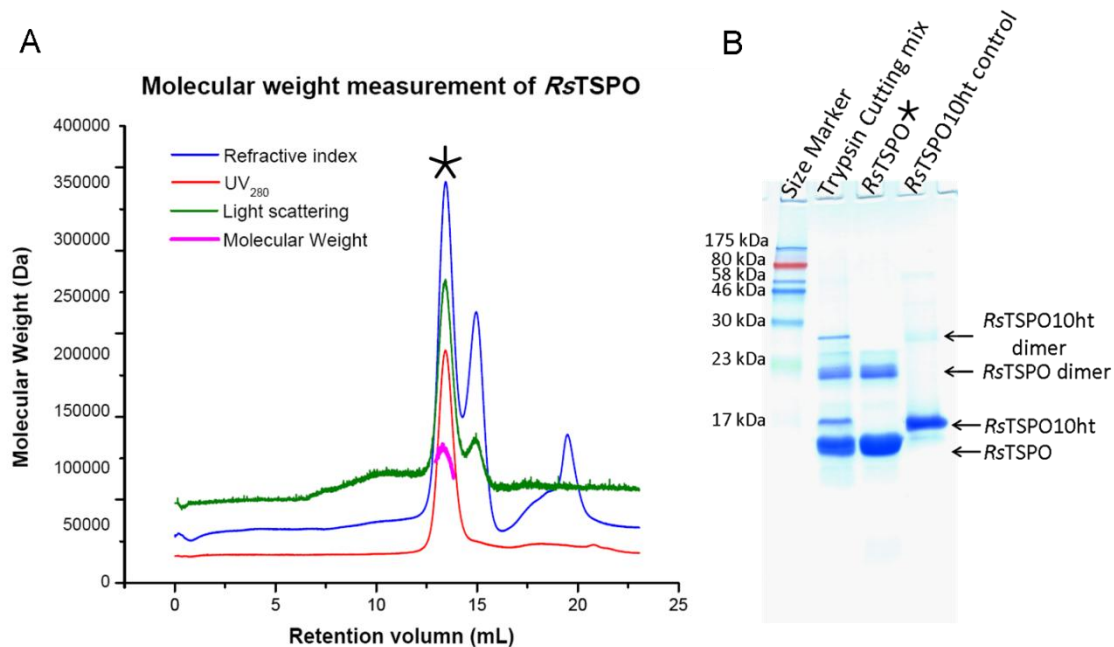
Figure 2.1. Purification and determination of the molecular weight of *Rs*TSPO.

(A) One representative trace of purified *Rs*TSPO on the triple detector array (Malvern ®). The peak of *Rs*TSPO is labeled with a star and the molecular weight was calculated as described and expressed on the Y axis. (B) SDS-PAGE for the purification of *Rs*TSPO. The lane of SEC-purified *Rs*TSPO is labeled with a star corresponding with the light scattering profile. The trypsin cutting mix represents the sample before SEC while a purified *Rs*TSPO10ht sample was use as the control.
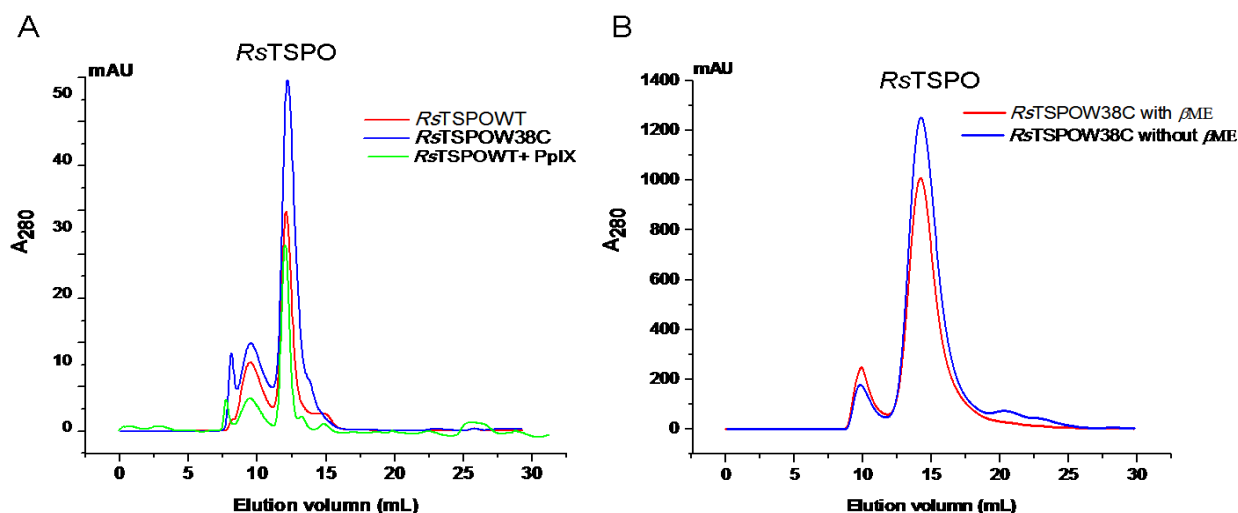
Figure 2.2. Investigation of the oligomeric state of purified RsTSPO by SEC.

(A) SEC profile of *Rs*TSPOWT, *Rs*TSPOW38C and *Rs*TSPOWT in the presence of 350 μM PpIX on a prepacked Superose® 12 300/10 column. (B) SEC profile of *Rs*TSPOW38C in the presence and absence of βME on a homemade Superose® 12 column.

Table 2.1. Molecular weight calculation from static light scattering measurement

Sample		$Mw_{complex}$	$f_{protein}$	$Mw_{protein}$	Monomer Mw_{Cal}	$N_{monomer}$
*Rs*TSPO	1st	98430	0.347	34155	17976	1.9
	2nd	104029	0.365	37971	17976	2.1
	3rd	97328	0.372	36206	17976	2.0
	4th	111620	0.362	40406	17976	2.2
	Ave.	102852	0.3615	37181	17976	2.1
Ovalbumin std		42757	0.982	41987	44287	0.95
DM std		37243	0	NA	NA	NA

Note: $Mw_{complex}$: molecular weight of the protein-detergent complex; $f_{protein}$: fraction of protein in the protein-detergent complex; $Mw_{protein}$: molecular weight of the protein without detergent; Mw_{cal}: molecular weight calculated from sequence; $N_{monomer}$: number of protein monomers in the protein-detergent complex.

The question of whether ligands influence the oligomeric state was investigated by incubating the *Rs*TSPO with the ligand PpIX prior to SEC. The SEC trace in the presence of PpIX showed the same size as that of the protein without ligand (Figure 2.2A). Since Yeliseev and Kaplan reported the W38C mutant to stabilize a dimer form in *R. sphaeroides* [34], a further question was whether a disulfide bond was involved in dimer formation, either through the W38C mutant or the naturally existent cysteine, C15, in the first transmembrane helix. There was in fact no apparent change in the amount or stability of the dimer form in the W38C mutant and no effect of addition of *ß*ME, as evidenced by no difference in the elution profile from SEC (Figure 2.2A, B). Therefore a disulfide bond is unlikely to be important in dimer formation.

These observations and the lack of detectable monomer form in SEC suggest that the dimer organization of *Rs*TSPO in the DM micelle is a very strong association, but through interactions other than disulfide bonds and independent of ligand binding. The persistence of a small fraction of dimer even in the SDS gels run under strongly denaturing conditions, also attests to the stability of the dimer.

We further explored the structure of the dimer *in vivo* by expressing in *E. coli* a dimer created by a gene fusion of two monomers. Three fusion proteins of *Rs*TSPO and *Hs*TSPO were constructed by making a direct connection between the C and N termini, resulting in a dimer with an anti-parallel configuration (Figure 2.3) as suggested to occur in the case of EmrE [56], a possible alternative to the parallel configuration supported by the cryo-EM and our modeling studies of TSPO (see below). *E. coli* cells carrying the gene fusion constructs were characterized by western blotting with antibodies against the histidine tag at the C-terminus of the fusion proteins. Our results show that the full length fusion proteins with *Rs*TSPO at the C-terminus and human or *Rhodobacter* at the N-terminus (*Hs-Rs*TSPO and *Rs-Rs*TSPO) were expressed (Figure

2.4) and inserted in the membrane without formation of a significant amount of inclusion bodies, implying a folded structure. In contrast, the dimer with the *Hs*TSPO portion at the C-terminus (*Rs-Hs*TSPO) was not detected, suggesting that this version of the fusion protein may not be correctly folded or inserted into the membrane.
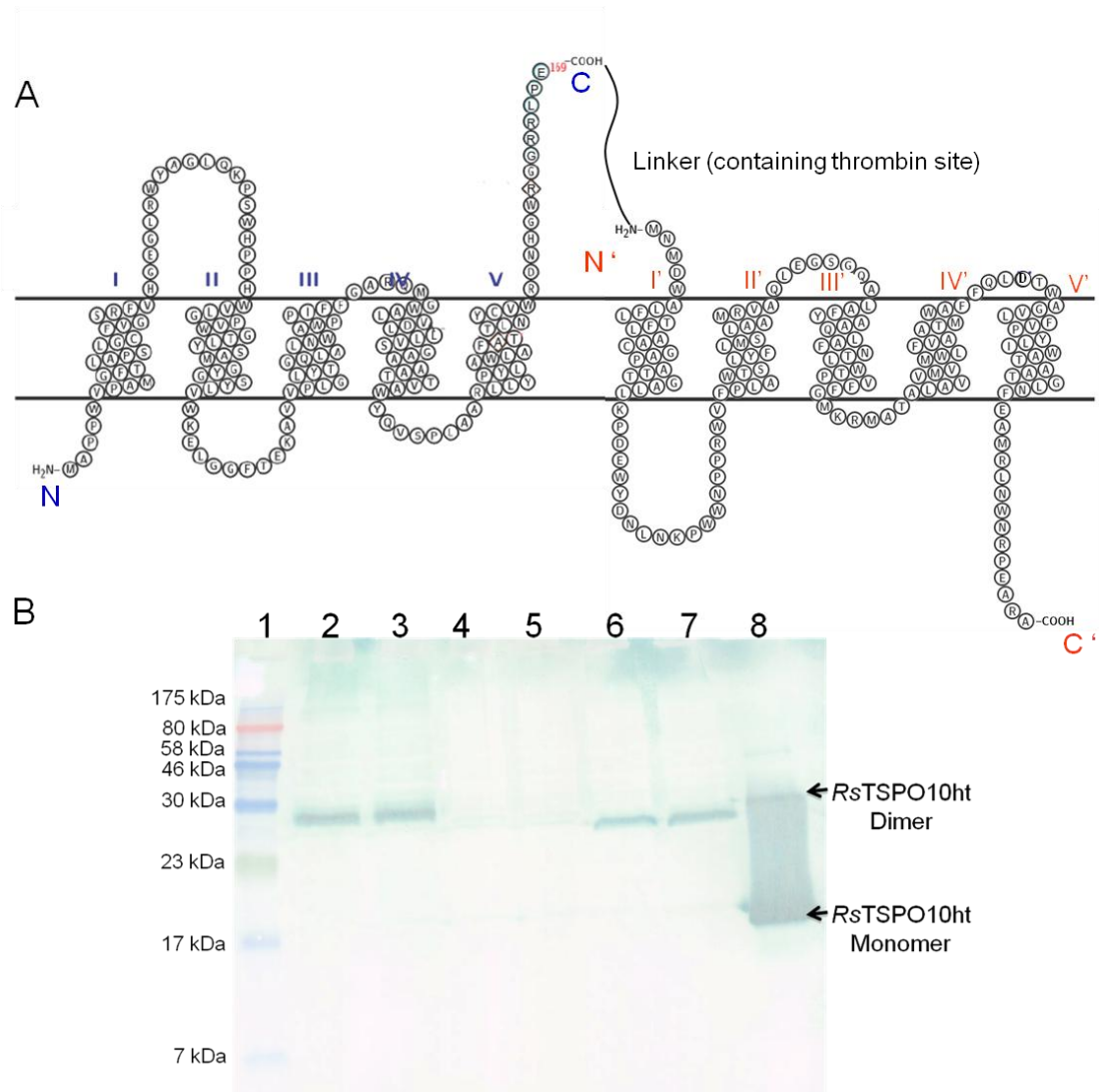
Figure 2.3. Expression of TSPO fusion proteins.

(A) Topology illustration of fusion proteins. All three fusion proteins have the same anti-parallel configuration. Shown in the figure is the *Hs-Rs*TSPO fusion construct, in which a thrombin site was placed in between the C-terminus of *Hs*TSPO and the N-terminus of the *Rs*TSPO. In the cases of *Rs-Hs*TSPO and *Rs-Rs*TSPO, the fusion proteins are constructed by directly connecting the C-terminus and the N-terminus. A 10-histag was constructed at the C-terminus of all the three fusion proteins. (B) Western blot of the whole cells expressing fusion proteins with antibodies against the C-terminal 10-histag. Lane 1: size marker; lane 2: *Hs-Rs*TSPO10ht after 7 hrs growth; lane 3: *Hs-Rs*TSPO10ht after 22 hrs growth; lane 4: *Rs-Hs*TSPO10ht after 7 hrs growth; lane 5: *Rs-Hs*TSPO10ht after 22 hrs growth; lane 6: *Rs-Rs*TSPO10ht after 7 hrs growth; lane 7: *Rs-Rs*TSPO10ht after 22 hrs growth; lane 8: positive control of purified *Rs*TSPO10ht. The fusion proteins were also found to be mainly in the membrane fraction of the fractionated cells, based on estimates from the yields of total membranes.

Although these results tell us little about the significance or existence of an anti-parallel dimer of TSPO, the observation that expression and insertion of the dimer depends on whether the *Rs* or *Hs* protein is at the C-terminal does suggest that membrane insertion of TSPO involves a C-terminal mechanism that may require additional machinery in the case of the mammalian protein, consistent with other evidence [57-59].

Overall, our studies are consistent with the dimer being the major structural unit of *Rs*TSPO as also implied by the cryo-EM studies of the purified *Rs*TSPO and our modeling analysis, which indicate a parallel dimer [46]. The possibility of an anti-parallel dimer and other homo- or hetero-oligomeric forms in the native membrane remain to be explored.

Tryptophan fluorescence quenching assay as a sensitive measure of K_d

We tested the validity of the tryptophan fluorescence quenching assay by measuring the binding of the known ligand, protoporphyrin IX (PpIX), to purified *Rs*TSPO (Figure 2.4). We determined a *Kd* for PpIX of 0.3 μM, lower than reported by Korkhov *et al.* [46] in a previous study (8.6 μM), possibly indicating the sensitivity of binding behavior to a variety of assay conditions (see discussion). The non-ligand porphyrin precursor δ-aminolevulinic acid (ALA) and the solvent DMSO were also measured and showed only a small quenching of the tryptophan fluorescence compared to PpIX, as did the steroid ursodeoxycholate (see below). A similar low micro-molar K_{app} for PpIX (2.4 μM) was also obtained with *Hs*TSPO (Figure 2.4), a result within the range of previous reports of PpIX binding affinity for mammalian TSPO [40,60]. (The presence of the contaminating protein GroEL, which has no tryptophan and does not contribute to the fluorescence [see Methods], may, however, give a somewhat higher binding constant for *Hs*TSPO due to ligand depletion.)
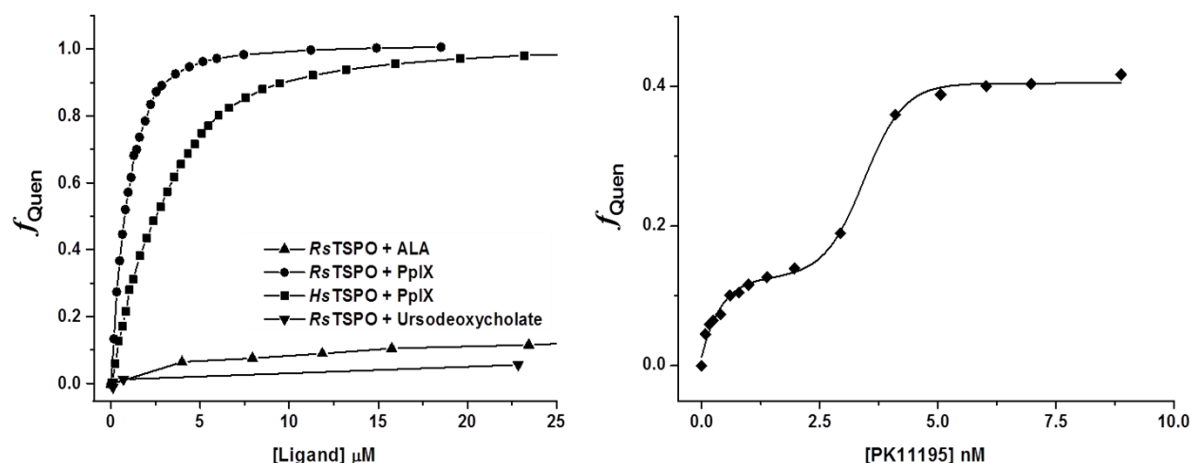
Figure 2.4. Binding of PpIX, ALA, and ursodeoxycholate to *Rs*TSPO and PK11195, PpIX to *Hs*TSPO.

(A) Binding curve of PpIX, ALA, and ursodeoxycholate to purified *Rs*TSPO and PpIX to partial purified *Hs*TSPO measured with tryptophan fluorescence quenching assay. (B) Binding curve of PK11195 to partially purified *Hs*TSPO.
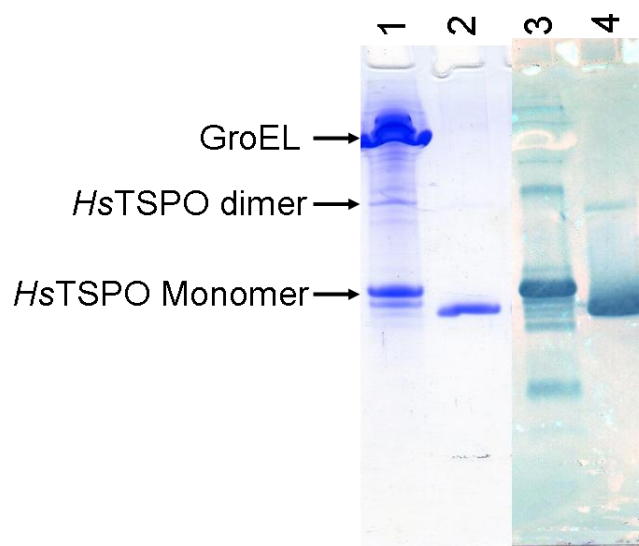
Figure 2.5. Purification of *Hs*TSPO.

Lane 1: Coomassie stain of purified *Hs*TSPO; lane 2: Coomassie stain of purified *Rs*TSPO as control; lane 3: western blot against histag of purified *Hs*TSPO; lane 4: western blot against histag of purified *Rs*TSPO as control.

We also tested the sensitivity of the assay by measuring the binding of HsTSPO to the diagnostic ligand PK11195 with expected binding affinity in the nano-molar range. Our measurements show two K_{app} of ~ 0.2 nM and 5 nM for PK11195 (Figure 2.4B), which agree with previous reports [35] and two different nano-molar binding affinities for PK11195 in both mouse liver [8] and a human Leydig cell line [61]. The results demonstrate the capability of the assay to characterize high-affinity binding.

Effect of detergent conditions on the binding assay

It was also important to find detergent conditions that maintained a stable protein and were compatible with the assay. The nano-molar binding affinity of PK11195 for HsTSPO (Figure 2.5B) was measured in 0.2 % DM. However, a previous report suggested that binding of PK11195 with mouse TSPO in the detergent SDS resulted in complete loss of affinity, emphasizing the importance of detergent conditions [39]. We tested the binding of PK11195 with RsTSPO in two different concentrations of DM, as well as in the common detergent used in NMR, Fos-Choline-12 (Figure 2.6). In 0.1 % DM, the binding affinity of purified RsTSPO for PK11195 was slightly increased compared to 0.2 % DM (7 μM vs 10 μM, respectively), while Fos-Choline-12 lowered the affinity to ~ 120 μM. Therefore, for standard assay conditions for ligand comparisons, 0.2 % DM was selected to keep purified RsTSPO stable while exhibiting good affinity for PK11195. (0.1 % DM is just below the critical micelle concentration (CMC) of DM and has a tendency to allow protein precipitation over time).
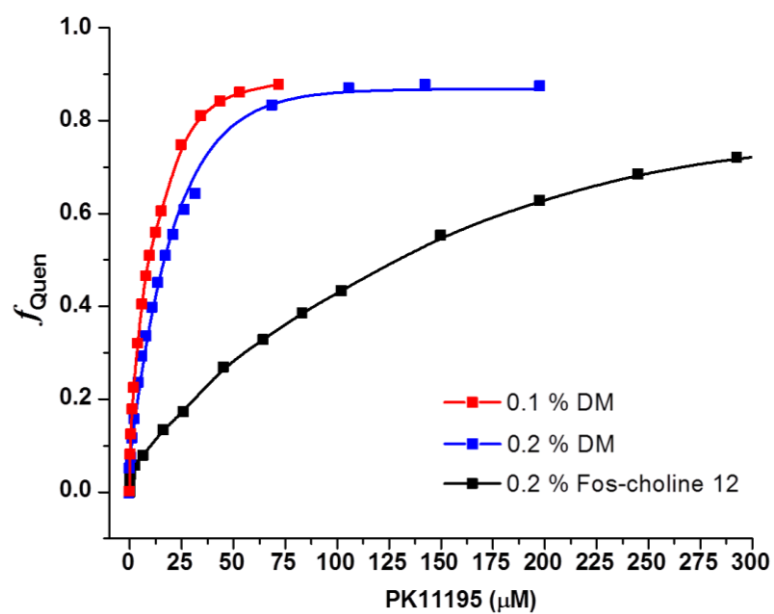
Figure 2.6. Binding curves of PK11195 with *Rs*TSPO in different detergent conditions as described in Methods.

_Rs_TSPO binds PK11195 and cholesterol at micro-molar affinity

In the pioneering study in 1997 [32], Yeliseev and colleagues reported that rat TSPO overexpressed in _Rhodobacter sphaeroides_ 2.4.1 displayed an affinity for PK11195 ranging from 4-12 nM, while the wild-type _Rs_TSPO showed no binding affinity above background. However, in our studies with purified _Rs_TSPO, the binding affinity of PK11195 was found to be 10 ± 1 μM, suggesting a binding site in _Rs_TSPO with lower but significant affinity compared to the mammalian proteins (Figure 2.7 and Table 2.2). In addition, the _Rs_TSPO form containing a W38C mutation located in the middle of loop 1 where both PpIX and PK11195 are proposed to bind [34,35] decreased the binding affinity of PK11195 by 3-fold. These results indicate that loop 1 contributes to PK11195 binding. PpIX binding to _Rs_TSPO was also influenced by the W38C mutation (Figure 2.7 and Table 2.2), showing a 6-fold decrease in affinity (2 μM _vs_ 0.3 μM), consistent with both binding sites involving W38C in the conserved region of loop 1. Although it is suggested PK11195 and PpIX bind in the same general area (loop 1) in both _Rs_TSPO and _Hs_TSPO, it should be noted that loop 1 is predicted to be flexible and shorter in _Rs_TSPO than in _Hs_TSPO, and the corresponding residue of W38 in _Hs_TSPO is S41. These differences would be expected to impact the affinity and specificity of ligand binding.
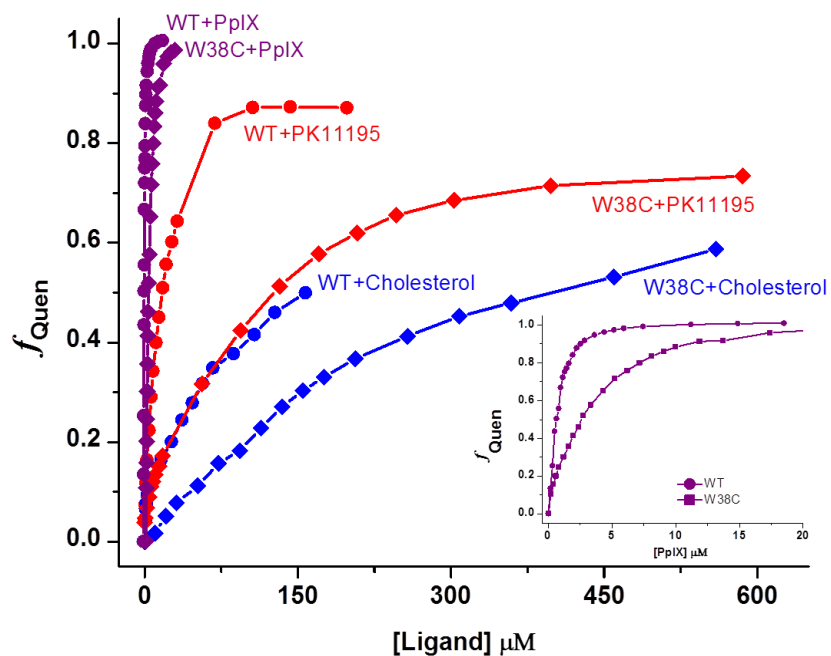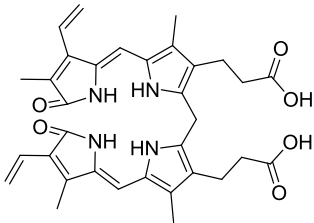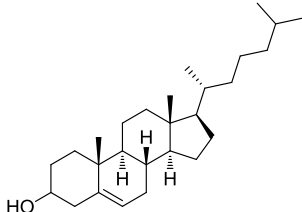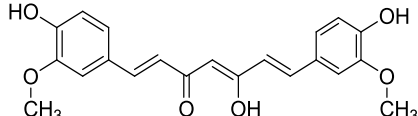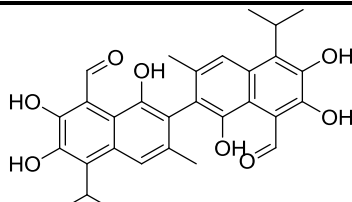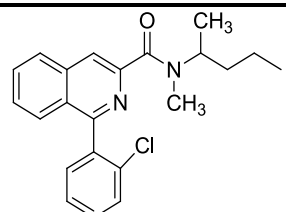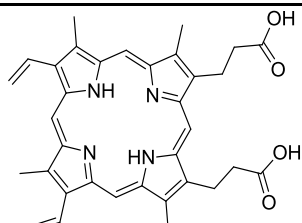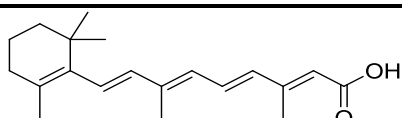
Figure 2.7. Binding of PpIX, PK11195 and cholesterol to purified *Rs*TSPO (WT) and *Rs*TSPOW38C (W38C).

All binding curves were obtained and plotted as described in the Methods. The inset shows a blow-up of the 0-20 μM region to better show the binding curve of the PpIX.

Table 2.2. Structure and K_d of ligands to RsTSPOWTand W38C mutant

ligands	Structure	K_d to RsTSPO (µM)	K_d to RsTSPOW38C (µM)
Bilirubin		4.7 ± 0.2	5.5 ± 0.3
Cholesterol		$K_{app} = 80$ [1]	$K_{app} = 200$ [1]
Curcumin		1.4 ± 0.1	2.6 ± 0.1
Gossypol		6.0 ± 0.2	3.9 ± 0.3
PK11195		10 ± 1	34 ± 2
Protoporphyrin IX (PpIX)		0.31 ± 0.01	2.0 ± 0.07
Retinoic acid		0.50 ± 0.02	1.6 ± 0.1

Note: 1: K_{app} is estimated from half-maximal quenching

2: Kd is obtained from fitting 3 independent titrations with equation (1) and standard error is reported.

Since cholesterol does not naturally occur in *Rhodobacter*, no data has been reported on its binding to *Rs*TSPO. However, *Rhodobacter* is one of the closest ancestors of mitochondria [28] and in fact has structural and functional analogs of cholesterol, hopanoids [37], in the membrane where *Rs*TSPO is located. In addition, the TSPO sequence alignment (Figure 1.6) shows a remarkably high similarity at the proposed cholesterol binding site (CRAC: -L/V-$(X)_{(1-5)}$-Y-$(X)_{(1-5)}$-R/K-) [36,62] across many species. In particular, 2 out of the 3 proposed critical residues in the CRAC sequence (Leu and Arg) are identical between *Rs*TSPO and *Hs*TSPO while the other is a conservative substitution of phenylalanine for tyrosine. Therefore, we expected that *Rs*TSPO might also bind cholesterol. Due to the low solubility of cholesterol in aqueous solution, we were unable to determine an accurate K_d, but we estimate from the binding curve a K_{app} of ~ 80 μM to *Rs*TSPO wild-type and ~ 200 μM for the W38C mutant (Figure 2.7), significantly lower affinity than reported for mammalian TSPO [27], possibly due to the variable region immediately preceding the CRAC sequence in helix V (residues 144-147) including the site of a human polymorphism [38,63]. In contrast, the steroid derivative ursodeoxycholate showed no detectable affinity for *Rs*TSPO (Figure 2.5A), suggesting that the binding of cholesterol, albeit low, is not just due to non-specific interactions.

Competition binding assay of PpIX, PK11195 and cholesterol

Loop 1 in the N terminal region has been proposed to be where drugs and porphyrin bind [27,64], while the cholesterol CRAC site is located at the C-terminal region of TSPO [36]. However, the small size of TSPO and the fact that it may function as dimer or higher oligomer introduces the possibility that these two sites are very close to each other and interacting. Nevertheless, in the case of PpIX and PK11195, we observe some difference in spectroscopic properties in the binding assay. The tryptophan fluorescence of *Rs*TSPO and *Hs*TSPO shows a

broad spectrum from 290 nm to 400 nm with a peak around 340 nm. PpIX quenches the tryptophan fluorescence evenly at all wavelengths and shows a maximum quenching close to 100 % (Figure 2.8 A, B). This indicates that the local environment of almost all tryptophans that contribute to the total tryptophan fluorescence for *Rs*TSPO is influenced by the binding of PpIX. In contrast, PK11195 quenches the fluorescence of *Rs*TSPO from 290 nm to 335 nm completely but not in the region of 330-340 nm (Figure 2.8C). This behavior suggests that PK11195 is interacting with a slightly different subset of the tryptophans compared to PpIX, implying some differences in their binding sites in the case of *Rs*TSPO.
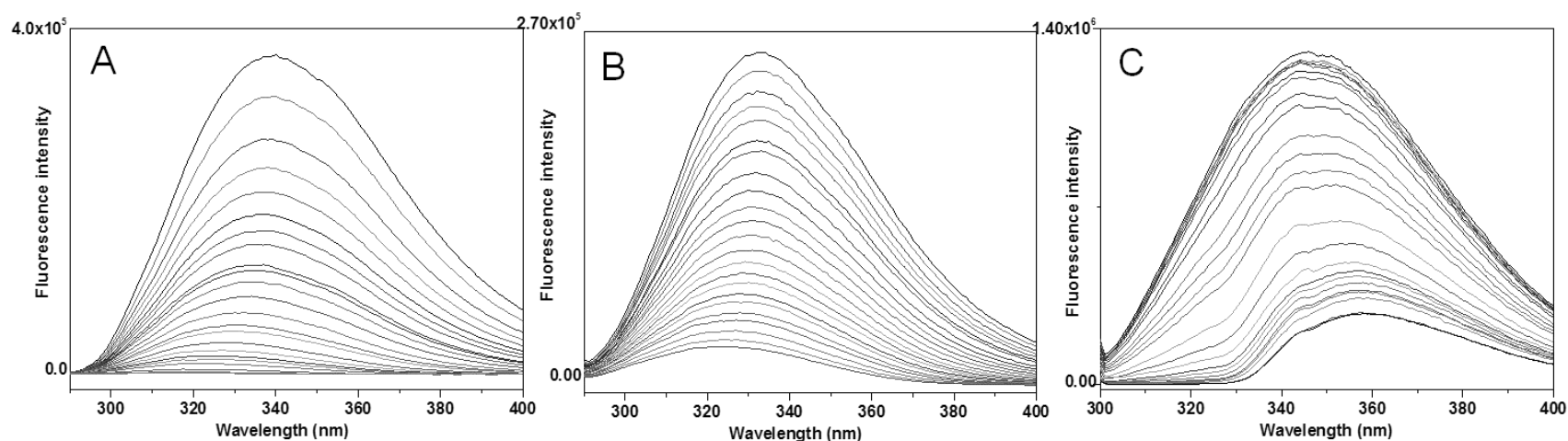
Figure 2.8. Tryptophan fluorescence quenching behavior of PpIX and PK11195.

Tryptophan fluorescence spectra of (A) *Rs*TSPO when binding with PpIX in 0.2 % DM; (B) *Hs*TSPO when binding with PpIX in 0.2 % DM; (C) *Rs*TSPO when binding with PK11195 in 0.2 % Fos-Choline-12. (PK11195 titration experiments done in 0.2 % DM show the same spectral behavior as the experiment shown, done in 0.2% Fos-Choline-12).

To further investigate possible overlap between the binding sites, competition binding assays were performed between PpIX, PK11195 and cholesterol (Figure 2.10). Purified RsTSPO was pre-incubated with either 50 μM cholesterol or 20 μM PK11195 or both on ice before the binding experiment.

The binding behavior of PpIX was somewhat affected by the presence of cholesterol, giving a K_d increase of 2-3 fold, suggesting some influence of cholesterol on the PpIX binding site. Interestingly, the presence of PK11195 caused a similar change in the binding of PpIX, ~ 3 fold increase in K_d, and PK11195 and cholesterol together had a greater effect of ~4 fold increase in K_d. This behavior (Figure 2.9) suggests that PK11195 and PpIX binding sites are interacting and that cholesterol is also altering the PpIX binding in manner that is somewhat additive with PK11195, consistent with partial overlap or allosteric effects of ligand binding at different sites.
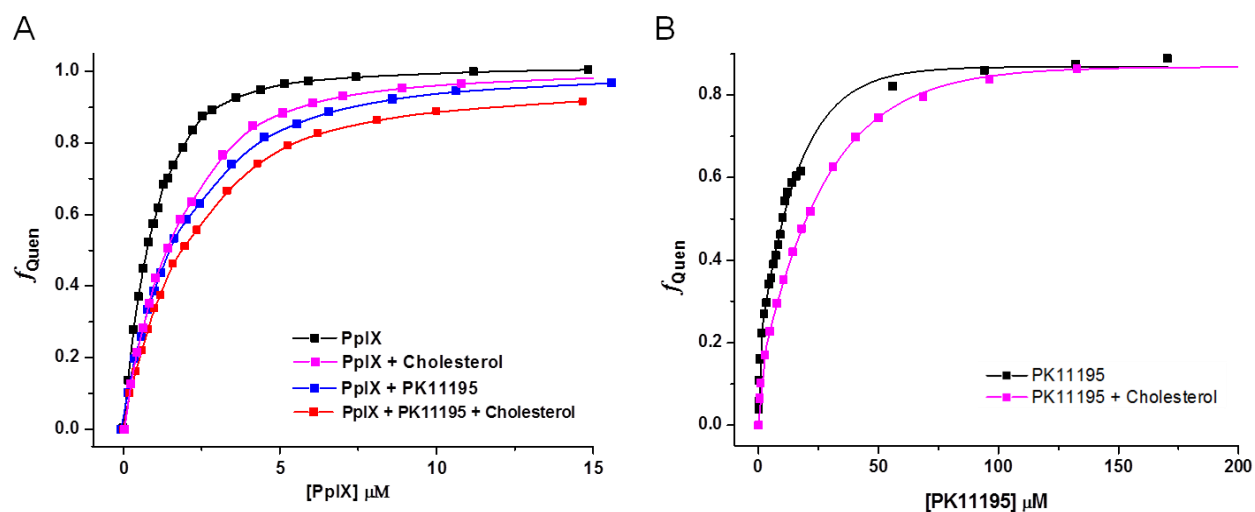
Figure 2.9. Competition binding studies between PpIX, PK11195 and cholesterol to *Rs*TSPO.

Experiments are done as described in Methods. (A) Competition between PpIX and cholesterol (preincubated at 50 µM cholesterol) and PK11195 (preincubated at 20 µM PK11195) as well as PK11195 plus cholesterol (preincubated with both). (B) Competition between PK11195 and cholesterol (preincubated at 50 µM cholesterol).

Compounds affecting apoptosis bind to *Rs*TSPO at micro-molar affinity

Besides the TSPO ligands PK11195, benzodiazepines, and PpIX, which all have been reported to either induce or prevent apoptosis [27], other compounds have been reported to affect apoptosis in human cell lines, but their targets are not well defined. In *R. sphaeroides,* TSPO is reported to facilitate the transport of intermediates of heme and carotenoid biosynthesis/breakdown pathways through the outer membrane [31,33,34]. Interestingly, in mammals the porphyrin breakdown product bilirubin and some carotenoid homologs (retinoids) have also been reported to induce apoptosis through the mitochondrial pathway [65-67]. These and other compounds reported to have effects on MPTP and apoptosis, including curcumin [68] and gossypol [69], were selected to test for their binding affinity to *Rs*TSPO. Binding studies with both wild-type and the W38C mutant show that several of these compounds bind to purified *Rs*TSPO at low micro-molar affinity similar to PpIX (Figure 2.10 and Table 2.2), which is suggestive that some of these apoptosis-inducing agents could function through direct interaction with TSPO.
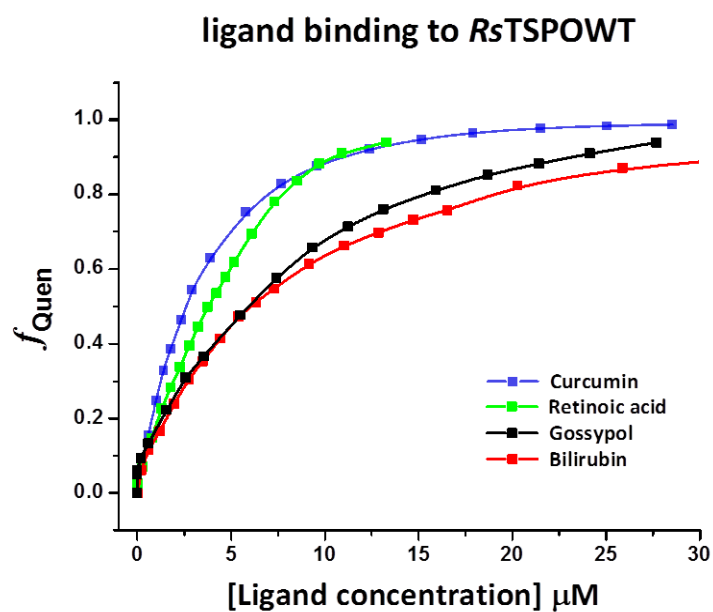
Figure 2.10. Binding curves of compounds affecting apoptosis: curcumin, retinoic acid, gossypol, and bilirubin

Models of the _Rs_TSPO dimer

The structural model of the _Rs_TSPO dimer was constructed using EM-Fold and Rosetta guided by the 10Å cryo-EM density map of _Rs_TSPO [46]. The two best-scoring models that were energetically more favorable (Figure 2.11) are displayed in Figure 2.12. The five next best-scoring topologies are provided in Figure 2.13 for comparison. At 10 Å resolution in the cryo-EM, the connectivity between trans-membrane helices was not resolved. The objective of the modeling study was to complete the model and use the Rosetta energy function to identify the global energy minimum, thereby adding atomic detail not visible in the experimental data. The seven topologies shown are energetically significantly more favorable than all alternative topologies (Figure 2.11). The two best scoring topologies have a significant energy gap of 28 to the best scoring model of an alternative topology. Therefore, we consider these two topologies as most likely for _Rs_TSPO.

Rosetta energy score of the top 20 topological fold
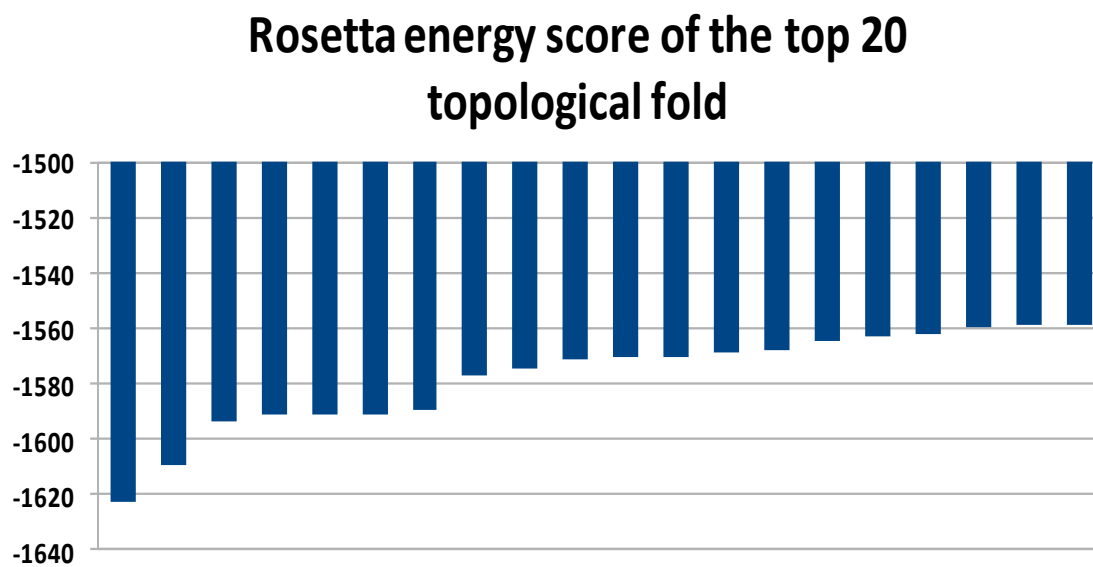
Figure 2.11. Rosetta energy score shows that the top 7 models are significantly better than the rest.
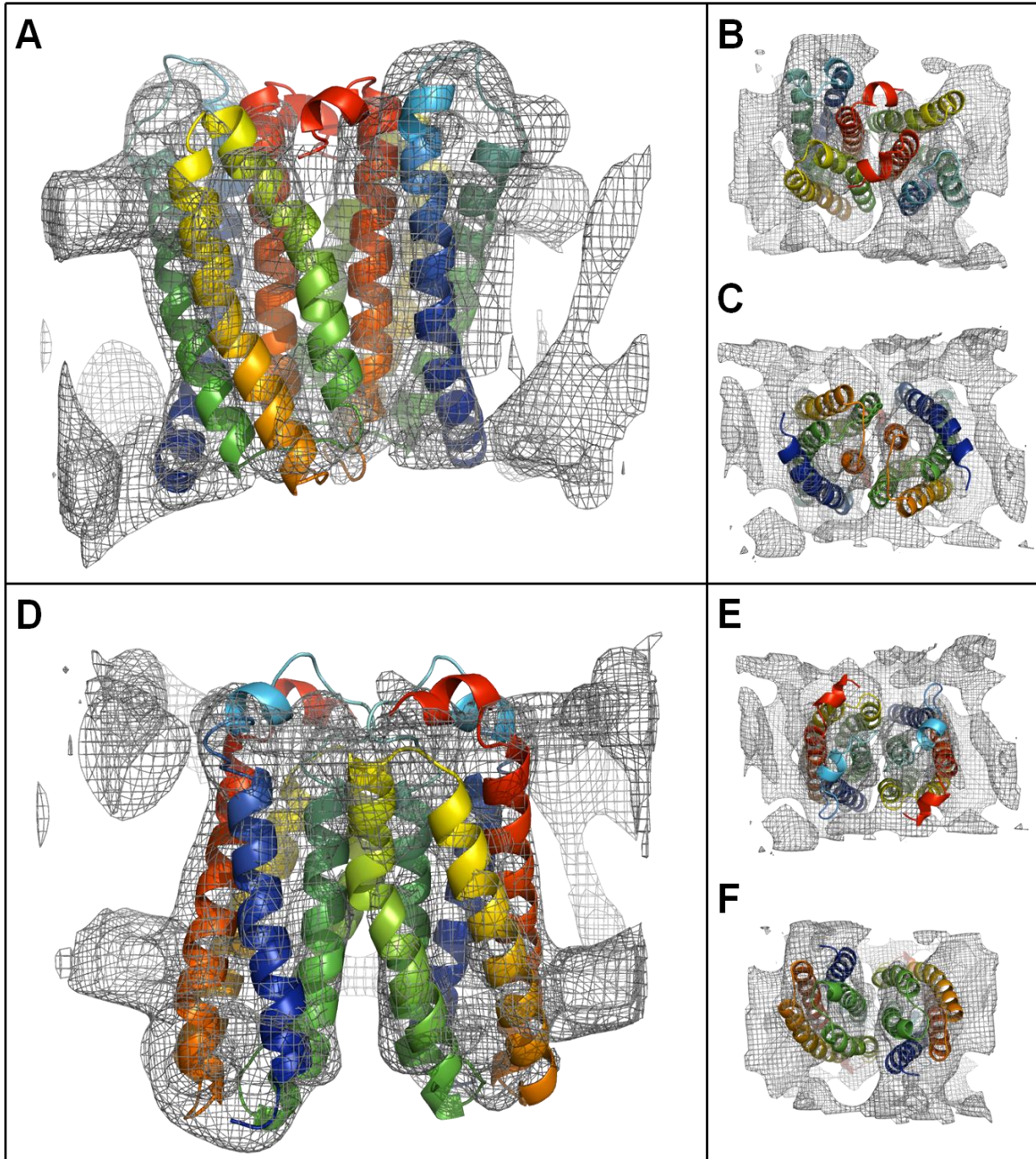
Figure 2.12. Top two models of a *Rs*TSPO dimer.

Model 1: (A) Side view, (B) top view, (C) bottom view. Model 2: (D) Side view, (E) top view, (F) bottom view. Electron density from the EM structure was contoured at 1.5 σ. Each monomer is colored with rainbow colors from blue to red corresponding to the N terminus to C terminus.
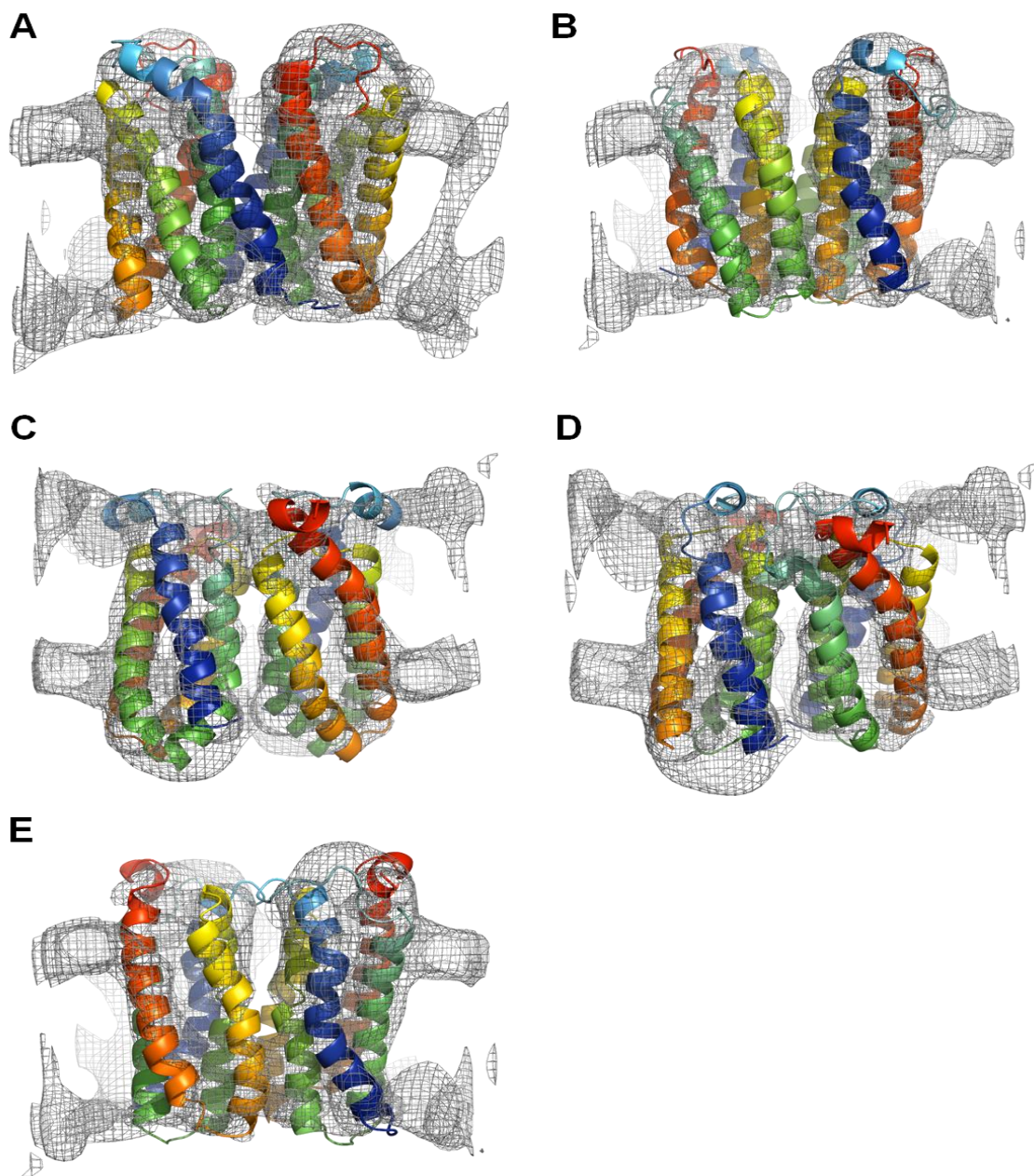
Figure 2.13. Top 3-5 scoring models of *Rs*TSPO dimer.
Models are displayed as rainbow diagram in order of ranking score. (A) Model 3, (B) Model 4, (C) Model 5, (D) Model 6, (E) Model 7.

Some common features are observed in the two top scoring models although the two *Rs*TSPO monomers are placed in opposite orientations within the EM density and have a different dimer interface (Figure 2.12). Both models place helix I and helix V close to each other, consistent with previous mutagenesis data [35]. In addition, helix I and helix II are on the same face, providing the possibility of helices I and II playing a role in substrate binding and transport together (see Discussion for details). The main differences are: 1) model 1 placed helix V in the dimer interface while the dimer interface in model 2 is composed of helices I, II and III; 2) model 1 has a relatively shorter loop 1 and a portion of predicted loop 1 forms a short helix that contributes to part of the transmembrane region, as compared to model 2. However, ligand binding at loop 1 is very likely to change the structure of this flexible region. Considering that TSPO has been reported to form higher oligomers [61], we fit the dimer into the larger density of the *Rs*TSPO helical crystal (Figure 2.14) and found an additional (though less strong) dimer interface mediated by helices I and II in model 1, as well as an additional dimer interface mediated by helices I and V in model 2. We have focused our binding analysis on model 2, which portrays helices I and II as being at the dimer interface while helix V is at the outside, leaving open the possibility of helix V interacting with another monomer, as suggested in Figure 2.14, or a partner protein for cholesterol translocation, as suggested by Papadopoulos *et al.* [57].
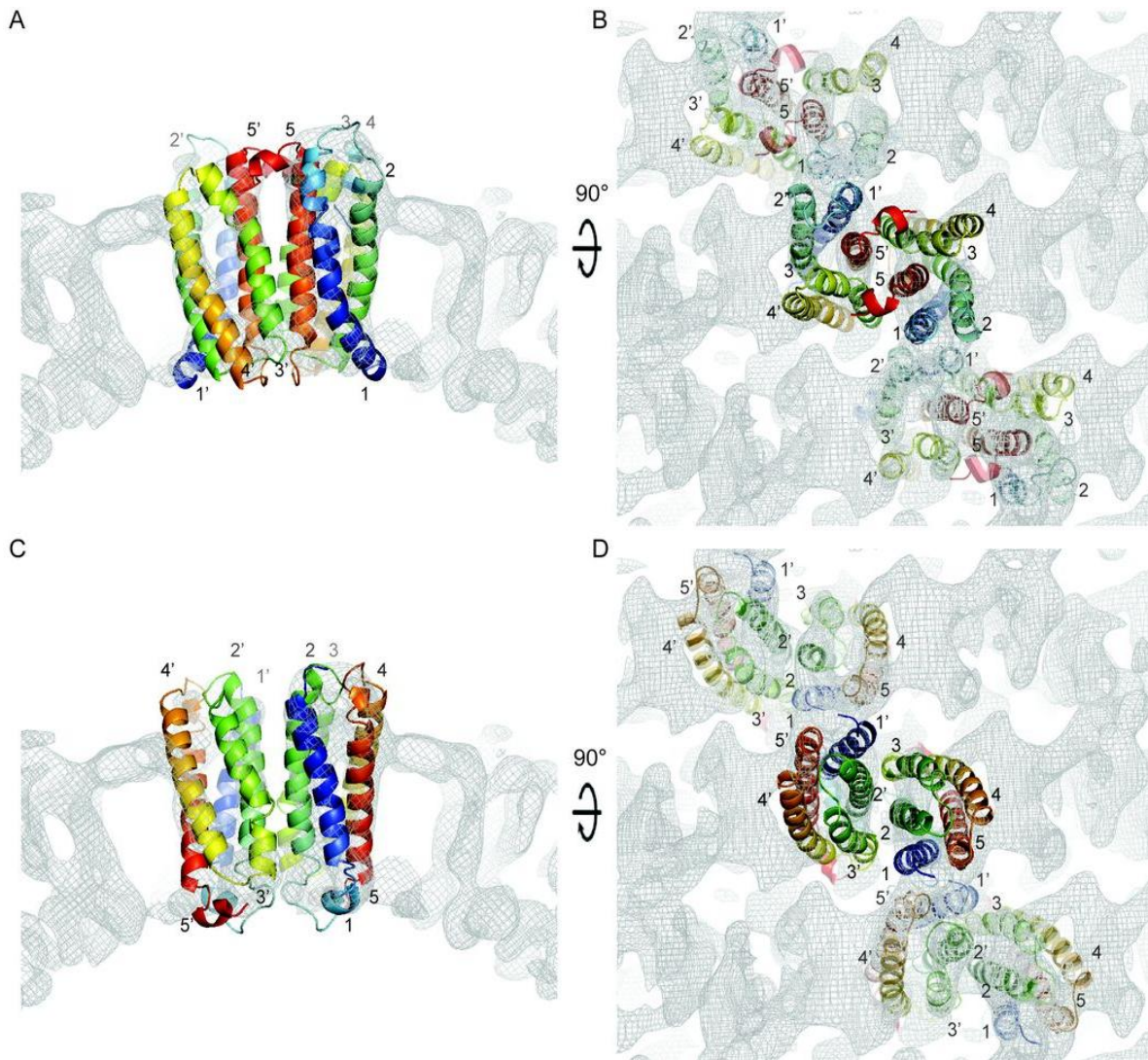
Figure 2.14. Oligomerization of *Rs*TSPO.

Models of *Rs*TSPO dimers were placed into the extended cryo EM electron density of the helical polymer crystal. (A) and (B): model 1; (C) and (D): model 2.

DISCUSSION

The ability of TSPO to bind to various ligands has been extensively investigated over the past 30 years, providing important information that has led to our current understanding of the function of TSPO. However, previous studies show significant variation in the binding properties of TSPO when measured in different cell lines or tissues or purified forms. It has also been suggested that TSPO functions *in vivo* as an oligomer [61], but details of the oligomerization and conditions that foster it are difficult to establish. To address these and other issues, we purified the homolog of human TSPO from *R. sphaeroides* and characterized the oligomeric state and binding behavior in a well-defined system. The bacterial protein *Rs*TSPO is important in itself, given its role in photosynthetic gene regulation and membrane transport in bacteria. The conserved aspects of sequence, along with some differences in ligand binding between the mammalian and *R. sphaeroides* proteins, provide opportunities to identify the potential determinants for the ligand interactions. In this study, we confirm that *Rs*TSPO forms a dimer *in vitro* and present models with atomic detail for the dimer form. Using one of these models, options for PpIX, PK11195 and cholesterol interaction sites are proposed. The binding behavior of other physiologically important ligands provides some new hints of the mechanism of potential regulation of MPTP by TSPO.

Evidence relating to the role of the dimer

In this work, we characterized the minimum <u>structural</u> unit of purified *Rs*TSPO as a dimer. It is reasonable to postulate that the minimum <u>functional</u> unit of *Rs*TSPO is also a dimer, considering several lines of evidence.

Because TSPO was first discovered and is best known as a receptor, the drug binding properties and the physiological effects of drug-related ligands were initially extensively

investigated. However, evidence has been obtained in both mammalian and *Rhodobacter* systems that TSPO also transports molecules including both cholesterol and the metabolites of heme and photosynthesis pathways [6,34,62]. It is reasonable to propose a monomer form of TSPO functions as a receptor, but given the small size of the protein, it is more difficult to postulate a mechanism for a monomer to transport either cholesterol or the heme/carotenoid metabolic intermediates. Yeliseev and Kaplan proposed that *Rs*TSPO forms a dimer *in vivo* and this dimer was stabilized by the W38C mutation [34]. Porphyrin has been reported to induce dimerization [34], although in our hands the already dimeric state of *Rs*TSPO was not influenced by the addition of PpIX. In our studies, no monomer form was ever observed under non-denaturing conditions during chromatography with or without βME, while a trace of dimer remained even under the strong denaturing conditions of urea/SDS-PAGE. In addition, the W38C mutant behaved very similarly to the wild-type in terms of dimer state, suggesting that *Rs*TSPO naturally forms a dimer by strong associations other than disulfide bonding. Similarly, the *E. coli* drug transporter EmrE [70] forms a dimer in the purified state that is uninfluenced by ligand binding. Biochemical and NMR data also show that EmrE can transport substrate as a dimer *in vivo* [71] and *in vitro* [72], while structural studies show a ligand at the dimer interface. In fact, a significant number of transporters function as dimers and/or show two-fold symmetry with substrate binding at the dimer or domain interface in the crystal structures [73,74], suggesting a common mechanism for substrate transport that could also apply to TSPO.

In view of the case of EmrE, which shows that a membrane protein can be inserted with dual topology [56] and given the apparently successful expression of our forced anti-parallel dimers, we considered the possibility that TSPO might also function as an anti-parallel structure to create a "5+5 inverted repeat" topology as reported in several cases [73,75]. Studies (reviewed

by Bowie [76]) suggest that rearrangement of the orientation of helices is possible as well as necessary in several cases for both large and small membrane proteins. However, the best cryo-EM and modeling evidence available so far indicates a parallel dimer, as modeled in this paper.

Taken together, our data as well as other studies indicate that *Rs*TSPO functions as a dimer, which is likely to be important for transporting substrates across the membrane. On the other hand, current models regarding the effect of drugs generally agree with the 1:1 drug to monomer ratio, suggesting that TSPO could perform receptor and transporter functions in different oligomer and hetero–oligomer states.

Effect of detergent on the structure and binding of *Rs*TSPO

Detergents play a critical role in the study of membrane proteins, allowing their characterization in a purified state. However, these artificial lipid-mimicking molecules may influence the binding of hydrophobic ligands, as observed in the case of a steroid binding site in cytochrome *c* oxidase where a systematic analysis of detergent effects led to a clearer understanding of competitive behavior between ligands and detergents and a more precise definition of the binding domain [77,78].

In this study, we also observed the influence of detergent upon the binding of ligands to purified *Rs*TSPO (Figure 2.6). Lacapere *et al.* [27] had previously reported that recombinant mouse TSPO lost its binding to PK11195 when purified with SDS as detergent but regained the binding ability when reconstituted into liposomes. In their hands, the binding of cholesterol was less influenced than the binding of PK11195 by SDS. In our studies, when a non-ionic detergent DM is used, a higher affinity PK11195 binding site appears to be maintained, as compared to using the charged detergents Fos-Choline-12 and SDS. Our observations are consistent with the

model that the PK11195 binding site involves the flexible extra-membrane loop 1 and the membrane interface where detergent/lipid head groups may have an impact, while cholesterol bound at the more deeply buried CRAC site on helix V may be less impacted by the detergent.

Using the TSPO dimer model to predict the binding sites for PpIX, cholesterol, and PK11195

Although we have demonstrated binding of both PK11195 and cholesterol to purified *Rs*TSPO, it is still a question as to what structural features result in an affinity for both ligands that is several orders of magnitudes lower than in mammalian TSPO. To attempt to obtain new insight into possible ligand interactions, models of *Rs*TSPO in the dimer form were generated (Figure 2.12). The top ranked candidate structures were compared and one (Model 2) was used to facilitate an interpretation of the binding behaviors of PpIX, cholesterol, and PK11195 to *Rs*TSPO.

Our preliminary competition binding studies (Figure 2.9) give evidence of some level of interaction between all three binding sites. The effects of PK11195 and cholesterol on the affinity of *Rs*TSPO for PpIX are almost additive, while the binding of PK11195 itself is less influenced by cholesterol. These results are consistent with PK11195 and PpIX interacting at somewhat different positions on the extra-membrane loop 1, and cholesterol acting at helix V of the C-terminus, with some allosteric influence on both.

We propose that PpIX, as one of the potential endogenous transport substrates of TSPO, binds initially at loop 1, en route to transport *via* the dimer interface, as illustrated in Figure 2.15. Previous *in vivo* studies, in particular mutation of residues W30, K36, W38, and W39 in *Rs*TSPO [34], as well as our data, show that loop 1 plays a critical role in the binding and export of porphyrins. However, loop 1 is not likely to be the only contributor to the binding of PpIX. The

observation that the tryptophan fluorescence was completely quenched by PpIX but not by PK11195 and other ligands binding (Figure 2.8) suggests that either PpIX interacts with a rather large area or induces a global conformational change, both of which are possible if PpIX is binding and being transported through the dimer interface. Initial PpIX binding at loop 1 is consistent with our observation that the W38C mutant reduced the affinity of PpIX for *Rs*TSPO by ~ 6 fold, while aromatic residues on transmembrane helix II, including highly conserved W44 and W50, also appear to play an important role in PpIX binding and transport, as evidenced by lower porphyrin export activity in phenylalanine mutants of both residues [34]. Our model (Figure 2.15) is consistent with helix II being a major part of the dimer interface where W44 and W50 are in the region of potential close interaction with PpIX.
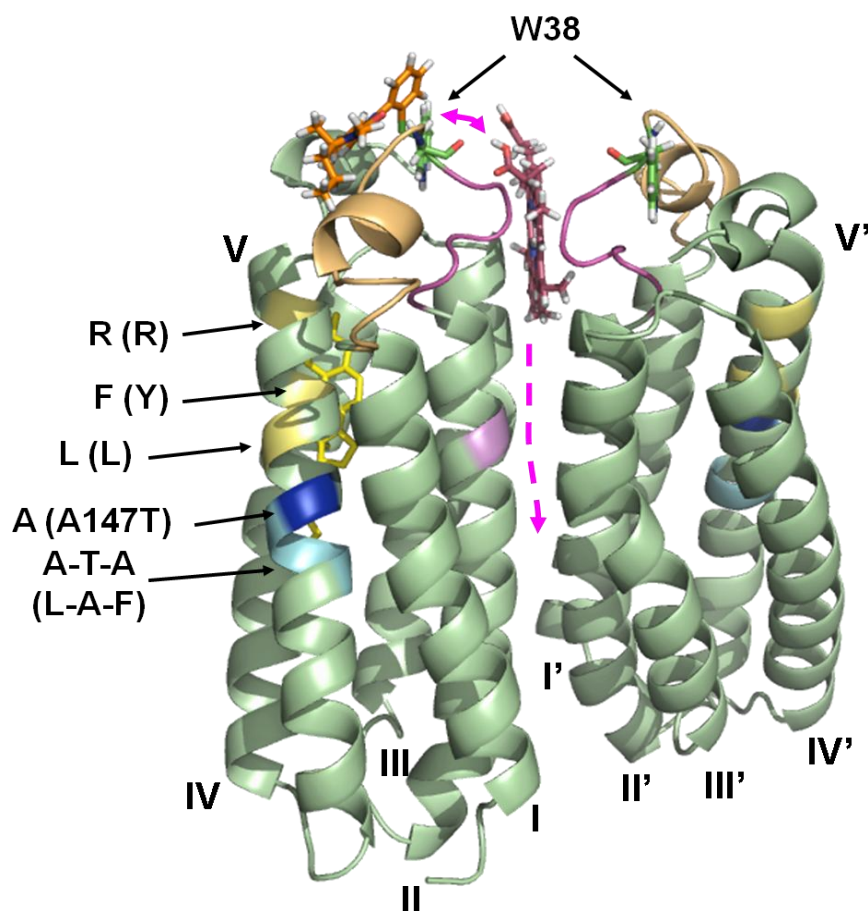
Figure 2.15. Proposed model of binding sites of PpIX, PK11195 and cholesterol on *Rs*TSPO.

Structures of PK11195 and PpIX were generated in ChemDraw ® 3D and cholesterol was taken from a published structure (PDB# 3D4S). Note that the computational model of *Rs*TSPO (Model 2) is generated based on EM density observed in a sample without ligand. Therefore, these models may represent a closed conformation, as indicated by close association of the monomers. Ligands are manually placed into the model of *Rs*TSPO on one monomer, for illustration of proposed locations. Helices are labeled with Roman numerals. W38 (green sticks); PK11195 (orange sticks); PpIX (dark purple sticks); cholesterol (yellow sticks). Highly conserved residues in the CRAC site are colored in light yellow and labeled according to the *Rhodobacter* sequence. Corresponding residues in the human sequence are shown in parentheses. Human polymorphism residue A139 (*Rs* number) is colored in dark blue, while the preceding Ala-Thr-Ala sequence is colored in cyan. The sequence in loop 1, before W38, that is proposed to play a role in PK11195 binding is colored in light orange corresponding to the ligand. The proposed PpIX binding sequence on loop 1 (including W44) is colored in light purple and the residue W50 on helix II is colored in pink. A loading and transport route for PpIX is indicated by a magenta dotted line, illustrating the potential role of the dimer in transport, which would require flexibility of the external loops.

Although PK11195 was also proposed to bind to TSPO at loop 1 and has been reported to compete with PpIX binding [40], the tryptophan quenching behavior suggests that PK11195 and PpIX do not bind in precisely the same location (Figure 2.8). As mentioned above, the last 2/3 of the loop 1 is highly conserved across all species, with conserved residues that play critical roles for PpIX binding, while the sequence in the first 1/3 is not. Thus the much lower binding affinity of PK11195 for RsTSPO compared to HsTSPO could be due in part to differences in the early part of loop 1. However, some overlap between PK11195 and PpIX binding is suggested by competition studies and the fact that the K_d of both PK11195 and PpIX were markedly reduced by the W38C mutant. Based on these independent lines of evidence, here we propose that PK11195 interacts mainly on the first half of loop 1 within the monomer, extending to residue W38 (S41 in human), and also harnesses some of the structural features of the helix I/membrane interface and the second half of loop 1 that binds the hydrophobic porphyrins. This interpretation is consistent with the observation that RsTSPO binds both PK11195 and PpIX at micro-molar affinity (Figure 2.6), while HsTSPO has nano-molar affinity for PK11195 but has similar affinity as RsTSPO for PpIX (Figure 2.6) [40]. Nevertheless, given the flexible nature of the loop, a high resolution structure with ligand bound will be essential to understand the details of the binding mechanisms.

In this study, we show that cholesterol does bind to purified RsTSPO but only with low affinity in the high micro-molar range. We note that the helix V and the C-terminus, where the CRAC sequence is located, is perhaps the most conserved region in the whole protein. However, the region right before the CRAC is much less conserved and shows some interesting features (Figure 1.6 and Figure 2.15). In the human and mouse TSPO proteins, where nano-molar affinities have been reported, a relatively hydrophobic sequence Leu-Ala-Phe (144-146)

precedes the CRAC, whereas in the *R. sphaeroides* sequence these residues are replaced by Ala-Thr-Ala (136-138), a much more hydrophilic combination. In fact, the spontaneous human polymorphism A147T, located right after the Leu-Ala-Phe, has been reported to reduce pregnenolone production [63] and binding of an imaging ligand by 2 orders of magnitude [38]. Our model of *Rs*TSPO (Figure 2.15) would allow the long hydrophobic tail of cholesterol to extend to the location of Ala-Thr-Ala, while the ring structure is interacting mainly with the CRAC site. The more hydrophobic character of the human helix V sequence may create a deeper binding site or reposition helix V to favor binding interactions for the hydrophobic rings.

Another interesting question is whether this region of helix V and cholesterol binding also affects other ligands. Besides our observations, extensive investigation of the binding of the original benzodiazepine ligand Ro5-4864 has concluded that the C-terminal region of TSPO, in particular residues 144-156 of helix V, which include both the CRAC site and the sequence preceding, plays a role in its binding [35] although involvement of loop 1 is also observed. The new PET ligand PBR28, a PK11195 related compound, shows a markedly reduced affinity for the *Hs*TSPO polymorphism A147T [38]. The same mutation in bacterial TSPO was recently reported to disrupt the binding of PpIX [79]. All together, helix V and the cholesterol binding region do appear to influence both PpIX and drug ligands. Our two top models (Figure 2.12 and 2.14) show that helix V and helix I are in close proximity within the dimer as well as the higher-order oligomer, providing the possibility of direct interaction between binding sites.

From these considerations, a tentative model (Figure 2.15) for the ligand binding sites of TSPO is proposed, suggesting that TSPO may perform its dual functions as transporter and receptor by binding the substrate PpIX at the dimer interface for transporting, while binding PK11195 and other ligands more superficially on loop 1. Cholesterol is proposed to bind at the

CRAC site located on helix V and we cite evidence that the 4 residues immediately preceding the CRAC site are also important for the binding of cholesterol and other ligands. In Model 1, these residues and the cholesterol binding site are located at the dimer interface, suggesting testable differences between the two models.

TSPO as a mediator of the regulation of MPTP and apoptosis.

Although numerous studies have implicated TSPO as a regulator of MPTP and apoptosis, the mechanism of the regulation is still unclear. In fact, Gonzalez-Polo *et al.* [42] reported that the diagnostic TSPO ligand PK11195 shows apoptosis-inducing effects independent of TSPO. Another important regulator of MPTP and apoptosis is the B-cell lymphoma 2 (Bcl-2) family of proteins (see review by R. Youle [80]), which can be either anti-apoptotic, such as Bcl-2 and Bcl-XL, or pro-apoptotic, as in the case of Bax, Bak and Bid. Bcl-2 family proteins are expressed in the cytosol and recruited during the process of apoptosis to the MPTP on the outer mitochondrial membrane, where TSPO is also localized. The fact that both TSPO and Bcl-2 family proteins regulate apoptosis and that the TSPO ligand PK11195 can reverse the cytoprotective effect of Bcl-2 [27] suggests a possible interaction of TSPO and Bcl-2 in the regulation of MPTP.

In this study we report binding of a number of apoptosis-inducing compounds to purified *Rs*TSPO with low micro-molar affinity, including PK11195, retinoic acid, curcumin, and bilirubin. This is consistent with a direct interaction of TSPO with these ligands and supports a role for TSPO during apoptosis. In addition, the binding of a known Bcl-2 inhibitor, gossypol, to purified *Rs*TSPO at low micro-molar affinity suggests a relationship between TSPO and Bcl-2 family proteins.

CONCLUSIONS

The current studies characterize the oligomeric state of purified TSPO from *R. sphaeroides* as a dimer and report the binding properties of a variety of ligands. New atomic resolution models of its dimer form are presented and used to predict TSPO's interaction with various ligands. Several novel ligands are reported, with implications for the role of TSPO in apoptosis and for facilitation of the crystallization of TSPO.

REFERENCES

REFERENCES

1. Braestrup C, Squires RF: **Specific benzodiazepine receptors in rat brain characterized by high-affinity (3H)diazepam binding**. *Proc Natl Acad Sci U S A* 1977, **74**:3805-3809.

2. Papadopoulos V, Baraldi M, Guilarte TR, Knudsen TB, Lacapere JJ, Lindemann P, Norenberg MD, Nutt D, Weizman A, Zhang MR, et al.: **Translocator protein (18 kDa): new nomenclature for the peripheral-type benzodiazepine receptor based on its structure and molecular function**. *Trends Pharmacol Sci* 2006, **27**:402-409.

3. Fan J, Lindemann P, Feuilloley MG, Papadopoulos V: **Structural and functional evolution of the translocator protein (18 kDa)**. *Curr Mol Med* 2012, **12**:369-386.

4. Krueger KE: **Molecular and functional properties of mitochondrial benzodiazepine receptors**. *Biochim Biophys Acta* 1995, **1241**:453-470.

5. Anholt RR, Pedersen PL, De Souza EB, Snyder SH: **The peripheral-type benzodiazepine receptor. Localization to the mitochondrial outer membrane**. *J Biol Chem* 1986, **261**:576-583.

6. Papadopoulos V, Amri H, Boujrad N, Cascio C, Culty M, Garnier M, Hardwick M, Li H, Vidic B, Brown AS, et al.: **Peripheral benzodiazepine receptor in cholesterol transport and steroidogenesis**. *Steroids* 1997, **62**.

7. Li H, Papadopoulos V: **Peripheral-type benzodiazepine receptor function in cholesterol transport. Identification of a putative cholesterol recognition/interaction amino acid sequence and consensus patterns**. *Endocrinology* 1998, **139**:4991-4997.

8. Taketani S, Kohno H, Furukawa T, Tokunaga R: **Involvement of peripheral-type benzodiazepine receptors in the intracellular transport of heme and porphyrins**. *J Biochem* 1995, **117**:875-880.

9. Verma A, Nye JS, Snyder SH: **Porphyrins Are Endogenous Ligands for the Mitochondrial (Peripheral-Type) Benzodiazepine Receptor**. *Pro Natl Ac Sci U S A* 1987, **84**:2256-2260.

10. Krueger KE, Papadopoulos V: **Mitochondrial benzodiazepine receptors and the regulation of steroid biosynthesis**. *Annu Rev Pharmacol Toxicol* 1992, **32**:211-237.

11. Chen MK, Guilarte TR: **Translocator protein 18 kDa (TSPO): molecular sensor of brain injury and repair**. *Pharmacol Ther* 2008, **118**:1-17.

12. Brown RC, Degenhardt B, Kotoula M, Papadopoulous V: **Location-dependent role of the

human glioma cell peripheral-type benzodiazepine receptor in proliferation and steroid biosynthesis. *Cancer Lett* 2000, **156**:125-132.

13. Hardwick M, Fertikh D, Culty M, Li H, Vidic B, Papadopoulos V: **Peripheral-type benzodiazepine receptor (PBR) in human breast cancer: correlation of breast cancer cell aggressive phenotype with PBR expression, nuclear localization, and PBR-mediated cell proliferation and nuclear transport of cholesterol**. *Cancer Res* 1999, **59**:831-842.

14. Ji B, Maeda J, Sawada M, Ono M, Okauchi T, Inaji M, Zhang MR, Suzuki K, Ando K, Staufenbiel M, et al.: **Imaging of peripheral benzodiazepine receptor expression as biomarkers of detrimental versus beneficial glial responses in mouse models of Alzheimer's and other CNS pathologies**. *J Neurosci* 2008, **28**:12255-12267.

15. Crompton M: **The mitochondrial permeability transition pore and its role in cell death**. *Biochem J* 1999, **341 (Pt 2)**:233-249.

16. Decaudin D, Castedo M, Nemati F, Beurdeley-Thomas A, De Pinieux G, Caron A, Pouillart P, Wijdenes J, Rouillard D, Kroemer G, et al.: **Peripheral benzodiazepine receptor ligands reverse apoptosis resistance of cancer cells in vitro and in vivo**. *Cancer Research* 2002, **62**:1388-1393.

17. Campanella M: **Editorial: The physiology and pharmacology of the mitochondrial 18 kDa translocator protein (TSPO): an emerging molecular target for diagnosis and therapy**. *Curr Mol Med* 2012, **12**:355.

18. Gatliff J, Campanella M: **The 18 kDa translocator protein (TSPO): a new perspective in mitochondrial biology**. *Curr Mol Med* 2012, **12**:356-368.

19. Rupprecht R, Papadopoulos V, Rammes G, Baghai TC, Fan J, Akula N, Groyer G, Adams D, Schumacher M: **Translocator protein (18 kDa) (TSPO) as a therapeutic target for neurological and psychiatric disorders**. *Nat Rev Drug Discov* 2010, **9**:971-988.

20. Xiao J, Liang D, Zhang H, Liu Y, Li F, Chen YH: **4'-Chlorodiazepam, a translocator protein (18 kDa) antagonist, improves cardiac functional recovery during postischemia reperfusion in rats**. *Exp Biol Med (Maywood)* 2010, **235**:478-486.

21. Kroemer G, Dallaporta B, Resche-Rigon M: **The mitochondrial death/life regulator in apoptosis and necrosis**. *Annu Rev Physiol* 1998, **60**:619-642.

22. Tait SW, Green DR: **Mitochondria and cell death: outer membrane permeabilization and beyond**. *Nat Rev Mol Cell Biol* 2010, **11**:621-632.

23. Jiang X, Wang X: **Cytochrome C-mediated apoptosis**. *Annu Rev Biochem* 2004, **73**:87-106.

24. McEnery MW, Snowman AM, Trifiletti RR, Snyder SH: **Isolation of the mitochondrial benzodiazepine receptor: association with the voltage-dependent anion channel and the adenine nucleotide carrier**. *Proc Natl Acad Sci U S A* 1992, **89**:3170-3174.

25. Leung AW, Halestrap AP: **Recent progress in elucidating the molecular mechanism of the mitochondrial permeability transition pore**. *Biochim Biophys Acta* 2008, **1777**:946-952.

26. Giorgio V, von Stockum S, Antoniel M, Fabbro A, Fogolari F, Forte M, Glick GD, Petronilli V, Zoratti M, Szabó I, et al.: **Dimers of mitochondrial ATP synthase form the permeability transition pore**. *Proc Natl Acad Sci U S A* 2013.

27. Krestinina OV, Grachev DE, Odinokova IV, Reiser G, Evtodienko YV, Azarashvili TS: **Effect of peripheral benzodiazepine receptor (PBR/TSPO) ligands on opening of Ca2+-induced pore and phosphorylation of 3.5-kDa polypeptide in rat brain mitochondria**. *Biochemistry (Mosc)* 2009, **74**:421-429.

28. Bui ET, Bradley PJ, Johnson PJ: **A common evolutionary origin for mitochondria and hydrogenosomes**. *Proc Natl Acad Sci U S A* 1996, **93**:9651-9656.

29. Armstrong GA, Alberti M, Leach F, Hearst JE: **Nucleotide sequence, organization, and nature of the protein products of the carotenoid biosynthesis gene cluster of *Rhodobacter capsulatus***. *Mol Gen Gen* 1989, **216, 254-268**.

30. Baker ME, Fanestil DD: **Mammalian peripheral-type benzodiazepine receptor is homologous to CrtK protein of *Rhodobacter capsulatus*, a photosynthetic bacterium**. *Cell* 1991, **65**:721-722.

31. Yeliseev AA, Kaplan S: **A sensory transducer homologous to the mammalian peripheral-type benzodiazepine receptor regulates photosynthetic membrane complex formation in *Rhodobacter sphaeroides* 2.4.1**. *J Biol Chem* 1995, **270**:21167-21175.

32. Yeliseev AA, Krueger KE, Kaplan S: **A mammalian mitochondrial drug receptor functions as a bacterial "oxygen" sensor**. *Proc Natl Acad Sci U S A* 1997, **94**:5101-5106.

33. Yeliseev AA, Kaplan S: **A novel mechanism for the regulation of photosynthesis gene expression by the TspO outer membrane protein of *Rhodobacter sphaeroides* 2.4.1**. *J Biol Chem* 1999, **274**:21234-21243.

34. Yeliseev AA, Kaplan S: **TspO of *Rhodobacter sphaeroides*. A structural and functional model for the mammalian peripheral benzodiazepine receptor**. *J Biol Chem* 2000, **275**:5657-5667.

35. Scarf AM, Auman KM, Kassiou M: **Is there any correlation between binding and functional effects at the translocator protein (TSPO) (18 kDa)?** *Curr Mol Med* 2012, **12**:387-397.

36. Li H, Yao Z, Degenhardt B, Teper G, Papadopoulos V: **Cholesterol binding at the cholesterol recognition/ interaction amino acid consensus (CRAC) of the peripheral-type benzodiazepine receptor and inhibition of steroidogenesis by an HIV TAT-CRAC peptide**. *Proc Natl Acad Sci U S A* 2001, **98**:1267-1272.

37. Rohmer M, Bouviernave P, Ourisson G: **Distribution of Hapanoid triperpene in Prokaryotes**. *Journal of General Microbiology* 1984, **130**:1137-1150.

38. Owen DR, Yeo AJ, Gunn RN, Song K, Wadsworth G, Lewis A, Rhodes C, Pulford DJ, Bennacef I, Parker CA, et al.: **An 18-kDa translocator protein (TSPO) polymorphism explains differences in binding affinity of the PET radioligand PBR28**. *J Cereb Blood Flow Metab* 2012, **32**:1-5.

39. Lacapère JJ, Papadopoulos V: **Peripheral-type benzodiazepine receptor: structure and function of a cholesterol-binding protein in steroid and bile acid biosynthesis**. *Steroids* 2003, **68**:569-585.

40. Wendler G, Lindemann P, Lacapère JJ, Papadopoulos V: **Protoporphyrin IX binding and transport by recombinant mouse PBR**. *Biochem Biophys Res Commun* 2003, **311**:847-852.

41. Scarf AM, Luus C, Da Pozzo E, Selleri S, Guarino C, Martini C, Ittner LM, Kassiou M: **Evidence for complex binding profiles and species differences at the translocator protein (TSPO) (18 kDa)**. *Curr Mol Med* 2012, **12**:488-493.

42. Gonzalez-Polo RA, Carvalho G, Braun T, Decaudin D, Fabre C, Larochette N, Perfettini JL, Djavaheri-Mergny M, Youlyouz-Marfak I, Codogno P, et al.: **PK11195 potently sensitizes to apoptosis induction independently from the peripheral benzodiazepin receptor**. *Oncogene* 2005, **24**:7503-7513.

43. Decaudin D, Castedo M, Nemati F, Beurdeley-Thomas A, De Pinieux G, Caron A, Pouillart P, Wijdenes J, Rouillard D, Kroemer G, et al.: **Peripheral benzodiazepine receptor ligands reverse apoptosis resistance of cancer cells in vitro and in vivo**. *Cancer Res* 2002, **62**:1388-1393.

44. Obame FN, Zini R, Souktani R, Berdeaux A, Morin D: **Peripheral benzodiazepine receptor-induced myocardial protection is mediated by inhibition of mitochondrial membrane permeabilization**. *J Pharmacol Exp Ther* 2007, **323**:336-345.

45. Schaller S, Paradis S, Ngoh GA, Assaly R, Buisson B, Drouot C, Ostuni MA, Lacapere JJ, Bassissi F, Bordet T, et al.: **TRO40303, a new cardioprotective compound, inhibits mitochondrial permeability transition**. *J Pharmacol Exp Ther* 2010, **333**:696-706.

46. Korkhov VM, Sachse C, Short JM, Tate CG: **Three-dimensional structure of TspO by electron cryomicroscopy of helical crystals**. *Structure* 2010, **18**:677-687.

47. Woetzel N, Lindert S, Stewart PL, Meiler J: **BCL::EM-Fit: rigid body fitting of atomic structures into density maps using geometric hashing and real space refinement**. *J Struct Biol* 2011, **175**:264-276.

48. Higuchi R, Krummel B, Saiki RK: **A general method of in vitro preparation and specific mutagenesis of DNA fragments: study of protein and DNA interactions**. *Nucleic Acids Res* 1988, **16**:7351-7367.

49. Studier FW: **Protein production by auto-induction in high density shaking cultures**. *Protein Expr Purif* 2005, **41**:207-234.

50. Slotboom DJ, Duurkens RH, Olieman K, Erkens GB: **Static light scattering to characterize membrane proteins in detergent solution**. *Methods* 2008, **46**:73-82.

51. Pettersen EF, Goddard TD, Huang CC, Couch GS, Greenblatt DM, Meng EC, Ferrin TE: **UCSF Chimera--a visualization system for exploratory research and analysis**. *J Comput Chem* 2004, **25**:1605-1612.

52. Karakaş M, Woetzel N, Staritzbichler R, Alexander N, Weiner BE, Meiler J: **BCL::Fold--de novo prediction of complex and large protein topologies by assembly of secondary structure elements**. *PLoS One* 2012, **7**:e49240.

53. DiMaio F, Leaver-Fay A, Bradley P, Baker D, Andr?? I: **Modeling symmetric macromolecular structures in Rosetta3**. *PLoS One* 2011, **6**:e20450.

54. DiMaio F, Tyka MD, Baker ML, Chiu W, Baker D: **Refinement of protein structures into low-resolution density maps using rosetta**. *J Mol Biol* 2009, **392**:181-190.

55. Yarov-Yarovoy V, Schonbrun J, Baker D: **Multipass membrane protein structure prediction using Rosetta**. *Proteins* 2006, **62**:1010-1025.

56. Nasie I, Steiner-Mordoch S, Gold A, Schuldiner S: **Topologically random insertion of**

EmrE supports a pathway for evolution of inverted repeats in ion-coupled transporters. *J Biol Chem* 2010, **285**:15234-15244.

57. Rone MB, Liu J, Blonder J, Ye X, Veenstra TD, Young JC, Papadopoulos V: **Targeting and insertion of the cholesterol-binding translocator protein into the outer mitochondrial membrane**. *Biochemistry* 2009, **48**:6909-6920.

58. Brambillasca S, Yabal M, Makarow M, Borgese N: **Unassisted translocation of large polypeptide domains across phospholipid bilayers**. *J Cell Biol* 2006, **175**:767-777.

59. Otera H, Taira Y, Horie C, Suzuki Y, Suzuki H, Setoguchi K, Kato H, Oka T, Mihara K: **A novel insertion pathway of mitochondrial outer membrane proteins with multiple transmembrane segments**. *J Cell Biol* 2007, **179**:1355-1363.

60. Verma A, Facchina SL, Hirsch DJ, Song SY, Dillahey LF, Williams JR, Snyder SH: **Photodynamic tumor therapy: mitochondrial benzodiazepine receptors as a therapeutic target**. *Mol Med* 1998, **4**:40-45.

61. Delavoie F, Li H, Hardwick M, Robert JC, Giatzakis C, Péranzi G, Yao ZX, Maccario J, Lacapère JJ, Papadopoulos V: **In vivo and in vitro peripheral-type benzodiazepine receptor polymerization: functional significance in drug ligand and cholesterol binding**. *Biochemistry* 2003, **42**:4506-4519.

62. Li H, Papadopoulos V: **Peripheral-type benzodiazepine receptor function in cholesterol transport. Identification of a putative cholesterol recognition/interaction amino acid sequence and consensus pattern**. *Endocrinology* 1998, **139**:4991-4997.

63. Costa B, Pini S, Gabelloni P, Da Pozzo E, Abelli M, Lari L, Preve M, Lucacchini A, Cassano GB, Martini C: **The spontaneous Ala147Thr amino acid substitution within the translocator protein influences pregnenolone production in lymphomonocytes of healthy individuals**. *Endocrinology* 2009, **150**:5438-5445.

64. Taketani S, Kohno H, Furukawa T, Tokunaga R: **Involvement of peripheral-type benzodiazepine receptors in the intracellular-transport of heme and porphyrins**. *J Biochem* 1995, **117**:875-880.

65. Keshavan P, Schwemberger SJ, Smith DL, Babcock GF, Zucker SD: **Unconjugated bilirubin induces apoptosis in colon cancer cells by triggering mitochondrial depolarization**. *Int J Cancer* 2004, **112**:433-445.

66. Korichneva I, Waka J, Hammerling U: **Regulation of the cardiac mitochondrial membrane potential by retinoids**. *J Pharmacol Exp Ther* 2003, **305**:426-433.

67. Pfahl M, Piedrafita FJ: **Retinoid targets for apoptosis induction**. *Oncogene* 2003, **22**:9058-9062.

68. Choudhuri T, Pal S, Agwarwal ML, Das T, Sa G: **Curcumin induces apoptosis in human breast cancer cells through p53-dependent Bax induction**. *FEBS Lett* 2002, **512**:334-340.

69. Oliver CL, Miranda MB, Shangary S, Land S, Wang S, Johnson DE: **(-)-Gossypol acts directly on the mitochondria to overcome Bcl-2- and Bcl-X(L)-mediated apoptosis resistance**. *Mol Cancer Ther* 2005, **4**:23-31.

70. Butler PJ, Ubarretxena-Belandia I, Warne T, Tate CG: **The Escherichia coli multidrug transporter EmrE is a dimer in the detergent-solubilised state**. *J Mol Biol* 2004, **340**:797-808.

71. Lloris-Garcerá P, Bianchi F, Slusky JS, Seppälä S, Daley DO, von Heijne G: **Antiparallel dimers of the small multidrug resistance protein EmrE are more stable than parallel dimers**. *J Biol Chem* 2012, **287**:26052-26059.

72. Morrison EA, DeKoster GT, Dutta S, Vafabakhsh R, Clarkson MW, Bahl A, Kern D, Ha T, Henzler-Wildman KA: **Antiparallel EmrE exports drugs by exchanging between asymmetric structures**. *Nature* 2012, **481**:45-50.

73. Radestock S, Forrest LR: **The alternating-access mechanism of MFS transporters arises from inverted-topology repeats**. *J Mol Biol* 2011, **407**:698-715.

74. Forrest LR, Krämer R, Ziegler C: **The structural basis of secondary active transport mechanisms**. *Biochim Biophys Acta* 2011, **1807**:167-188.

75. Krishnamurthy H, Piscitelli CL, Gouaux E: **Unlocking the molecular secrets of sodium-coupled transporters**. *Nature* 2009, **459**:347-355.

76. Bowie JU: **Structural biology. Membrane protein twists and turns**. *Science* 2013, **339**:398-399.

77. Qin L, Mills DA, Buhrow L, Hiser C, Ferguson-Miller S: **A conserved steroid binding site in cytochrome *c* oxidase**. *Biochemistry* 2008, **47**:9931-9933.

78. Hiser C, Buhrow L, Liu J, Kuhn LA, Ferguson-Miller SM: **A conserved amphipathic ligand binding region influences K-path dependent activity of cytochrome *c* oxidase**. *Biochemistry* 2013.

79. Ginter C, Kiburu I, Boudker O: **Chemical catalysis by the translocator protein (18 kDa)**.

Biochemistry 2013.

80. Youle RJ, Strasser A: **The BCL-2 protein family: opposing activities that mediate cell death**. *Nat Rev Mol Cell Biol* 2008, **9**:47-59.

CHAPTER 3

Identification of a key cholesterol binding enhancement motif in Translocator Protein 18 kDa

This chapter will be submitted in part as "Fei Li, Jian Liu, Lance Valls, Shelagh Ferguson-Miller. Identification of a key cholesterol binding enhancement motif in Translocator Protein 18 kDa"

Lance Valls (undergraduate student) performed all binding assays and Dr. Jian Liu did the protein co-evolution analysis on *Rs*TSPO.

INTRODUCTION

Translocator Protein 18 kDa (TSPO) is a widely distributed integral membrane protein initially discovered as a peripheral tissue binding site for anxiolytic benzodiazepine drugs [1] and therefore known as the peripheral benzodiazepine receptor (PBR). It was renamed in 2006 to more accurately reflect its far-reaching phylogeny and increasing evidence of involvement in a number of complex cellular processes, including cholesterol transport, inflammation, tumor progression, Alzheimer disease and regulation of the mitochondrial permeability transition associated with apoptosis [2-8]. Deletion of TSPO was found to be developmentally lethal in the mouse [9].

In mammals, TSPO is expressed at highest levels in the outer membrane of mitochondria in steroid hormone producing tissues, where it functions to facilitate cholesterol transport and is proposed to be a rate-limiting step in steroidogenesis [10,11] (but see [12]). High expression is also observed in the most metastatic cancers [13] and in regions of inflammation [14,15], possibly relating to a role in corticosteroid production in response to stress [16] and leading to the use of TSPO ligands for sensitive positron emission tomography (PET) imaging of damage in the brain [17]. A conserved cholesterol recognition/interaction amino acid consensus sequence (CRAC: $L/V\text{-}_{x(1\text{-}5)}\text{-}Y\text{-}_{x(1\text{-}5)}\text{-}R/K$) near the C-terminus of the predicted transmembrane helix V was identified as the cholesterol binding site in mammalian TSPO [18]. Despite sharing the majority of the CRAC sequence ($L\text{-}_{x(1)}\text{-}F\text{-}_{x(3)}\text{-}R$), the homolog from *Rhodobacter sphaeroides* (*Rs*TSPO) shows more than 1000-fold lower affinity for cholesterol than mammalian TSPO. A clue to this disparity was provided by recent publications reporting a spontaneous human polymorphism A147T in the region immediately preceding the CRAC site. This change correlated with reduced pregnenolone production [19] and bipolar disorder [20] as well as lower

imaging ligand binding [21], drawing attention to this region.

Comparing the sequences of bacterial and mammalian proteins, we noted that the helix V region containing CRAC is generally well conserved, except that three residues preceding the human polymorphism A147T are highly variable in bacteria but conserved in the mammalian proteins and much more hydrophobic, suggesting that this region is a possible contributor to the differing affinities. We therefore designed a mutant to test the functional implications of this region preceding the human polymorphism site. *Rhodobacter* is a good model system for investigating the cholesterol binding function of TSPO due to its dramatically different affinity and availability in purified form [19]. Using a combination of biochemical and evolutionary analysis, we identified a motif that correlates with nM affinity for cholesterol. The cholesterol binding enhancement motif is highly conserved within mammalian TSPOs and is also observed in other mammalian membrane proteins, indicating broad significance for cholesterol/protein interactions and providing new evidence relevant to the recent debate on the role of TSPO in cholesterol transport [12].

MATERIAL AND METHODS

Cloning, expression and purification of protein.

The coding sequence of *Rs*TSPO was subcloned into the pUC12 vector for mutagenesis. Mutant *Rs*TSPO was made by QuikChange Mutagenesis$^{©}$ (Stratagene). The construct was confirmed by sequencing and ligated into the pRK415 expression vector with KpnI and HindIII restriction sites. The expression vector containing the desired TSPO coding sequence was introduced into the *E. coli* expression strain BL21 λDE3. Purification procedures are as previously described for the *Rs*TSPO-WT protein [22] except for the modified procedure for the *Rs*TSPO-LAF, which is described in the text.

Tryptophan fluorescence quenching binding assay.

Binding of ligands to RsTSPO proteins is measured as previously described [22] on an Agilent Eclipse$^{®}$ fluorescence spectrometer. K_d was calculated by fitting the binding curve with equations previously developed for single site binding mode [22] when possible. In the cases where complicated binding behavior occurred or the precipitation of ligand at higher concentrations prevented accurate fitting, an apparent K_d was estimated from the half-maximal quenching. Each reported K_d is an average from three independent experiments.

TLC analysis of the purified RsTSPO_LAF sample.

One μl samples were spotted on a Si-60 thin layer chromatography (TLC) plate (EMD). Samples contained either: 1) 0.1 % Cholesteryl hemisuccinate (CHS) standard in 50 mM Tris, 150 mM NaCl buffer pH 8; 2) rescue buffer (50 mM Tris, 150 mM NaCl, 10% glycerol, 0.2% DM and 0.01% CHS, pH 8); or 3) purified RsTSPO-LAF, 21 μM in size exclusion chromatography (SEC) buffer (50 mM Tris, 150 mM NaCl, 10% glycerol, 0.2% DM, pH 8). The plate was run in chloroform:methanol:ammonia (63:35:5) and air dried before spraying with a cholesterol specific staining solution (20% sulfuric acid) and baked in 110 ℃ for ~5 mins. Cholesterol and cholesterol esters are stained wine-red.

Covariance analysis with PsiCOV.

A total of 2332 sequences homologous to RsTSPO were obtained from the non-redundant (nr) protein sequence database using the DELTA-Blast (Domain Enhanced Lookup Time Accelerated BLAST) web server. Multiple sequence alignments of these sequences were done with the Cobalt Constraint-based Multiple Protein Alignment Tool. PsiCOV was then used to calculate the contact pair covariance of this alignment. The initial value of Glasso regulation

parameter ρ is set to 0.001.

Phylogenetic analysis of the enhancement motif.

Sequences of TSPO proteins were obtained from the NCBI database using the accession number provided in [3]. Sequences of full length TSPO proteins were aligned with Clustal Omega [23] and the picture was created in the Aline [24] program. Phylogenetic analysis was done on the aligned full length TSPO sequences with the default NJ method in MEGA6 [25] software.

Survey of the enhancement motif in human membrane protein database.

A database containing 5183 human membrane proteins was downloaded from the UniProtKB/Swiss-Prot database with human, transmembrane, and helical as keyword filters. The search pattern $[L/V]_{x1-5}-[Y]_{x1-5}-[R]$ was used to search for the CRAC motif with the Fuzzpro program within the EMBOSS suite. The pattern $[L]-[A]-[F]_{x2-5}-[L/V]_{x1-5}-[Y]_{x1-5}-[R]$ was used to search for the LAF-CRAC with enhancement motif.

RESULTS AND DISCUSSION

Rationale and design of mutations in *Rs*TSPO.

TSPO from *Rhodobacter* shows more than 34 % amino acid identity compared to the human protein [26] and rat TSPO is able to rescue the function of a *Rs*TSPO knock-out mutant *in vivo* [27], suggesting a conserved functional relationship. More importantly, helix V of *Rs*TSPO has a high degree of similarity to the mammalian sequence (Figure 3.1), but with some distinctive differences. The CRAC site is highly conserved, but nevertheless, human TSPO has >1000-fold higher affinity for cholesterol than *Rs*TSPO [22]. The observation of a human polymorphism (A147T in human and A139T in *Rhodobacter*) immediately preceding the CRAC motif that appeared to affect ligand binding affinity, along with the fact that the three residues

prior to A139T were highly variable in bacteria, led us to propose a role for this region in cholesterol binding.
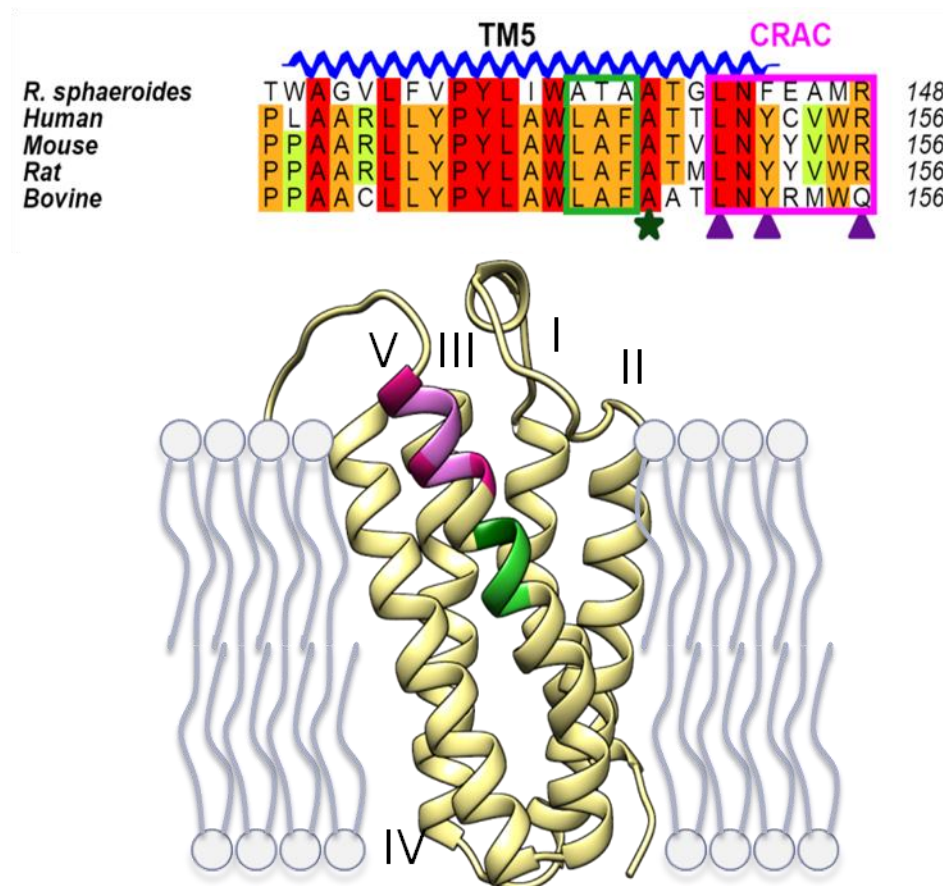
Figure 3.1. Location of the triple mutation of *Rs*TSPO in relation to the CRAC sequence.

Upper panel shows the sequence alignment of the C-terminal helix V region of TSPO from *R. sphaeroides* (*Rs*), human, mouse, rat and bovine. The CRAC motif is boxed with magenta and the three critical residues are labeled with dark magenta triangles. The location of the human polymorphism A147 (A139 in *Rs*TSPO) is labeled with a dark green star. Residues mutated in this study are boxed green. Lower panel shows the location of aforementioned residues on a model of *Rs*TSPO colored coded: magenta for the CRAC region with dark magenta representing the 3 critical residues, dark green for A139 and green for LAF.

To test our hypothesis, we created a mutant of *Rs*TSPO, *Rs*TSPO-A136L/T137A/A138F (*Rs*TSPO-LAF), to mimic human TSPO by replacing the *Rhodobacter* sequence Ala-Thr-Ala (136-138) with the more hydrophobic human counterpart Leu-Ala-Phe (144-146). We predicted this region to be deeply buried in the membrane, with the possibility of better interacting with the alkyl tail of cholesterol and increasing cholesterol binding affinity. Since the C-terminus including helix V is not suggested to play a major role in the binding of the specific diagnostic ligand PK11195 [28] or protoporphyrin IX (PpIX), we also tested the binding of these ligands to the mutant form.

Rs TSPO-LAF exhibits a tendency to aggregate when concentrated, but CHS can rescue it from precipitation.

The triple mutant *Rs*TSPO-LAF was well expressed and initially purified following the same procedure as *Rs*TSPO-WT [22] but it was observed to precipitate during the concentration step after Ni-NTA purification. Addition of buffer supplemented with 0.01% CHS rescued *Rs*TSPO-LAF during the concentration step and His-tag removal. The final purification by SEC was performed in regular buffer without CHS and yielded considerably lower amounts of protein, likely due to the loss from some precipitation before SEC.

Interestingly, we found that CHS was retained and enriched by *Rs*TSPO-LAF during this purification method, as shown in the TLC plate in Figure 3.2A. The *Rs*TSPO-LAF to which CHS was added during concentration and then further purified without any CHS by SEC retained 2-3 fold more CHS than the buffer itself used for rescue in the previous steps. *Rs*TSPO-LAF was also purified by replacing the concentrating step with a spin column buffer exchange step to remove the imidazole after Ni-NTA elution and foregoing the concentration and SEC purification step. Previous experience with *Rs*TSPO-WT had shown that protein after Ni-NTA purification

has similar high purity compared to that treated with trypsin and purified by an additional SEC step and has no observable difference in ligand binding. Since the protein concentration used in the binding assay is very low, *Rs*TSPO-LAF protein from the spin column could be used directly in the binding assays and compared with samples purified after treatment with CHS. Given the lower stability of the LAF mutant, we did a control experiment which confirmed that the fluorescence reading was not significantly decreased during the time course of the binding assay indicating little precipitation in the course of the experiments (Figure 3.2B). A SDS-PAGE of the purified *Rs*TSPO-LAF protein is shown in Figure 3.2C.
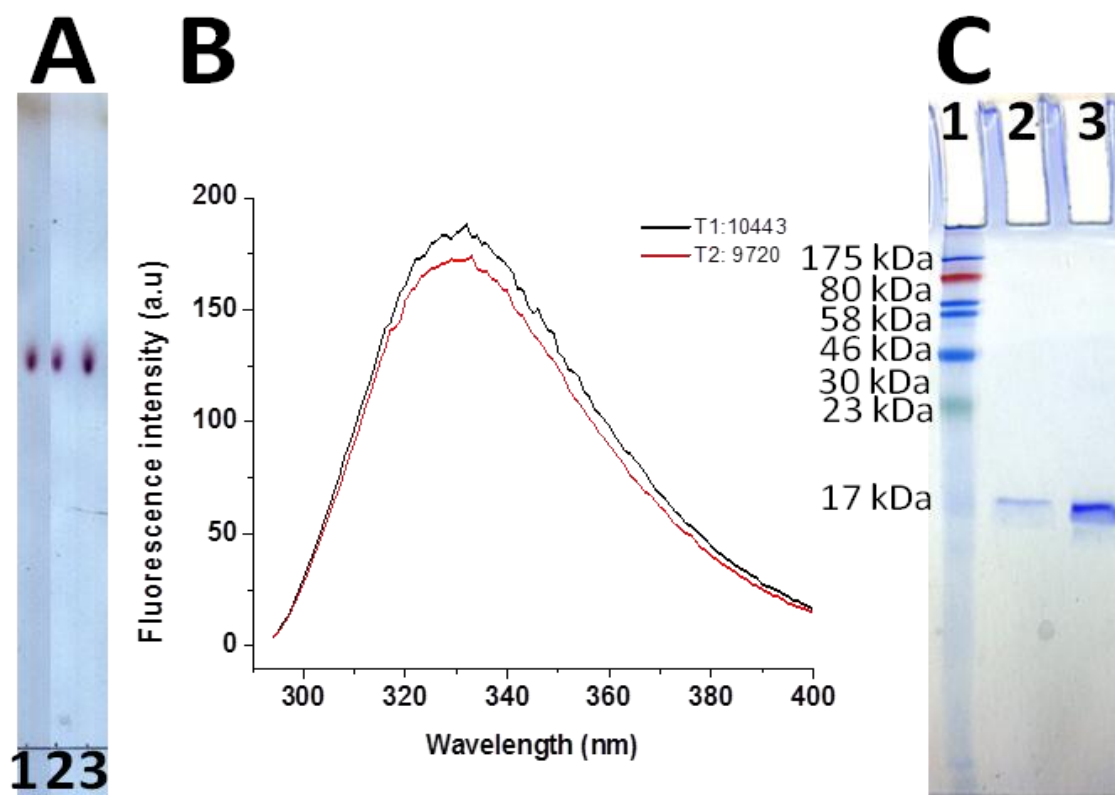
Figure 3. 2. Purification of *Rs*TSPO-LAF and the rescue with cholesterol hemisuccinate.

(A) TLC of *Rs*TSPO-LAF. 1: CHS standard (0.1%) in 50 mM Tris-150 mM NaCl pH 8 buffer; 2: rescue buffer containing CHS (50 mM Tris, 150 mM NaCl, 10% glycerol, 0.2% DM, pH 8, supplemented with 0.01% CHS); 3: *Rs*TSPO-LAF after CHS rescue and further purified in SEC buffer without CHS. (B) Fluorescence spectra of *Rs*TSPO-LAF. T1 and T2 are two time points one hour apart, representing the start and end of a typical fluorescence quenching experiment. The integration areas, which are used in calculating the fraction of quenching of both curves, are noted in the figure. This experiment shows only ~5% of fluorescence decay during the binding experiment for the *Rs*TSPO-LAF protein, confirming that the slight decay, likely due to some tendency to aggregate, will not influence the binding results. (C) SDS-PAGE of purified *Rs*TSPO proteins. 1: size marker; 2: Ni-NTA purified *Rs*TSPO-LAF; 3: *Rs*TSPO-WT

***Rs*TSPO-LAF binds cholesterol with nM affinity.**

Freshly purified *Rs*TSPO-LAF protein not exposed to CHS was used in the binding assay with cholesterol. Our results (Figure 3.3) show a high affinity cholesterol binding site in the LAF mutant, with a K_d of ~ 20 nM, similar to the affinity of mouse and human TSPO previously reported [18,29]. It is difficult to calculate an accurate K_d for the low affinity cholesterol binding in WT since saturating concentrations could not be achieved due to the limited solubility of cholesterol. Nevertheless, Figure 3.3 clearly shows that introducing the LAF motif causes the affinity for cholesterol to greatly increase in the initial phase of the binding titration, from an apparent K_d in the low μM range for WT to the low nM range for LAF. In addition, the samples originally purified in the presence of CHS and retaining that ligand showed dramatically lower apparent affinity for cholesterol similar to WT, suggesting CHS is binding at the same site as cholesterol. This finding is consistent with the observation that CHS co-purifies with the mutant form (Figure 3.2 and Figure 3.3). These results strongly support a role of the LAF motif in determining the nM affinity of cholesterol for mammalian TSPO, since introduction of the three amino acid changes are sufficient to account for the 1000-fold enhanced affinity.
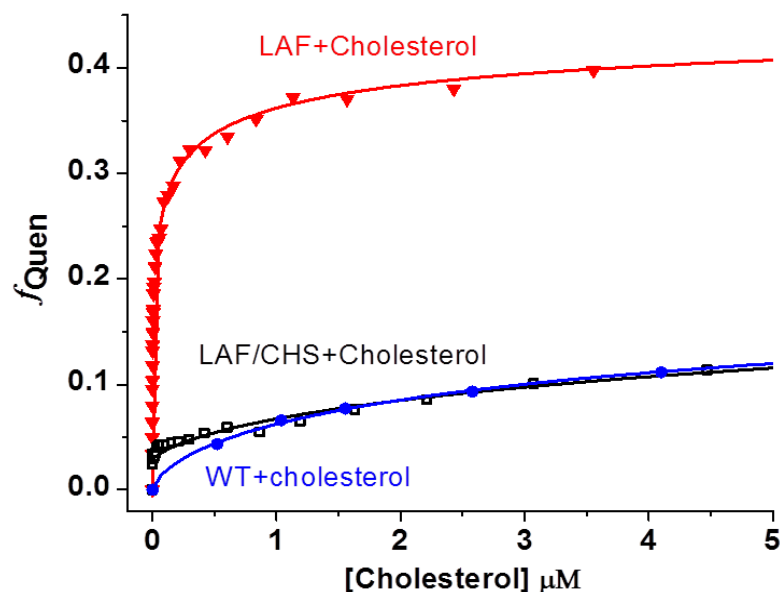
Figure 3.3 *Rs*TSPO-LAF binds to cholesterol at nM affinity.

Binding curve of *Rs*TSPO-LAF with cholesterol compared to WT and *Rs*TSPO-LAF purified in the presence of CHS. Binding data for cholesterol with WT were previously reported [22] and shown here for comparison with the mutant form. All binding assays were done with the same protein concentration (2.5 μM) and the same buffer conditions as previously described [22] (50 mM Tris, 150 mM NaCl, 10% glycerol, 0.2% DM, pH 8). Error bars for each data point are not provided because individual data points are not repeated; rather, the complete binding curve for each ligand was repeated 3 times.

Two binding orientations of cholesterol to the CRAC site have been suggested [30,31], with the hydroxyl group facing in or out of membrane. Considering our previous finding that ursodeoxycholate, which has a similar ring structure as cholesterol but with a carboxyl attached to the alkyl chain, does not bind to *Rs*TSPO-WT [22], our results support a model with cholesterol binding with the hydroxyl group facing out, the ring structure interacting with the highly conserved CRAC site, and the alkyl chain interacting with the LAF motif towards the center of the membrane. Consistent with this model, pregnenolone, testosterone and progesterone, all with shorter and more hydrophilic tails, were not observed to be transported by mouse TSPO expressed in *E. coli* [18].

Binding behavior of *Rs*TSPO-LAF with PK11195 and PpIX.

We also tested the binding of PK11195 and PpIX with *Rs*TSPO-LAF. Our results (Figure 3.4) show that the *Rs*TSPO-LAF mutant has some influence on the binding of PK11195 and PpIX but not nearly as dramatic as the effects on cholesterol binding. Notably, the distinctive emission spectrum previously seen in PK11195 quenching curves with the *Rs*TSPO-WT protein [22] was also seen in the mutant, suggesting that the binding site of PK11195 was not strongly influenced by the mutation. Importantly, the modest effects of the three amino acid substitution in *Rs*TSPO-LAF on binding of ligands other than cholesterol indicate that it is not causing a generalized change in structure, but rather a specific localized one.
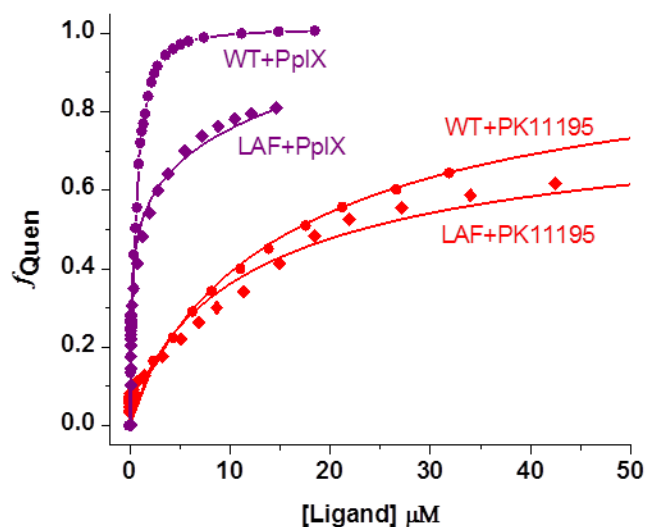
Apparent K_d values of WT and LAF mutant

	PK11195	PpIX
WT	$10 \pm 1 \ \mu M$	$0.31 \pm 0.01 \ \mu M$
LAF	$15 \pm 4 \ \mu M$	$1.1 \pm 0.1 \ \mu M$

Figure 3.4. Binding of *Rs*TSPO-LAF with PK11195 and PpIX.

Upper panel shows the binding curves for *Rs*TSPO-LAF and *Rs*TSPO WT with PpIX and PK11195. Lower panel reports the calculated K_d. Buffer conditions are as in Fig 3.3.

Interactions between helix IV and V are critical for protein stability.

Covariance analysis is a method to identify interacting residues within proteins based on the concept that residues which interact in the structure have a higher probability of undergoing parallel mutations during evolution to maintain protein function and stability. This method provides independent information to identify critical interactions between residues as well as powerful constraints for computational modeling [32]. We analyzed the sequences of TSPO with the covariance method to investigate critical residue interactions as an independent test of our previous models based on computational analysis and cryo-electron microscopy [22] as well as to provide information regarding the source of observed instability of *Rs*TSPO-LAF.

Several software packages [33-35] were used to analyze TSPO sequences and gave very similar results. The top scoring interacting residue pairs predicted by PsiCOV on the basis of 2332 sequences are plotted on the predicted topology map of *Rs*TSPO (Figure 3.5). Our analysis identified a number of high scoring interactions between helix IV and helix V, while there were very few between other helices, suggesting that these two helices may be critical for the stability of TSPO. In fact, in an early effort to obtain NMR structures of TSPO fragments, Jamin and colleagues showed that helix IV itself could not form a stable helix [31] but is stabilized by a strong interaction with helix V and maintains this association when purified in various detergents [36]. The recent NMR structure of a monomer form of mouse TSPO also shows helix IV−V association [37].
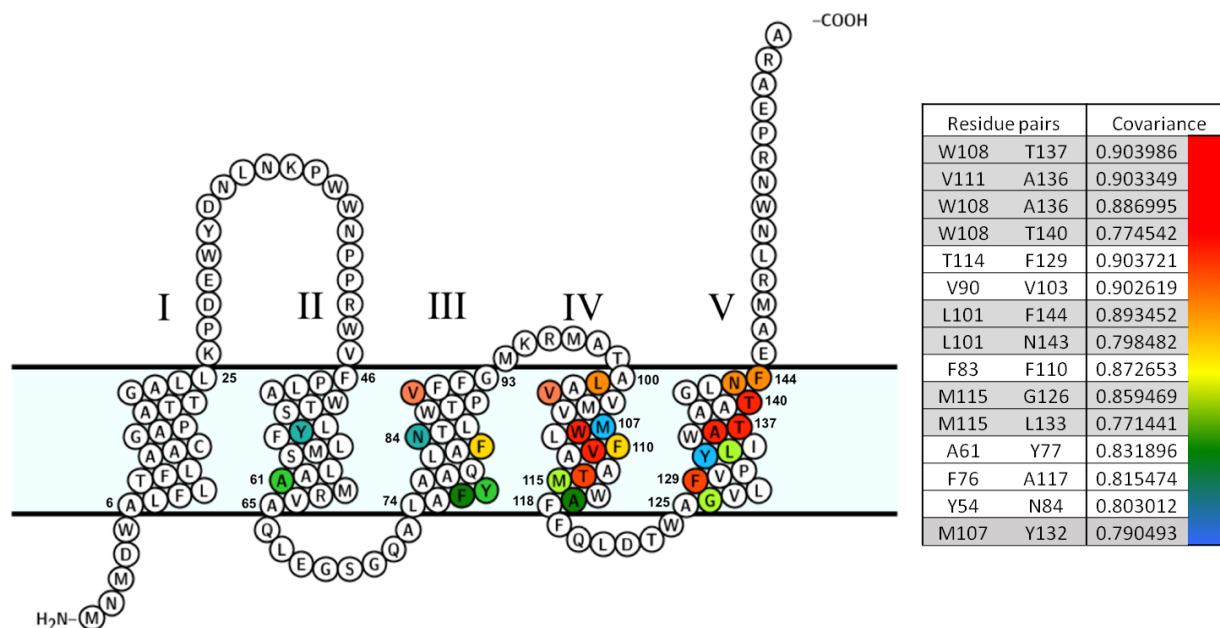
Figure 3.5. Topology diagram of *Rs*TSPO showing contact pairs predicted by covariance analysis.

Helices are marked with Roman numerals. Predicted residue contact pairs are rendered in the same color. Their covariances are calculated with PsiCOV [33]. Top 15 helical residue contact pairs are shown (covariance > 0.77).This diagram is produced with the Protter web application [38]. The sequence and helix information is from Toppred [11].

The two highest scoring interactions predicted by this covariance analysis are exactly within the ATA/LAF region (*Rs* residues 136,137 shown in red in Figure 3.5), providing an explanation for the observed lower stability of the TSPO-LAF mutant. Independently, the hydrogen/deuterium (H/D) exchange analysis performed by an NMR group also shows that these residues on helix IV and V are the most stable core in the whole protein [37]. In the wild type *Rs*TSPO, A136 and T137 on helix V are predicted to have strong interactions with V111 and W108 on helix IV. In our *Rs*TSPO-LAF mutant, we have created a better binding site for cholesterol at the expense of weakening some of these critical interactions, accounting for the observed lesser stability. For instance, in *Rs*TSPO-WT, alanine136 on helix V is predicted to pair with bulky residues, either tryptophan108 or valine111 on helix IV, while in the human/mouse protein the larger leucine of LAF, the equivalent of 136, is paired with a smaller serine at the equivalent of 108 or a smaller alanine at the equivalent of V111. By making double mutants that take into account these pairings, a more stable form with high cholesterol affinity might be achieved.

Evolution of the cholesterol binding enhancement motif.

The region immediately preceding the previously identified CRAC motif is suggested to be important for the function of human TSPO on the basis of the characteristics of a human polymorphism A147T [19,21]. In addition to A147, we further identify a motif that includes residues L144-A145-F146 in human TSPO (136,137,138 in *Rs*TSPO) as playing an important role in determining the high affinity of mammalian TSPO for cholesterol, a property not found in the bacterial proteins which lack this LAF sequence.

To investigate the evolutionary significance of the LAF motif, we analyzed the sequences of TSPO proteins from a set of different species previously described [3,39]. Our analysis shows

that the cholesterol binding enhancement motif is very well conserved within mammals as Leu-Ala-Phe (LAF, Figure 3.6 A&C), including human and mouse where extensive studies have shown that TSPO plays a critical role in cholesterol transport into mitochondria and steroidogenesis [40,41]. While bacteria and archaea have a similar CRAC sequence with the central Y replaced by F, their LAF motifs are very diverse. Hopanoids, which have a very similar ring structure to cholesterol, have been identified in bacteria [42,43] as serving a similar function to cholesterol in the higher animals. However, they can have quite different tails as shown by two representative hopanoids in Figure 3.6B, suggesting the tail could range from very long and hydrophilic to very short and hydrophobic. The more variable motif in bacteria and other lower orders may reflect the need to accommodate the distinctive tails of the hopanoids in different bacteria, or to accommodate alternative ligands. Note that helix IV is also much more conserved within mammals as compared to bacteria. Taken together with the covariance evidence that helices IV and V interact and co-evolve, our results are consistent with the increasing functional importance of cholesterol and its metabolic products in higher animals, supplying a selection pressure for the evolution of high affinity cholesterol binding involving the enhancement motif. Indeed, all mammals that metabolize cholesterol in mitochondria as the sole source of steroid hormones seem to preserve the high affinity LAF sequence in this motif.
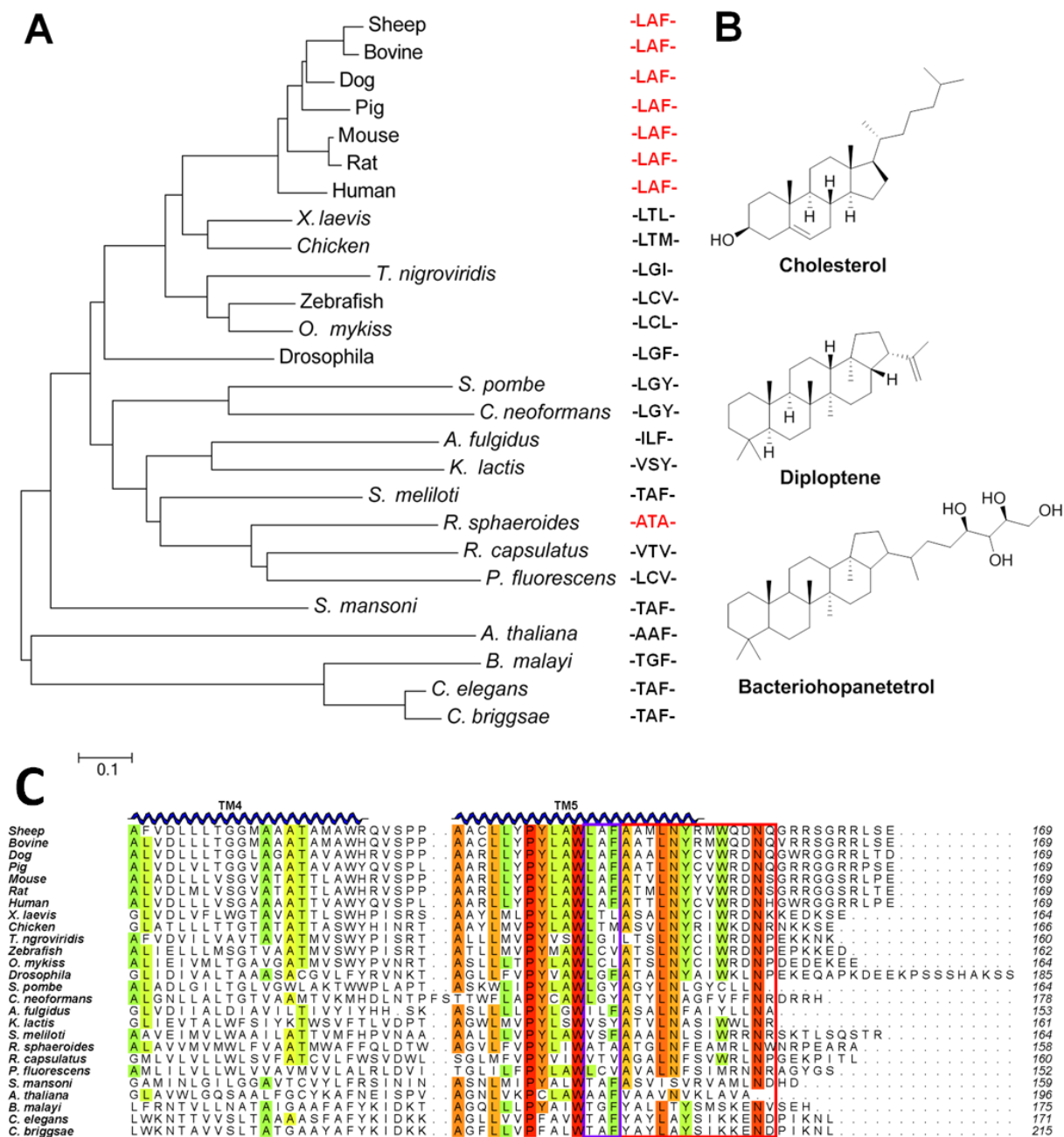
Figure 3.6. Evolution of TSPO and correlation with LAF motif.

(A) Phylogenetic tree of TSPO from selected species showing the presence/absence of the LAF motif; (B) structure of cholesterol and of two representative hopanoids; (C) sequence alignment of helix IV and helix V of TSPO from selected species.

The cholesterol binding enhancement motif exists in other membrane proteins and may indicate the presence of high affinity cholesterol binding sites.

Cholesterol is a major component of the membranes of higher animals, accounting for around 30% of the lipid bilayer [44], and it plays a critical role as the source of all steroid hormones as well as regulating the chemical and physical properties of membranes and thus membrane embedded proteins. Interest in this latter role of cholesterol has been stimulated by the increasing number of high resolution membrane protein structures in which cholesterol binding sites are observed or predicted [45-48]. The identification of the CRAC site in TSPO [18,29] led to its recognition in other membrane proteins and suggested its general importance, but other motifs have also been found [48,49]. In this study, we identify a motif adjacent to the CRAC site in TSPO which enhances cholesterol binding and is highly conserved in mammals. Some interesting questions are raised by our findings: 1) is this enhancement motif also present in other membrane proteins that are regulated by cholesterol; 2) is this motif found in all mammalian CRAC sites or only a subset; and 3) is the presence of this enhancement motif in other membrane proteins associated with any common characteristic?

To address some of these questions, we surveyed 5183 currently identified human membrane proteins from the UniProtKB/Swiss-Prot database. Both CRAC and LAF-x(2-5)-CRAC, which allows 2-5 residues between the LAF and CRAC sites, were searched by the Fuzzpro program. A total of 28627 CRAC sites were identified in 4684 human membrane proteins, about 6 sites per protein on average, while only 66 LAF-$_{x(2-5)}$-CRAC sites were identified in 66 membrane proteins, including members from all major membrane protein families (Table 3.1). Although the finding of 6 CRAC sites/protein in so many proteins is theoretically possible, the result is more consistent with this broadly defined motif having relatively low predictive ability, as concluded

by Sanders *et al.* [50]. In contrast, the much smaller subset found with the extended motif suggests more predictive value.

Table 3.1 Classification of human membrane proteins with the cholesterol binding enhancement motif

Membrane protein family	Within transmembrane helix	In extracellular domains	Total
Receptors	16 (33%)	2 (12 %)	18 (27%)
Transporters	8 (16%)	0 (0%)	8 (12%)
Ion channels	4 (8.2%)	2 (12%)	6 (9.1%)
Enzymes	2 (4.1%)	8 (47%)	10 (15%)
Others	19 (39%)	5 (29%)	24 (36%)
Total	49 (100%)	17 (100%)	66 (100%)

Out of the 66 identified sites, 49 are in the later half of transmembrane helices, similar to the location in TSPO and topologically consistent with the hydroxyl of cholesterol being close to the membrane surface. The significance of sites identified by the LAF-CRAC motif remains to be determined as more cholesterol-regulated membrane proteins are characterized biochemically and structurally, but it seems likely that they represent higher affinity binding modes with functional significance beyond that conferred by cholesterol as solvent. The location of TSPO in mitochondria, which are low in cholesterol [44], and the function of TSPO as part of a cholesterol transport system, are consistent with a requirement for the enhancement motif we have identified in mammalian TSPO to provide significantly increased affinity for cholesterol. Indeed a LAF-CRAC sequence is identified in the predicted transmembrane helix 2 of the StAR-related lipid transfer protein 3 (STARD3). This protein has a steroidogenic acute regulatory protein domain (StAR) in the extracellular domain and has been proposed to translocate cholesterol between endosomes and mitochondria [51,52] similar to the proposed TSPO-StAR transport system [53]. Also identified in our survey to have the enhanced cholesterol binding motif is the sodium-dependent bile acid transporter (SLC10A2). The substrate, a derivative of cholesterol, is seen in crystals of a bacterial homolog [54] to occupy a binding pocket where the LAF-CRAC sequence is also found in the human homolog [55]. Since cholesterol has been shown to be a regulator of this bile acid transporter [56] the proximity of these sites could be significant.

Our survey suggests that cholesterol binding sites with the enhancement motif are fairly widespread and could be critical for high affinity binding involved in transport or regulation, while the CRAC sequence alone and other motifs may represent sites important for other membrane-mediated cholesterol effects such as protein/protein association and domain formation

[50].

SUMMARY

Biochemical, mutational and evolutionary covariance studies of the purified bacterial homolog of mitochondrial TSPO identify a cholesterol-binding enhancement motif that is highly conserved in mammalian but not bacterial proteins. This motif in the C-terminal transmembrane helix V of TSPO, adjacent to the previously identified CRAC sequence and a human single polymorphism associated with bipolar disorder, significantly affects affinity for cholesterol. The altered properties of a purified mutant form are consistent with genetic covariance analysis and previous NMR studies that show this region to be of critical importance to the structure and function of TSPO. The cholesterol binding enhancement motif associated with CRAC is conserved in mammalian TSPO and also identified in many human membrane proteins. Our survey suggests that the enhancement motif may be useful for identifying high affinity cholesterol binding regions with functional and regulatory significance.

REFERENCES

REFERENCES

1. Braestrup C, Squires RF: **Specific benzodiazepine receptors in rat brain characterized by high-affinity (3H)diazepam binding**. *Proc Natl Acad Sci U S A* 1977, **74**:3805-3809.

2. Papadopoulos V, Baraldi M, Guilarte TR, Knudsen TB, Lacapère JJ, Lindemann P, Norenberg MD, Nutt D, Weizman A, Zhang MR, et al.: **Translocator protein (18kDa): new nomenclature for the peripheral-type benzodiazepine receptor based on its structure and molecular function**. *Trends Pharmacol Sci* 2006, **27**:402-409.

3. Fan J, Lindemann P, Feuilloley MG, Papadopoulos V: **Structural and functional evolution of the translocator protein (18 kDa)**. *Curr Mol Med* 2012, **12**:369-386.

4. Krueger KE: **Molecular and functional properties of mitochondrial benzodiazepine receptors**. *Biochim Biophys Acta* 1995, **1241**:453-470.

5. Crompton M: **The mitochondrial permeability transition pore and its role in cell death**. *Biochem J* 1999, **341 (Pt 2)**:233-249.

6. Verma A, Snyder SH: **Peripheral type benzodiazepine receptors**. *Annu Rev Pharmacol Toxicol* 1989, **29**:307-322.

7. Barron AM, Garcia-Segura LM, Caruso D, Jayaraman A, Lee JW, Melcangi RC, Pike CJ: **Ligand for translocator protein reverses pathology in a mouse model of Alzheimer's disease**. *J Neurosci* 2013, **33**:8891-8897.

8. Lin R, Angelin A, Settimo FD, Martini C, Taliani S, Zhu S, Wallace DC: **Genetic analysis of dTSPO, an outer mitochondrial membrane protein, reveals its functions in apoptosis, longevity, and Aβ42-induced neurodegeneration.** *Aging Cell*. 2014, **13**:507-518.

9. Papadopoulos V, Amri H, Boujrad N, Cascio C, Culty M, Garnier M, Hardwick M, Li H, Vidic B, Brown AS, et al.: **Peripheral benzodiazepine receptor in cholesterol transport and steroidogenesis**. *Steroids* 1997, **62**:21-28.

10. Anholt RR, Pedersen PL, De Souza EB, Snyder SH: **The peripheral-type benzodiazepine receptor. Localization to the mitochondrial outer membrane**. *J Biol Chem* 1986, **261**:576-583.

11. Cserzö M, Wallin E, Simon I, von Heijne G, Elofsson A: **Prediction of transmembrane alpha-helices in prokaryotic membrane proteins: the dense alignment surface method**. *Protein Eng* 1997, **10**:673-676.

12. Morohaku K, Pelton SH, Daugherty DJ, Butler WR, Deng W, Selvaraj V: **Translocator protein/peripheral benzodiazepine receptor is not required for steroid hormone biosynthesis**. *Endocrinology* 2014, **155**:89-97.

13. Hardwick M, Fertikh D, Culty M, Li H, Vidic B, Papadopoulos V: **Peripheral-type benzodiazepine receptor (PBR) in human breast cancer: correlation of breast cancer cell aggressive phenotype with PBR expression, nuclear localization, and PBR-mediated cell proliferation and nuclear transport of cholesterol**. *Cancer Res* 1999, **59**:831-842.

14. Chen MK, Guilarte TR: **Translocator protein 18 kDa (TSPO): molecular sensor of brain injury and repair**. *Pharmacol Ther* 2008, **118**:1-17.

15. Bird JL, Izquierdo-Garcia D, Davies JR, Rudd JH, Probst KC, Figg N, Clark JC, Weissberg PL, Davenport AP, Warburton EA: **Evaluation of translocator protein quantification as a tool for characterising macrophage burden in human carotid atherosclerosis**. *Atherosclerosis* 2010, **210**:388-391.

16. Lucki NC, Li D, Sewer MB: **Sphingosine-1-phosphate rapidly increases cortisol biosynthesis and the expression of genes involved in cholesterol uptake and transport in H295R adrenocortical cells**. *Mol Cell Endocrinol* 2012, **348**:165-175.

17. Chauveau F, Boutin H, Van Camp N, Dollé F, Tavitian B: **Nuclear imaging of neuroinflammation: a comprehensive review of [11C]PK11195 challengers**. *Eur J Nucl Med Mol Imaging* 2008, **35**:2304-2319.

18. Li H, Papadopoulos V: **Peripheral-type benzodiazepine receptor function in cholesterol transport. Identification of a putative cholesterol recognition/interaction amino acid sequence and consensus pattern**. *Endocrinology* 1998, **139**:4991-4997.

19. Costa B, Pini S, Gabelloni P, Da Pozzo E, Abelli M, Lari L, Preve M, Lucacchini A, Cassano GB, Martini C: **The spontaneous Ala147Thr amino acid substitution within the translocator protein influences pregnenolone production in lymphomonocytes of healthy individuals**. *Endocrinology* 2009, **150**:5438-5445.

20. Colasanti A, Owen DR, Grozeva D, Rabiner EA, Matthews PM, Craddock N, Young AH: **Bipolar Disorder is associated with the rs6971 polymorphism in the gene encoding 18 kDa Translocator Protein (TSPO)**. *Psychoneuroendocrinology* 2013, **38**:2826-2829.

21. Owen DR, Yeo AJ, Gunn RN, Song K, Wadsworth G, Lewis A, Rhodes C, Pulford DJ, Bennacef I, Parker CA, et al.: **An 18-kDa translocator protein (TSPO) polymorphism explains differences in binding affinity of the PET radioligand PBR28**. *J Cereb Blood Flow Metab* 2012, **32**:1-5.

22. Li F, Xia Y, Meiler J, Ferguson-Miller S: **Characterization and modeling of the oligomeric state and ligand binding behavior of purified translocator protein 18 kDa from** *Rhodobacter sphaeroides*. *Biochemistry* 2013, **52**:5884-5899.

23. Sievers F, Wilm A, Dineen D, Gibson TJ, Karplus K, Li W, Lopez R, McWilliam H, Remmert M, Söding J, et al.: **Fast, scalable generation of high-quality protein multiple sequence alignments using Clustal Omega**. *Mol Syst Biol* 2011, **7**:539.

24. Bond CS, Schüttelkopf AW: **ALINE: a WYSIWYG protein-sequence alignment editor for publication-quality alignments**. *Acta Crystallogr D Biol Crystallogr* 2009, **65**:510-512.

25. Tamura K, Stecher G, Peterson D, Filipski A, Kumar S: **MEGA6: Molecular Evolutionary Genetics Analysis version 6.0**. *Mol Biol Evol* 2013, **30**:2725-2729.

26. Yeliseev AA, Kaplan S: **TspO of** *Rhodobacter sphaeroides*. **A structural and functional model for the mammalian peripheral benzodiazepine receptor**. *J Biol Chem* 2000, **275**:5657-5667.

27. Yeliseev AA, Krueger KE, Kaplan S: **A mammalian mitochondrial drug receptor functions as a bacterial "oxygen" sensor**. *Proc Natl Acad Sci U S A* 1997, **94**:5101-5106.

28. Farges R, Joseph-Liauzun E, Shire D, Caput D, Le Fur G, Ferrara P: **Site-directed mutagenesis of the peripheral benzodiazepine receptor: identification of amino acids implicated in the binding site of Ro5-4864**. *Mol Pharmacol* 1994, **46**:1160-1167.

29. Li H, Yao Z, Degenhardt B, Teper G, Papadopoulos V: **Cholesterol binding at the cholesterol recognition/ interaction amino acid consensus (CRAC) of the peripheral-type benzodiazepine receptor and inhibition of steroidogenesis by an HIV TAT-CRAC peptide**. *Proc Natl Acad Sci U S A* 2001, **98**:1267-1272.

30. Rupprecht R, Papadopoulos V, Rammes G, Baghai TC, Fan J, Akula N, Groyer G, Adams D, Schumacher M: **Translocator protein (18 kDa) (TSPO) as a therapeutic target for neurological and psychiatric disorders**. *Nat Rev Drug Discov* 2010, **9**:971-988.

31. Jamin N, Neumann JM, Ostuni MA, Vu TK, Yao ZX, Murail S, Robert JC, Giatzakis C, Papadopoulos V, Lacapère JJ: **Characterization of the cholesterol recognition amino acid consensus sequence of the peripheral-type benzodiazepine receptor**. *Mol Endocrinol* 2005, **19**:588-594.

32. de Juan D, Pazos F, Valencia A: **Emerging methods in protein co-evolution**. *Nat Rev Genet* 2013, **14**:249-261.

33. Jones DT, Buchan DW, Cozzetto D, Pontil M: **PSICOV: precise structural contact prediction using sparse inverse covariance estimation on large multiple sequence alignments**. *Bioinformatics* 2012, **28**:184-190.

34. Yang J, Jang R, Zhang Y, Shen HB: **High-accuracy prediction of transmembrane inter-helix contacts and application to GPCR 3D structure modeling**. *Bioinformatics* 2013, **29**:2579-2587.

35. Kamisetty H, Ovchinnikov S, Baker D: **Assessing the utility of coevolution-based residue-residue contact predictions in a sequence- and structure-rich era**. *Proc Natl Acad Sci U S A* 2013, **110**:15674-15679.

36. Galvagnion C, Montaville P, Coïc YM, Jamin N: **Production and initial structural characterization of the TM4TM5 helix-loop-helix domain of the translocator protein**. *J Pept Sci* 2013, **19**:102-109.

37. Jaremko L, Jaremko M, Giller K, Becker S, Zweckstetter M: **Structure of the mitochondrial translocator protein in complex with a diagnostic ligand**. *Science* 2014, **343**:1363-1366.

38. Omasits U, Ahrens CH, Müller S, Wollscheid B: **Protter: interactive protein feature visualization and integration with experimental proteomic data**. *Bioinformatics* 2014, **30**:884-886.

39. Fan J, Papadopoulos V: **Evolutionary origin of the mitochondrial cholesterol transport machinery reveals a universal mechanism of steroid hormone biosynthesis in animals**. *PLoS One* 2013, **8**:e76701.

40. Papadopoulos V, Amri H, Boujrad N, Cascio C, Culty M, Garnier M, Hardwick M, Li H, Vidic B, Brown AS, et al.: **Peripheral benzodiazepine receptor in cholesterol transport and steroidogenesis**. *Steroids* 1997, **62**.

41. Papadopoulos V, Lecanu L, Brown RC, Han Z, Yao ZX: **Peripheral-type benzodiazepine receptor in neurosteroid biosynthesis, neuropathology and neurological disorders**. *Neuroscience* 2006, **138**:749-756.

42. Rohmer M, Bouviernave P, Ourisson G: **Distribution of hapanoid triperpene in prokaryotes**. *J Gen Micro*1984, **130**:1137-1150.

43. Poger D, Mark AE: **The relative effect of sterols and hopanoids on lipid bilayers: when comparable is not identical**. *J Phys Chem B* 2013, **117**:16129-16140.

44. van Meer G, Voelker DR, Feigenson GW: **Membrane lipids: where they are and how they**

behave. *Nat Rev Mol Cell Biol* 2008, **9**:112-124.

45. Singh AK, McMillan J, Bukiya AN, Burton B, Parrill AL, Dopico AM: **Multiple cholesterol recognition/interaction amino acid consensus (CRAC) motifs in cytosolic C tail of Slo1 subunit determine cholesterol sensitivity of Ca2+- and voltage-gated K+ (BK) channels**. *J Biol Chem* 2012, **287**:20509-20521.

46. Barrett P, Song Y, Van Horn W, Hustedt E, Schafer J, Hadziselimovic A, Beel A, Sanders C: **The amyloid precursor protein has a flexible transmembrane domain and binds cholesterol**. *Science* 2012, **336**:1168-1171.

47. Picazo-Juárez G, Romero-Suárez S, Nieto-Posadas A, Llorente I, Jara-Oseguera A, Briggs M, McIntosh TJ, Simon SA, Ladrón-de-Guevara E, Islas LD, et al.: **Identification of a binding motif in the S5 helix that confers cholesterol sensitivity to the TRPV1 ion channel**. *J Biol Chem* 2011, **286**:24966-24976.

48. Hanson MA, Cherezov V, Griffith MT, Roth CB, Jaakola VP, Chien EY, Velasquez J, Kuhn P, Stevens RC: **A specific cholesterol binding site is established by the 2.8 A structure of the human beta2-adrenergic receptor**. *Structure* 2008, **16**:897-905.

49. Baier CJ, Fantini J, Barrantes FJ: **Disclosure of cholesterol recognition motifs in transmembrane domains of the human nicotinic acetylcholine receptor**. *Sci Rep* 2011, **1**:69.

50. Song Y, Kenworthy AK, Sanders CR: **Cholesterol as a co-solvent and a ligand for membrane proteins**. *Protein Sci* 2014, **23**:1-22.

51. Alpy F, Tomasetto C: **MLN64 and MENTHO, two mediators of endosomal cholesterol transport**. *Biochem Soc Trans* 2006, **34**:343-345.

52. Charman M, Kennedy BE, Osborne N, Karten B: **MLN64 mediates egress of cholesterol from endosomes to mitochondria in the absence of functional Niemann-Pick Type C1 protein**. *J Lipid Res* 2010, **51**:1023-1034.

53. Rone MB, Fan J, Papadopoulos V: **Cholesterol transport in steroid biosynthesis: role of protein-protein interactions and implications in disease states**. *Biochim Biophys Acta* 2009, **1791**:646-658.

54. Hu NJ, Iwata S, Cameron AD, Drew D: **Crystal structure of a bacterial homologue of the bile acid sodium symporter ASBT**. *Nature* 2011, **478**:408-411.

55. Hussainzada N, Banerjee A, Swaan PW: **Transmembrane domain VII of the human apical sodium-dependent bile acid transporter ASBT (SLC10A2) lines the substrate**

translocation pathway. *Mol Pharmacol* 2006, **70**:1565-1574.

56. Alrefai WA, Sarwar Z, Tyagi S, Saksena S, Dudeja PK, Gill RK: **Cholesterol modulates human intestinal sodium-dependent bile acid transporter**. *Am J Physiol Gastrointest Liver Physiol* 2005, **288**:G978-985.

CHAPTER 4

Crystallization strategies of small *α* helical integral membrane proteins: a case study of Translocator Protein 18 kDa from *Rhodobacter sphaeroides* (*Rs*TSPO)

INTRODUCTION

Membrane proteins play important roles in all living organisms, promoting a strong interest in understanding their structures and functions in detail. Recent developments in biochemistry and biophysics have greatly improved our ability to investigate membrane proteins. In particular, the technical developments in the field of membrane protein crystallography, including development of alternative crystallization methods for membrane proteins [1,2], high throughput robotic machines [3], and the optimization of synchrotron beamlines for membrane protein crystals [4] have allowed us to obtain high resolution structures of important membrane proteins at an unprecedented rate (http://blanco.biomol.uci.edu/mpstruc/#Latest). As a result, our understanding of various processes involving membrane proteins has tremendously improved over the past decades, providing critical information for understanding the fundamental mechanisms of membrane proteins as well as for rational design of drugs targeting membrane proteins. Despite these developments, obtaining high resolution crystal structures of membrane proteins remains a formidable task, and often requires significant experimentation and optimization. Every successfully solved membrane protein crystal structure, especially those with unique properties and/or those that are underrepresented in the current PDB, provides valuable information to help us with mastering the art of membrane protein crystallization.

TSPO from *Rhodobacter sphaeroides* (*Rs*TSPO) represents a type of small membrane protein that is mainly composed of α-helices without big cytoplasmic domains for mediating crystal contacts. The structure determination of *Rs*TSPO was a challenging project in that significant optimization was needed in almost every step to achieve the final high resolution structures of this unique membrane protein. Investigation and optimization of the crystallization strategies for *Rs*TSPO was systematic and extensive, spanning from the traditional vapor

diffusion method to the newly developed lipidic cubic phase (LCP) method. From this perspective, the optimization process to obtain crystals of *Rs*TSPO is a valuable case study that provides important lessons for optimizing crystallization conditions for similar types of small and hydrophobic integral membrane proteins.

Over the past 20 years, alternative crystallization methods for membrane proteins have been developed and optimized, and have shown great potential. In general, these methods aim to provide a more natural environment for membrane proteins during crystallization. Such an environment has a bilayer structure with more lipid content compared to the protein-detergent complexes used in the regular vapor diffusion method. One example of these methods is the bicelle method [2], proposed and popularized by Dr. James Bowie's group, that reconstitutes the detergent solubilized membrane protein into small bilayer-like discs before setting up a regular vapor diffusion crystallization experiment. Other alternatives involve addition of detergent and/or lipids during steps of purification and crystallization and have been successful in various cases [5,6].

The LCP (also know as *in meso*) crystallization method first pioneered by Landau and Rosenbusch [7] and further developed by Dr. Martin Caffrey's group [1] aims to better mimic the continuous bilayer environment during crystallization with the use of bilayer forming lipids to host membrane proteins. The LCP method has shown great success with multiple classes of membrane proteins including beta-barrels [8], alpha-helical transmembrane proteins [9], and challenging membrane protein complexes [10]. The LCP method takes advantage of the phase behavior of monoacylglycerol (MAG) lipids when mixed with aqueous solutions (i.e., protein solutions). A bicontinuous three-dimensional highly curved lipid bilayer consisting of interpenetrating but non-communicating aqueous channels forms spontaneously when the MAG

is mixed with a protein-water solution at a certain ratio. The specific structure formed is named as the cubic phase or Pn3m phase [7]. This continuous bilayer serves as the stabilizing matrix for membrane proteins incorporated in it, as well as providing the channels and portals allowing diffusion and crystallogenesis [1].

Despite extensive screening with the vapor diffusion method, it failed to produce good diffraction quality crystals of *Rs*TSPO under all conditions tested. The choice of the LCP crystallization method, which promotes type I crystal packing, was the key breakthough in obtaining *Rs*TSPO crystals. Additionally, additives such as ligands and lipids also play important roles in stabilizing the purified membrane protein and are frequently screened during the optimization [11,12]. In the case of *Rs*TSPO, the addition of high affinity ligands significantly improved the crystal size and quality, which eventually allowed structure determination. In addition, a mutant form designed to mimic a human polymorphism, A147T (A139T in *Rs*TSPO), that is associated with anxiety related disease, was found to give the most stable and well diffracting crystals.

MATERIAL AND METHODS

Materials

Chemicals were purchased from Sigma-Aldrich. All detergents were purchased from Anatrace (Maumee, OH). Lipids were purchased from Avanti Polar Lipids. The *Rs*TSPO expression plasmid was a gift from Dr. Samuel Kaplan from the University of Texas. *Pfu* Turbo[®] polymerase was purchased from Agilent Technologies (Santa Clara, CA). Restriction enzymes and T4 ligase were purchased from New England Biolabs (Ipswich, MA).

Methods

Protein expression and purification

The pRK415 plasmid containing the coding sequence of RsTSPO with a C-terminal 10 Histag (RsTSPO10ht) was transformed into the *E. coli* BL21 λDE3 strain. The transformed bacteria were cultured at 30 °C in 100 mL LB medium containing appropriate antibiotics overnight. Fifteen mL of the overnight culture were then transferred into 1 L of auto-induction media (ZYM-5025) [13] containing glycerol, glucose and lactose and the appropriate antibiotics. Cultures were grown at 30 °C. Cells were harvested when the OD_{600} reached above 4.0 (usually after overnight growth). Harvested cells were resuspended in lysis buffer (50 mM KH_2PO_4 pH 6.5, 1 mM EDTA) supplemented with Roche ® protease inhibitor cocktail and were lysed by two passes through a French press homogenizer at 20,000 p.s.i. Broken cells were centrifuged at 200 x g for 5 mins, 10,000 x g for 30 mins and 150,000 x g for 90 mins at 4 °C to isolate the membranes. Isolated membranes were resuspended with buffer A (50 mM Tris-HCl, pH 8, 150 mM NaCl, 10 % glycerol) and quick-frozen with liquid nitrogen and stored at -70 °C before purification.

Membranes were thawed on ice, resuspended to 10 mg/ml total protein in buffer A, solubilized by adding detergent, 1 mM PMSF and Roche ® protease inhibitor cocktail (no EDTA) and stirred at 4 °C for 1 hr. Solubilized membranes were centrifuged at 150,000 x g for 30 mins to remove the unsolubilized fraction. The supernatant was loaded on a 10 mL Ni-NTA (Qiagen ®) gravity column pre-equilibrated with 3 column volumes (CV) of buffer A followed by 1 CV of buffer A with 10 mM imidazole. After extensive washing with buffer A supplemented with detergent at the appropriate concentration and 50 mM imidazole, fractions containing the desired

protein were eluted using buffer A supplemented with detergent at appropriate concentration and 300 mM imidazole over two CV. Absorption at 280 nm was used to monitor the washing and elution process. Fractions containing the desired protein were pooled and concentrated with a 50 kDa molecular weight cut off (MWCO) Amicon Filter (Millipore [®]). Protein purified in this way was either loaded on SEC column directly to test whether the selected detergent will result in a homogenous peak of *Rs*TSPO10ht or washed with no imidazole buffer and treated with trypsin at 4 °C overnight before further purification by SEC. The purity of the protein was determined on SDS-PAGE stained with Coomassie blue.

Determination of detergent content of purified *Rs*TSPO by thin layer chromatography (TLC) and a colorimetric method

The detergent species and levels during purification was monitored by both TLC [14] and a colorimetric [15] method. Briefly, standard solutions containing known concentrations of maltoside or glucoside detergents were spotted on TLC plates together with the purified protein sample and run under the same conditions. The TLC plates were stained with iodine and alpha naphthol. Detergent present in the sample was identified by comparing the *Rf* with standards, while the density of the stained spot was quantified by using ImageJ [16] and used to calculate the concentration of detergent in the sample based on a standard curve. In the colorimetric method, standards as well as protein samples were mixed with reaction solution containing phenol and sulfuric acid and the absorbances at 490 nm were measured with a PerkinElmer [®] spectrometer. Concentrations were similarly calculated from a standard curve based on A_{490}.

Detergent exchange

Several schemes were used to exchange the detergent as well as to reduce the total detergent

concentration in the purified *Rs*TSPO samples. One way to reduce the detergent concentration was simply to wash the purified protein with no-detergent buffer during concentration. In this method, purified protein solution was mixed with equivalent buffer with no detergent at a 1:1 ratio and concentrated with the Amicon concentrator containing an appropriate MWCO membrane. The process was repeated several times to achieve the desired detergent concentration. A cholate washing step was also tried because it has been shown that cholate can help break the filament structure formed by DDM and reduce the detergent level [17]. In this method, cholate was added into the protein solution to a final concentration of 6 % followed by incubation on ice for 1 hr. An equal volume of buffer with no detergent was added and the solution was concentrated with the appropriate Amicon concentrator. Alternatively, the Pierce detergent-removal spin column was used to exchange and reduce the detergent concentration with an in-house protocol. Briefly, the spin column was equilibrated 4 times with buffer containing the desired detergent at 5x critical micelle concentration (CMC) by spinning at 1000 x *g*. Three hundred µL of the buffer containing 2x CMC of the desired detergent was then added into a clean collecting tube and 100 µL of protein sample in purification buffer containing DM was loaded onto the column, followed by centrifugation for 2 mins at 1000 x g. The protein sample in the desired final buffer was then removed from the collecting tube and concentrated with a 0.5 mL 50 kDa MWCO Amicon concentrator. The final sample was quick-frozen in liquid nitrogen and analyzed by the TLC methods previous described.

Screening for solubilizing detergent

Membranes of *E. coli* containing 10 mg/ml total protein (as determined by the bicinchoninic acid assay (BCA) assay using bovine serum albumin (BSA) as the standard) were solubilized by shaking with buffer containing 20x CMC of detergent for 2 h at 4 ℃ and centrifuged at 200,000

x *g* for 30 min. The effectiveness of solubilization was judged by comparing the supernatant with membranes solubilized by 1 % DDM by using a Western blot. Solubilized supernatant was also kept at 4 ºC to test for long time stability.

Screening and optimization of the purification detergent with SEC

Detergents were also screened directly with SEC for their ability to produce a homogeneous sample for crystallization. In this method, membranes containing *Rs*TSPO were solubilized with 1% DM and purified as previously described on a Ni-NTA column with buffer containing 0.2 % DM and 10 % glycerol. *Rs*TSPO10ht was then directly loaded onto a Superose12 $^{®}$ gel filtration column equilibrated with buffer containing 50 mM NaCl, 150 mM NaCl, 10 % glycerol and the desired detergent.

Optimization of SEC conditions

For any detergent that was able to give a homogeneous peak of *Rs*TSPO10ht, the SEC conditions were fine-tuned by testing if the Histag and glycerol influence the purification. *Rs*TSPO10ht samples were purified as described previously and run in buffer without glycerol. Concentrated *Rs*TSPO10ht samples were washed once and diluted with no-imidazole buffer to 10 ml and incubated with trypsin overnight to remove the Histag. Samples were then concentrated with a 30 kDa MWCO Amicon filter unit down to 250 uL and loaded on the Superose12 $^{®}$ gel filtration column. Samples of good quality were concentrated and used in crystallization screening directly.

The optimized purification procedure were to purify *Rs*TSPO with buffer containing 0.2 % DM and 10 % glycerol up to the setup of the SEC. Ni-NTA purified *Rs*TSPO10ht was concentrated to less than 1 mL with a 50 kDa MWCO Amicon filter unit and washed with 10 mL

buffer with no imidazole. This sample was concentrated again to less than 250 uL before being diluted to 10 mL and adding trypsin for digestion overnight. The trypsin treated *Rs*TSPO sample was then concentrated with a 30 kDa MWCO Amicon filter unit down to 250 uL and run on a Superdex 200 gel filtration column with buffer containing 0.2 % DM but no glycerol.

Crystallization screening of *Rs*TSPO with the vapor diffusion method

The traditional vapor diffusion method [18] was first used to grow crystals with samples purified by Ni-NTA and SEC. Both *Rs*TSPO10ht and *Rs*TSPO purified with various detergent conditions were screened. High throughput screening plates were set up with the Crystal Gryphon ® (Art Robbins Instruments) robot with 200 nL protein:200 nL screen solution ratio with a wide range of commercial crystallization screens. Different protein:screen solution ratios at 1:2, 1:3 and 2:1 were also tested. Wells were examined under regular light as well as polarized light with a microscope periodically. Scaled-up sitting drop or hanging drop trays were set up for conditions that showed promising results from the initial screens. Initial leads were scaled up and optimized with 1 µL protein:1 µL screen solution in both sitting drop and hanging drop formats. All crystals were harvested with cryoloops and directly frozen in liquid nitrogen before being tested for diffraction quality.

Crystallization screening of *Rs*TSPO with the LCP method

Initial high throughput screening for crystallization conditions of *Rs*TSPO with the LCP method was done at the NIH-supported membrane protein center of Dr. Stroud at UCSF. *Rs*TSPO was purified in 0.2 % DM buffer without glycerol and concentrated to 30 mg/ml with a 30 kDa MWCO Amicon concentrator. Purified *Rs*TSPO (30 mg/mL) was incorporated into monoolein (MO) (v/v 2:3) by mechanical mixing. One hundred nL of the protein-lipid mixture

was dispensed onto the plastic plates by the LCP Mosquito$^®$ robot and 1 µL of precipitant solution was laid on top of the protein-lipid bolus. Plates were sealed by covering the well with another plastic cover and incubated at 20 ºC. Plates were monitored under bright light as well as with the polarizer and UV light to confirm the growth of protein crystals.

Optimization of crystal leads with the LCP method

Further optimization of the lead conditions with both the LCP and sponge phase methods was done at MSU. In the sponge phase method, 0.5 µL protein-MO mixture was covered with 2 µL precipitant solution and set up in a hanging drop setup with 125 µL reservoir solution. Initial crystallization conditions were more finely screened by varying the pH, PEG concentration, additive, and host lipid. Glass plates and coverslips were used in all optimization plates to enable crystal harvesting.

Crystals were harvested with Mitigen$^®$ microloops or micromesh by using published protocols [19,20]. Briefly, the glass coverslip was cut open with a capillary cutter and screen solutions were laid on top before opening the well. Screen solution was also injected into the well through holes opened at the corner of the cut coverslip. Broken glass was carefully removed piece by piece with fine tweezers while screen solution was added to keep the LCP bolus from drying. Crystals were harvested from the LCP bolus with a microloop or micromesh matching the size of the crystal and immediately frozen with liquid nitrogen. The entire process was monitored under the microscope with a polarizer to keep track of small crystals that were only visible by this approach.

Preparation of heavy metal derivative of the *Rs*TSPO A139T crystal

A tantalum bromide cluster $(Ta_6Br_{12})Br_2$ was soaked into A139T crystals at 1 mM final

concentration, while another potential heavy metal derivative was obtained by co-crystallizing the A139T protein with mercury thiocyanide, Hg(SCN), under the same crystallization conditions, but the concentrated heavy metal stock solution was pre-spotted and dried on the crystallization plate before setting up crystals. Sixteen different heavy metal containing solutions were used at two different concentrations each. The A139T crystal containing the Hg derivative appeared after around two weeks.

Data collection and processing

Diffraction data on crystals from the vapor diffusion conditions were collected at 100 K at LS-CAT (beamlines 21ID-G and 21ID-F) at the Advanced Photon Source (APS), Argonne National Laboratory. Data on crystals from LCP conditions were collected at GM/CA-CAT (beamline 23ID-B and 23ID-D) at APS. Crystals buried in the LCP bolus on the micromesh were located by X-ray diffraction with an attenuated beam with proper rastering strategies before data collection. Data were collected with a 5 μm micro-focusing beam at full beam intensity. Wedges containing 10-30 degrees of data were individually processed with the XDS software (Version March 20, 2013) [21] and merged and scaled with Aimless (CCP4 6.3.0) [22,23] to make the complete dataset for structure determination. Data from the heavy metal derivative crystals were collected using either the peak wavelength of the tantalum L3 edge (1.255 keV) or of the mercury L3 edge (1.007 Å) at the 23ID-B beamline (Advanced Photon Source). Complete (360˚) datasets for each derivative were acquired from single crystals by using a 10 μm minibeam at 20x attenuation with 1˚ oscillation and 1 s exposure per frame; the data were collected in 30˚ wedges with direct and inverse beams, combined with a helical rotation strategy to minimize the radiation damage and maximize the anomalous signal. The Ta dataset was integrated and scaled to 3.7 Å resolution and the Hg dataset was integrated and scaled to 3.2 Å by using HKL2000

(HKL Research) and XDS [21].

Structure determination and refinement

The A139T mutant structure was solved by using multiple isomorphous replacement-anomalous scattering phasing with the Ta and Hg datasets combined with the high resolution native dataset method in SHARP (version 2.8.2) [24]. Complete models for the three *Rs*TSPO monomers in the A139T C2 asymmetric unit, except for loop 1 from one of the 3 monomers, were easily autotraced and built in SHARP after the initial rounds of density modification. The structure of wild type *Rs*TSPO was solved by molecular replacement with a partially refined model of the A139T mutant. Initial refinement for all structures was performed iteratively with Phenix.refine [25] followed by manual examination and model rebuilding with the program Coot 7.2 [26] against 2Fo-Fc and Fo-Fc maps. Final refinement were done with Phenix-1.9-1692 [25], followed by iterative rebuilding of the model with Coot 7.2 [26] against 2Fo-Fc, Fo-Fc, and feature-enhanced maps (Phenix-1.9-1692).

RESULTS

Initial crystallization screening with *Rs*TSPO purified in DM indicated inhibition of crystallization by detergent

The initial purification scheme developed by Dr. Ferguson-Miller in collaboration with Dr. John Lee (UCSF) gave good yield of *Rs*TSPO in high purity (Figure 4.1). A time course of trypsin digestion showed that trypsin immediately cut around 50 % of *RsT*SPO10ht while the SEC showed a major homogenous peak of *Rs*TSPO at around 44 kDa. One percent DDM was used for membrane solubilization in this method while all purification, including both Ni-NTA and SEC, was done in buffer supplemented with 0.2 % DM and 10 % glycerol. The main peak P3 (Figure 4.1A) was screened with several commercial high throughput crystallization kits at 6

mg/mL, 10 mg/mL and 15 mg/mL protein concentrations. Quasi-crystals started to appear in multiple conditions after around two weeks while a large percentage of the conditions showed phase separation. These behaviors usually indicate that the detergent concentration present in the crystallization drop was too high and therefore inhibiting crystallization.
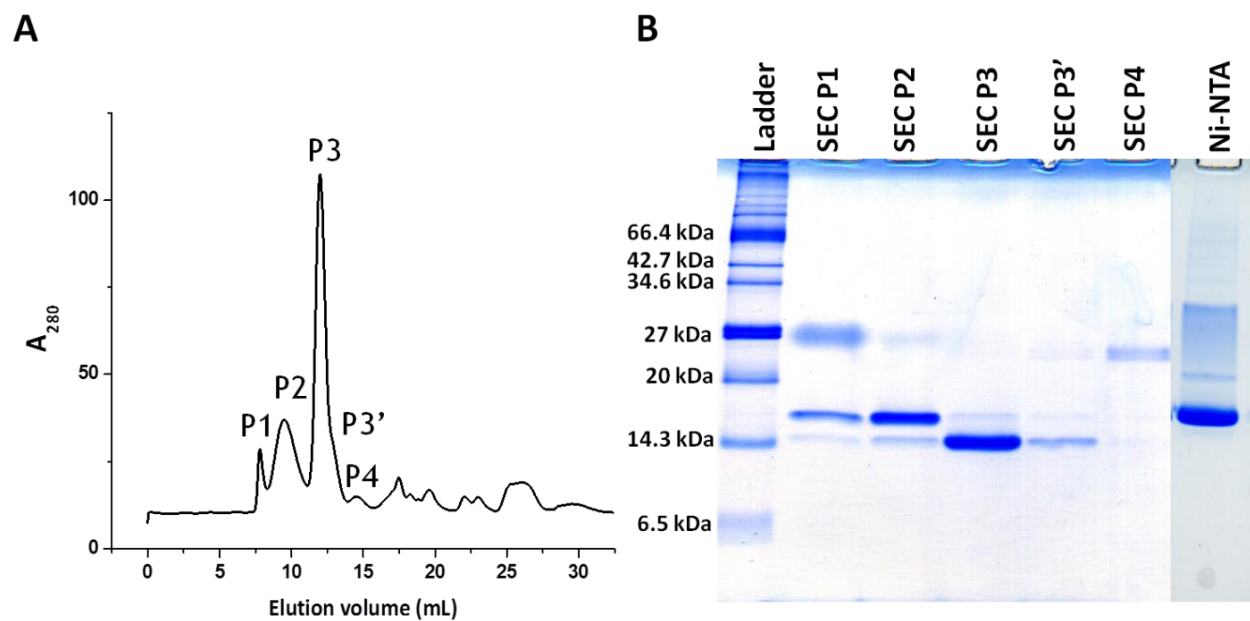
Figure 4.1 *Rs*TSPO was purified by metal affinity and size exclusion chromatography (SEC) and analyzed by SDS PAGE.

(A): SEC profile of *Rs*TSPO. (B): Coomassie stained SDS-PAGE gel of SEC fractions of purified *Rs*TSPO showed that Peak 3 (SECP3) was fully cleaved by trypsin and highly purified.

Although DDM and DM are very good at stabilizing membrane proteins, they also tend to inhibit crystal formation due to masking of potential crystal contacts by the detergents. Given that *Rs*TSPO is a very small protein, the use of DDM and DM in the purification may be detrimental to crystallization. Additionally, the micelle size of DDM and DM is much bigger than the monomer of *Rs*TSPO. This will result in a very high DDM/DM concentration in the purified *Rs*TSPO sample because the detergent micelles will be concentrated together with *Rs*TSPO during the concentration step. This will further inhibit crystallization, as suggested by the observed phase separation behavior.

Two methods were established and used to determine the detergent concentration in the purified *Rs*TSPO samples. Both the TLC method and colorimetric method showed good linearity at the desired concentration range and had good agreement (Figure 4.2). Several purified and concentrated *Rs*TSPO and *Rs*TSPO10ht samples used in crystallization were measured and one representative TLC and one standard curve is shown in Figure 4.2A. All samples show > 5 % DM/DDM concentration, which is more than 200x CMC for both detergents. Figure 4.2A also shows that the DM concentration was significantly increased after concentrating the protein on a 50 kDa MWCO Amicon concentrator. These results confirmed that the detergent was indeed significantly concentrated and was at a much too high a concentration for optimium crystal growth.
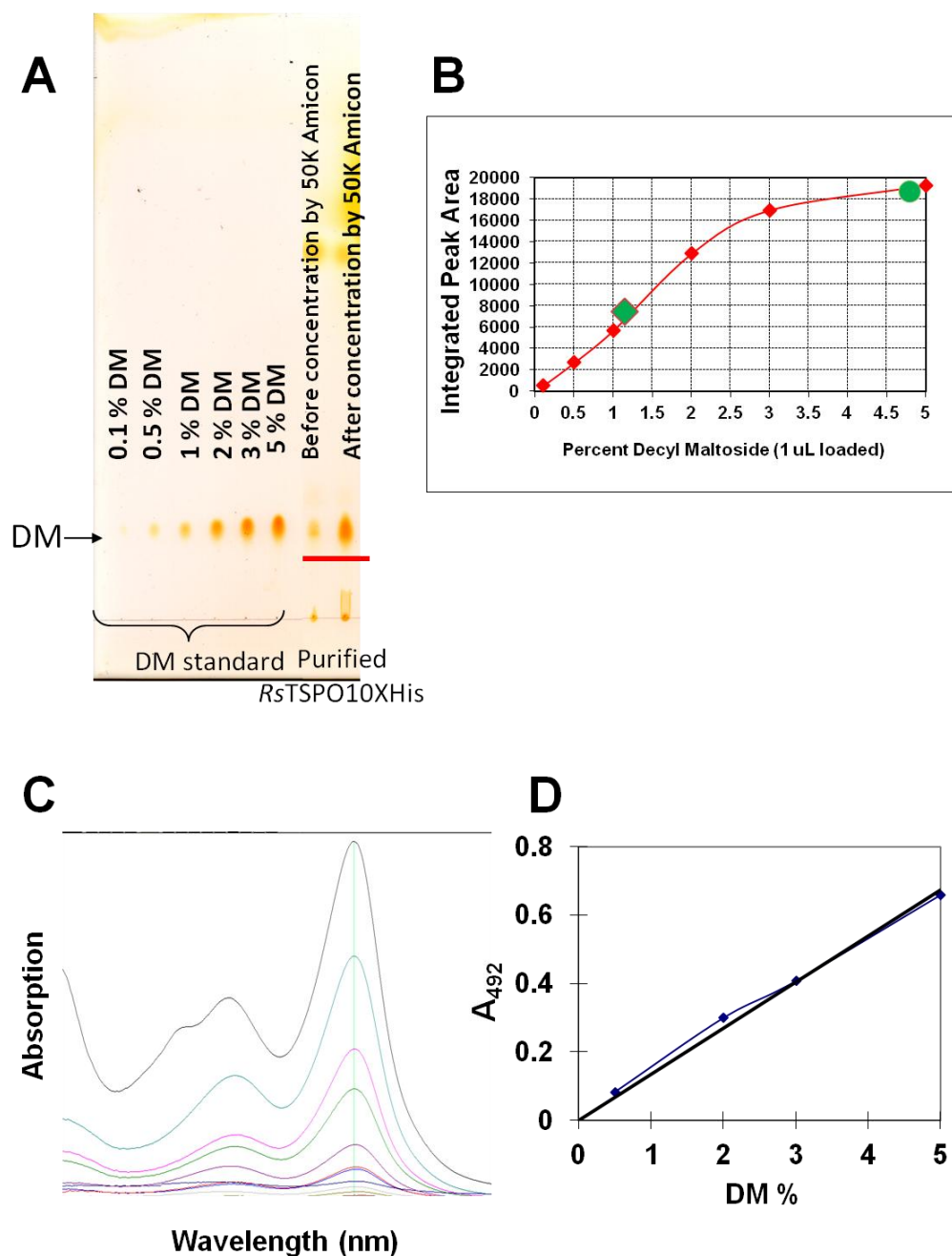
Figure 4.2 Determination of detergent concentration of purified *Rs*TSPO samples.

(A) TLC plate stained with iodine. (B) Standard curve of detergent concentration of samples in (A) where the concentrations of detergent in the purified protein sample before (green diamond) and after (green circle) the concentration step are indicated on the standard curve. (C) Colorimetric assay of DM (see Methods) showing a strong peak at 492 nm that was used for quantifying the sugar content (i.e., maltose detergent content). (D) Standard curve of detergent concentration of samples in (C).

As a result, two strategies were explored to optimize the detergent in the purification procedures to promote crystallization: 1) screening and optimization of purification conditions with various detergents and buffer conditions to achieve a suitable detergent concentration in the crystallization sample; and 2) screening for alternative detergents with smaller micelle size and higher CMC for solubilization. Various methods and techniques were tested and optimized iteratively with one final goal of maximizing the protein to detergent ratio for the purified *Rs*TSPO sample used in crystallization.

DM level in purified *Rs*TSPO was successfully reduced and exchanged for smaller detergents

Excessive amounts of detergent are known to inhibit the crystallization of membrane proteins. This problem is usually dealt with by concentrating purified membrane proteins with a concentrator that has large enough pores to let the detergent micelles go through and thus keep the detergent concentration in the concentrated samples roughly the same as in the unconcentrated samples at around 2x CMC. However, in the case of *Rs*TSPO, the detergent micelles of both DDM and DM are in fact larger than the protein, which makes it unavoidable to concentrate the detergent while concentrating the protein. DDM is also known to bind to membrane proteins strongly at very low concentrations, which makes it a favorable choice for solubilization of larger membrane proteins but not a good choice for *Rs*TSPO. To avoid this complication, the solubilization detergent was changed to 1 % DM, which was shown in the solubilization test to be equally good (see below).

Since DM was able to be used to successfully purify *Rs*TSPO to homogeneity and produce good yields for crystallization experiments, efforts were focused on reducing the DM concentration in the concentrated *Rs*TSPO sample. A simple dilution and wash method was tried

143

first based on the fact that the DM concentration in the concentrated *Rs*TSPO sample was several hundred fold higher than the CMC. Therefore, no-detergent buffer was used to dilute the sample to reduce the DM concentration below 2x CMC and the sample was re-concentrated. This procedure was repeated several times based on the rationale that the DM will be concentrated again during protein concentration, but repeating the process should reduce the DM concentration to just enough to keep the protein in solution. *Rs*TSPO remained soluble after dilution with the no-detergent buffer but precipitated during re-concentrating.

A cholate wash procedure was then tested since cholate has been reported to break the filament structure formed by DDM [17]. We suspected that DM has a similar filament forming property and therefore the cholate washing would also help DM to go through the membrane during the concentrating step. As shown in Figure 4.3A, the cholate washing procedure dramatically decreased the DM concentration in the final sample and the sample was then used in crystallization screening. However, both *Rs*TSPO and cholate formed heavy precipitation in crystallization conditions, suggesting that the detergent concentration after this procedure was too low.

A modified detergent removal procedure with the Pierce detergent-removal spin column was also used to reduce the DM concentration or to exchange DM for other detergents. Figure 4.3 B&C clearly shows that this procedure was very effective in removing the DM in the sample and replacing it with detergents with smaller micelles, such as octyl-glucoside (OG) or nonyl-glucoside (NG). This procedure was also used to reduce the DM level by spinning the samples into buffer containing 0.17 % DM in the collection tube. However, TLC results showed that more than 5 % DM remained in the sample after the removal procedure, suggesting that OG or NG used to equilibrate the column also played a role in facilitating the detergent removal,

possibly by breaking the detergent micelle formed by DM or forming mixed-micelles with smaller sizes. Samples treated with these methods were used in the crystallization screening with commercial screen kits.
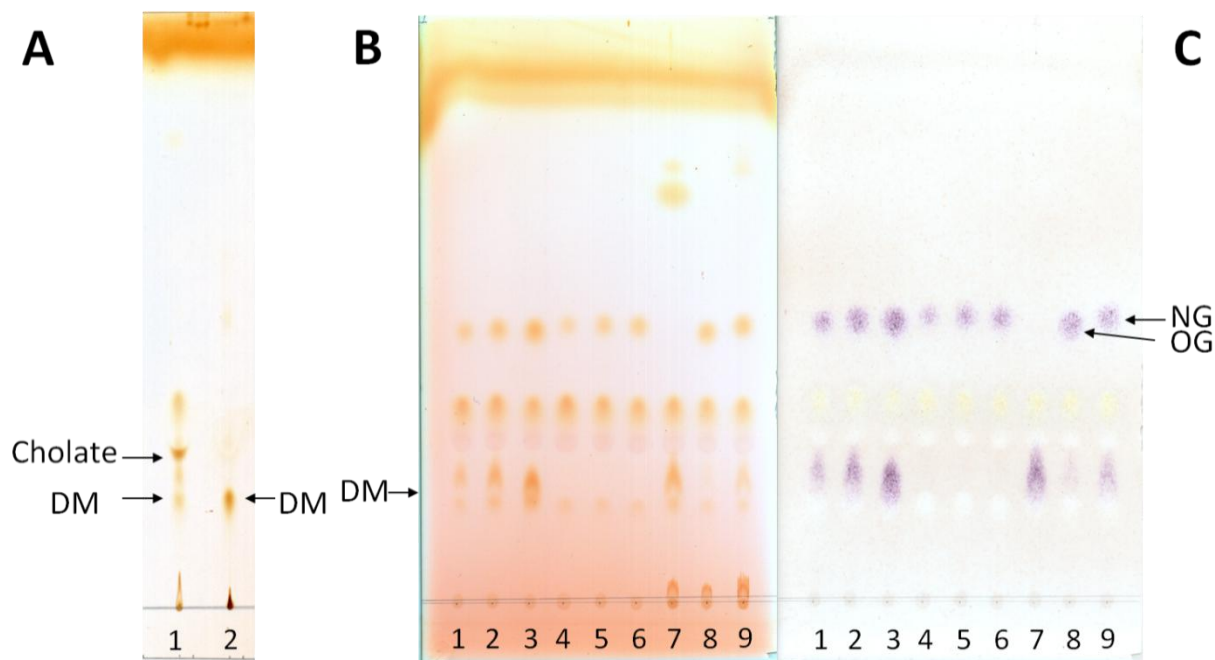
Figure 4.3 Detergent exchange results determined by TLC.

(A) Cholate wash result, plate stained with iodine. Lane 1: *Rs*TSPO sample washed with 6 % cholate; lane 2: untreated *Rs*TSPO sample. (B) Detergent exchange results with the Pierce detergent-removal spin column, stained with iodine. Lane 1: mixed standard of 0.5 % DM and 0.5 % OG; lane 2: 1 % DM and 1 % OG; lane 3: 2 % DM and 2 % OG; lane 4: 0.4 % NG; lane 5: 0.8 % NG; lane 6: 1 % NG; lane 7: *Rs*TSPO10ht directly from Ni-NTA; lane 8: *Rs*TSPO10ht exchanged into OG; lane 9: *Rs*TSPO10ht sample exchanged into NG. (C) Same plate as in (B) stained with alpha naphthol that detects the sugar moiety of detergents.

Samples treated by these various detergents and procedures were all monitored by TLC and tested by small scale crystallization screening with a wide range of commerial screens by using the vapor diffusion method. Experiments were carefully monitored and the results were documented (Table 4.1) to guide the optimization of purification and crystallization. However, no crystal were obtained from these treated samples.

Table 4.1 High throughput small scale crystallization screening results of *Rs*TSPO

Screen Kit	Protein concentration (mg/ ml)	Detergent used in purification	Washing with cholate	Detergent level quantified by TLC	Screen set-up Protein :Screen nl: nl	Results
Cryo I/II	6	0.2 % DM	NO	N/A	200:200	30% clear, 30% phase separation
	10					30 % precipitation, usually oily precipitation, 5 % phase separation
Crystal screen 1/2	10	0.2 % DM	NO	N/A	200:200	30% precipitation and phase separation
Axygen I	5	0.3 % DM	YES	0.1- 0.5 % DM	200:200	Precipitation condensed in the middle
	7					
Axygen IV	10	0.2 % DM	NO	N/A	200:200	> 50% phase separation, oily spread precipitation
Axygen V	5	0.3 % DM	YES	0.1- 0.5 % DM	200:200	Most wells show precipitation, some condensed in the middle of well
	7					
MemGold	5	0.15 % DM	YES	0.1- 0.5 % DM ~ 1% Cholate	200:200	Heavy precipitation possibly due to cholate
	7	0.3 % DM	NO	0.5 % - 1 % DM	200:200	Most wells are clear
			YES	0.1- 0.5 % DM		
	5	0.3 % DM	YES	N/A	200:100	<1% phase amorphous separation, 60% precipitation, several wells show heavy precipitation at first and changed to clear sheet
MemStart/sys	7	0.3 % DM	NO	0.5 % - 1 % DM	200:200	30% clear, 30% amorphous precipitation
			YES	0.1- 0.5 % DM		30% clear, 30% precipitation

RsTSPO was successfully extracted by several detergents

Several representative detergents belonging to different chemical classes that have been used successfully to facilitate membrane protein crystallization were tested (Figure 4.4A). Zwittergen 3-12, C12E8 and LDAO are all popular detergents for membrane protein crystallization with higher CMCs and smaller micelles compared to DM and DDM. Experience shows that it is easier to grow membrane protein crystals purified with these detergents if the protein is stable. However, membrane proteins tend to precipitate in buffer with these detergents because of their charge and because their micelles are not big enough to effectively protect the hydrophobic regions of membrane proteins. LAPAO was tested because it was successfully used in purification and crystallization of another related mitochondrial alpha-helical transmembrane protein, the adenine nucleotide translocator (ANT) [27]. Cymal-type detergents were designed as derivatives of DDM, acting as mild non-ionic detergents to keep the native properties of membrane proteins but with higher CMCs and smaller micelles. Cymal-5 was chosen based on the consideration of the size of RsTSPO as well as its success with several other membrane proteins [28,29]. The protein yield using these various detergents to solubilize membranes containing RsTSPO10ht was compared with 1 % DDM (Figure 4.4 B). All selected detergents extracted RsTSPO from membranes equally well based on a western blot of supernatants reacted with an antibody against the Histag. The sample treated with LDAO precipitated right after solubilization. All other samples were kept at 4 °C to test for long time stability. The sample in DDM buffer was stable for more than 2 months while others were able to keep the protein stable for 3-5 weeks, roughly the time for a crystallization experiment.
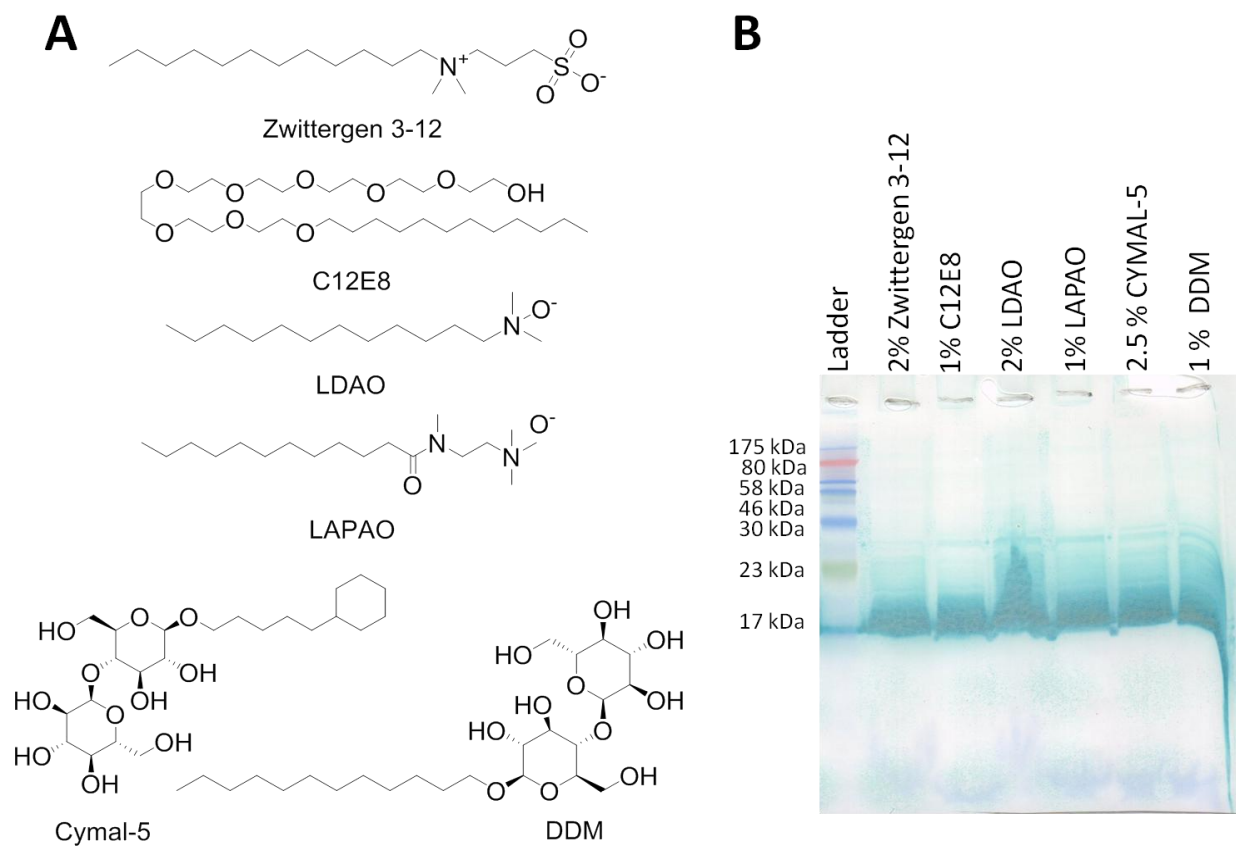
Figure 4.4 Detergent solubilization screening results.
(A) Structures of selected detergents used in the solubilization screen. (B) Western blot of supernatants reacted with antibodies against the Histag showing the results of the solubilization screen.

Identification of the optimal detergent by size exclusion chromatography

A SEC method was also used to exchange and test detergents for their suitability to support *Rs*TSPO crystallization. The advantage of the SEC method is that the homogeneity of the sample, which is critical for crystallization, was also monitored. Briefly, *Rs*TSPO10ht was solubilized in 1 % DM and purified on Ni-NTA with buffer supplemented with 0.2 % DM and 10 % glycerol, in which it has very good stability. Two times the CMC of the selected detergent was used in the SEC step to replace the 0.2 % DM. The suitability of the detergent was judged by the SEC profile. A minimal aggregation peak at the void volumn (~7.5 mL) and a tight homogeneous dimer peak of *Rs*TSPO10ht (~12.5-14 mL depending on the specific detergent) is a good indication that the selected detergent was good.

Representative SEC profiles are shown in Figure 4.5. As expected, C10E5 and Zwittergent 3-12 were not able to stabilize *Rs*TSPO, perhaps due to the small size of their micelles. On the other hand, maltose detergents (DM, NM, OM, cymal-5) were much more effective in stabilizing *Rs*TSPO in solution with minimum void volumn and two homogeneous peaks as shown in the SEC profiles. However, the two peaks representing the oligomer and dimer forms of *Rs*TSPO were not well separated in most cases. High throughput crystallization trials were set up with both peaks purified in maltose detergents but no crystal hits were found with any of the commercial screens.
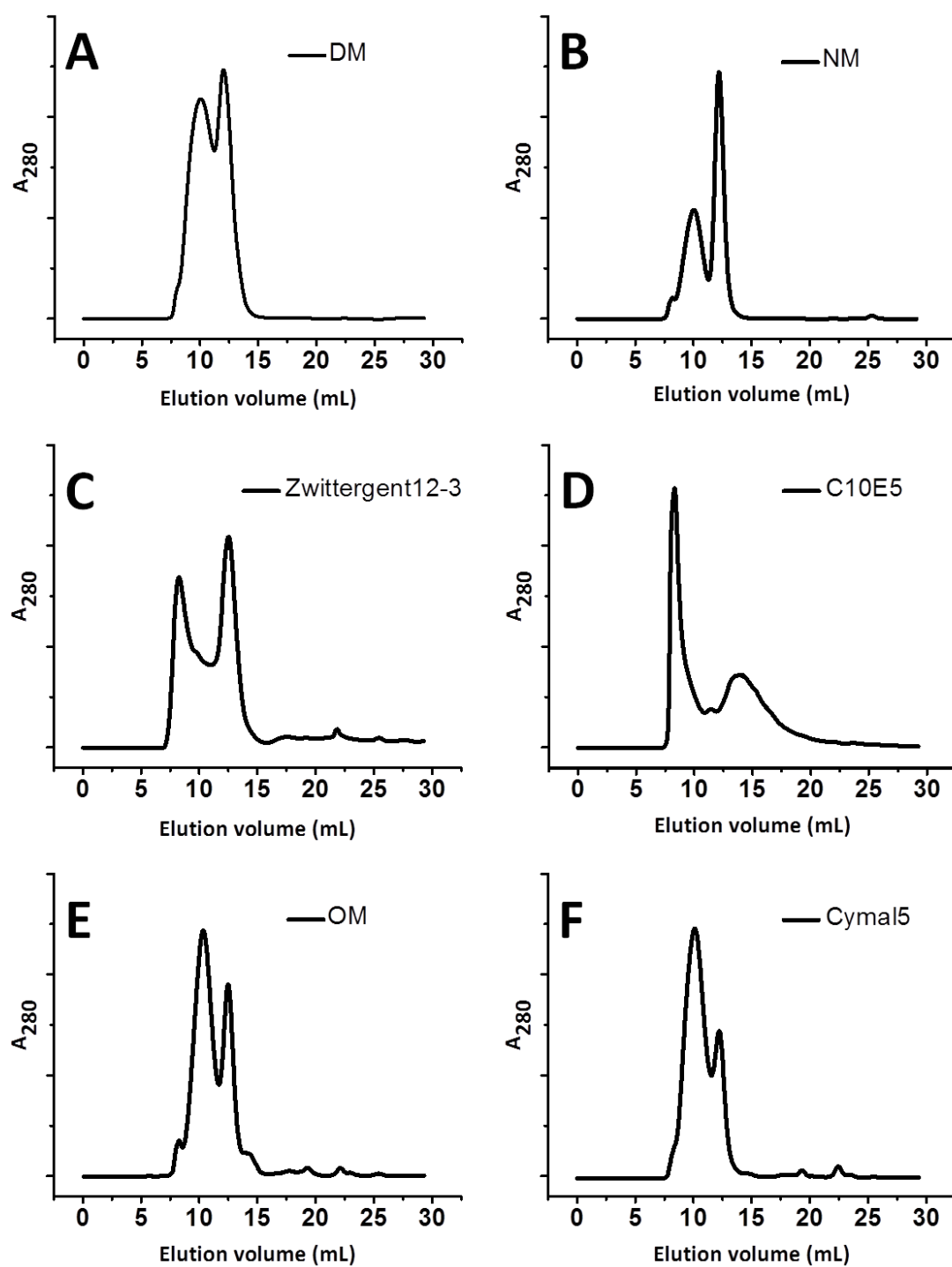
Figure 4.5 SEC profiles of *Rs*TSPO10ht purified in different detergents.
(A) DM, (B) NM, (C) Zwittergent 3-12, (D) C10E5, (E) OM, (F) cymal-5.

Identification of the optimum purification procedure by SEC

Despite extensive screening of detergents, DM proved to be the best detergent for solubilization and purification of *Rs*TSPO10ht in terms of good yield from extraction as well as long time stability. However, samples purified in DM never succeeded in producing diffraction quality crystals. Given the extremely small size of *Rs*TSPO10ht, the thought was perhaps the micelles of DM were too big and too stable such that no area of the protein was exposed to the solution and therefore no crystal contacts could be formed. The SEC profile with DM also showed that the separation of the oligomer and dimer peaks was not optimum (Figure 4.5A), a potential factor that could inhibit crystallization. On the other hand, C10E5 type detergents usually form smaller micelles but have shown to be de-stabilizing to *Rs*TSPO10ht (Figure 4.5B). To create the best balance of stability versus crystallizability, C10E5 was added to DM to modulate and promote crystallization. A similar procedure was used successfully in the optimization of crystallization conditions for the *E. coli* glycerol-3-phosphate transporter by mixing DDM and C12E9 [30]. When *Rs*TSPO10ht was purified with buffer containing 0.2 % DM/0.06 % C10E5 (Figure 4.6 C), the aggregation peak was eliminated while the two peaks of dimer and oligomer were better separated. The dimer peak was subsequently concentrated and used in crystallization screening. Indeed, this sample successfully grew small crystals that diffracted to around 16 Å (Figure 4.8A).
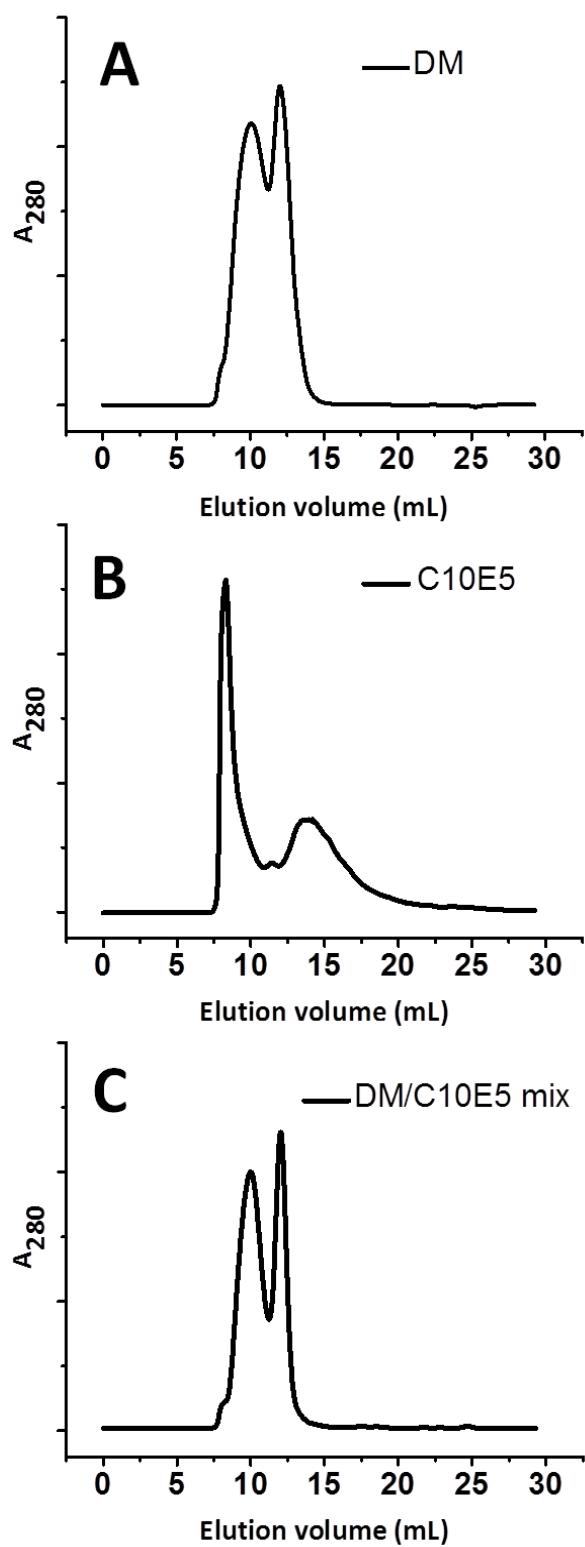
Figure 4.6. SEC profiles of *Rs*TSPO10ht purified in (A) DM alone, (B) C10E5 alone, and (C) DM/C10E5 mixture.

Ten percent glycerol was used in the original purification protocol as a general stabilizing reagent but its effect was never tested. Therefore, a modified purification procedure was tested to see if removing the glycerol is beneficial. Ten percent glycerol was used in all buffers in the same way as in the original protocol up to the SEC step to maintain the maximum stability of the protein. A buffer with the same detergent but no glycerol was used in the final SEC step. No precipitation was observed during and after the SEC for proteins purified with the no glycerol buffer, while the SEC profiles were improved slightly as suggested by a tighter major peak (Figure 4.7 A, C, E, F).

The histidine tag has been shown to mediate crystal contacts in some cases [31] and can be particularly useful if the target protein does not have big cytosolic regions for making crystal contacts, for instance in the case of *Rs*TSPO. However, it can also cause heterogeneity and is usually removed during the final purification step. Removal of the 10-Histag was therefore tested and the SEC profile showed that this step was extremely effective in suppressing the oligomerization of *Rs*TSPO (Figure 4.7 C, D).

Figure 4.7 shows that the combination of removing the glycerol and the 10-Histag produced the best purification result in terms of having a tight, single major peak at the dimer size. All DM, NM and DM/C10E5 mixtures were able to purify *Rs*TSPO to good quality. *Rs*TSPO proteins purified in all three detergents were tested in crystallization screening. Protein purified with DM/C10E5/no glycerol continued to produce crystals of similar quality as previously described while protein purified with DM without glycerol was able to produce small crystals that diffracted to around 20 Å for the first time. However, these conditions failed in further scale-up and optimization. On the other hand, protein purified in NM buffer precipitated quickly after setting up, suggesting that 10 carbons is the minimum alkyl tail length for a suitable detergent.
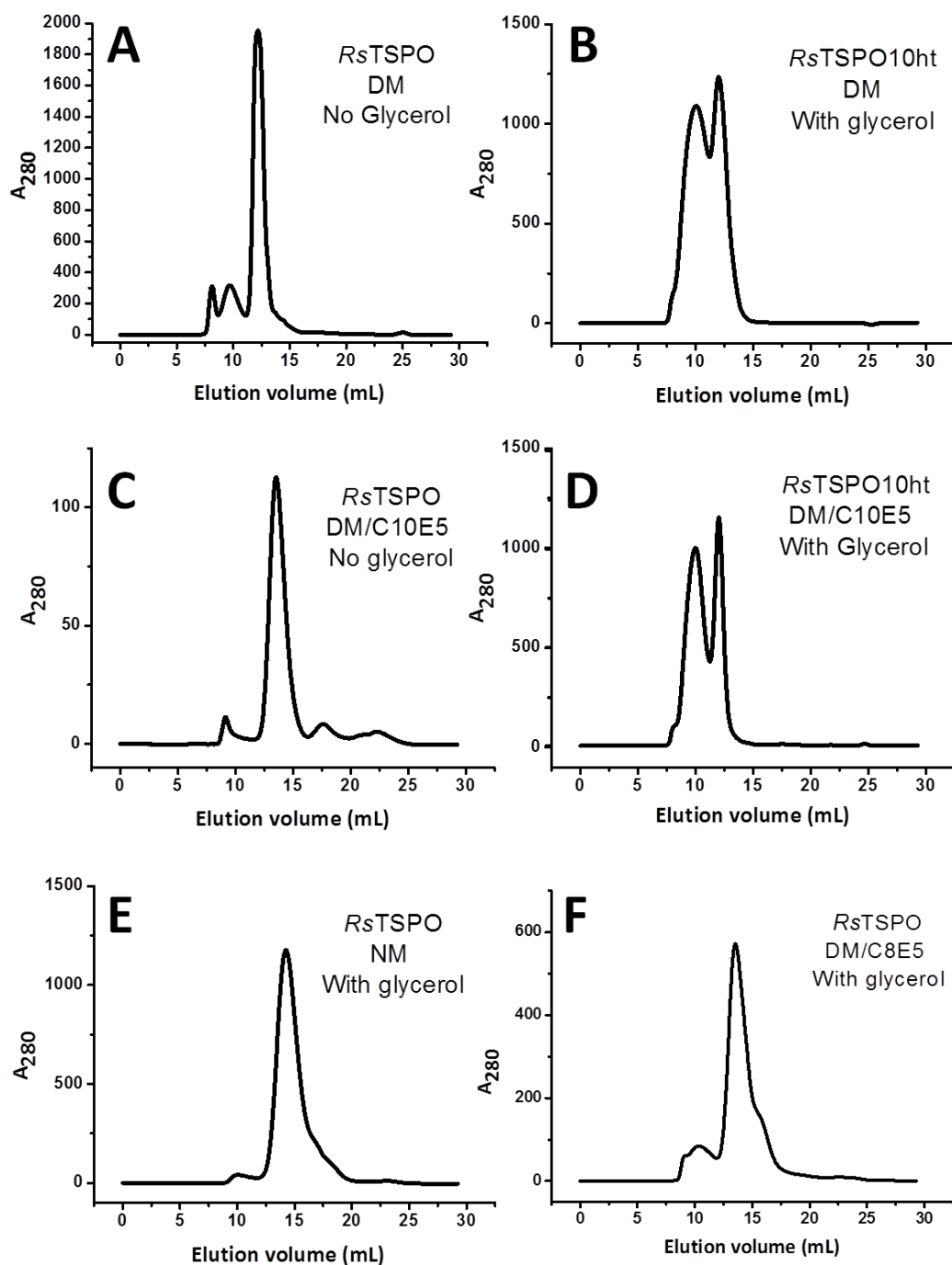
Figure 4.7. SEC profiles for testing effects of glycerol and histag.
*Rs*TSPO10ht (B&D) runs at around 12.5 mL (around 66kDa) while *Rs*TSPO (A,C,E&F) runs at around 14-15 mL (around 44 kDa) on the Superose 12 column. The histag promotes oligomerization and results in less well separated peaks between the oligomer and the dimer while glycerol slightly increases the width of the peak

156

Results of crystallization and optimization with the vapor diffusion method

In addition to the extensive optimization of the purification procedure and detergents, more than 1000 crystallization conditions with various protein ratios and temperatures were screened to identify the lead for optimization. Although some conditions were able to produce small crystals (Figure 4.8 A, B) occasionally, the results were not consistent and they all failed in scale-up experiments. In addition, all crystals grown in the vapor diffusion method never diffracted to better than 13 Å. Among all the potential lead conditions, one was worth mentioning. The condition of 0.05 M NaCl, 0.02 M glycine pH 10, 33% PEG 1000 produced the best crystal in the vapor diffusion method with a sample purified in 0.2% DM/ 0.06% C10E5, and this crystal diffracted to 16 Å. Addition of 2-propanol slightly increased the resolution to 13 Å. Interestingly, the lead identified with the LCP method also contained ~32% PEG 1000 and addition of 2-propanol significantly increased the size and the quality of the crystals (see discussion below).
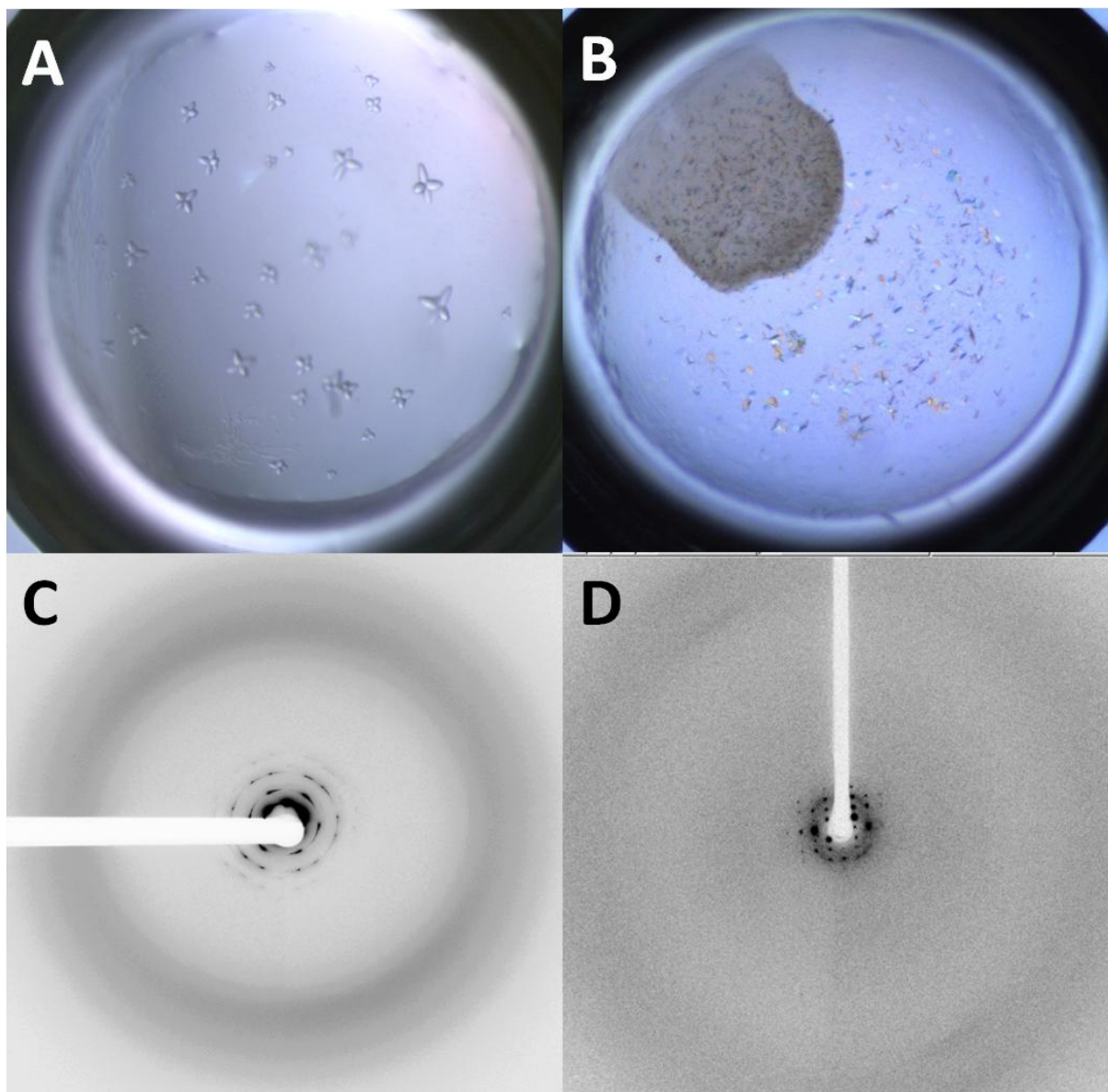
Figure 4.8 Representative *Rs*TSPO crystals grown with the vapor diffusion method and their diffraction patterns.

(A) *Rs*TSPO purified in 0.2% DM/ 0.06% C10E5 buffer with no glycerol, and grown in 0.05 M NaCl, 0.02 M glycine pH 10, 33% PEG1000, 20 °C; (B) *Rs*TSPO purified in 0.2% DM buffer with no glycerol, and grown in 26-33% PEG400, CaCl$_2$, pH 6.5-8.5,4 °C; (C) diffraction pattern of crystal in (A); (D) diffraction pattern of crystal in (B).

Initial screening with the LCP method

The failure of the extensive screening and optimization of crystallization conditions with vapor diffusion confirmed our concern that *Rs*TSPO is not suitable for crystallization by the traditional vapor diffusion method and prompted us to consider the alternative methods. Given that TSPO lacks large extra-membrane loops to mediate crystal contacts in type II crystals and the fact that it successfully produced 2D crystals for cryo-EM structure determination [32], we considered trying to promote the type I crystallization by using the LCP method.

*Rs*TSPO was purified with the same optimized procedure, which uses 0.2 % DM throughout the purification and no-glycerol buffer in the final SEC step and concentrated to 30 mg/mL with a 30 kDa MWCO filter. Initial high throughput screening was done as described in the Methods. Small crystals started to appear after about 10 days of incubation at 20 ℃. More crystals were observed after 2-3 weeks in conditions containing zinc acetate ($Zn(OAC)_2$), MES buffer pH 6.0 and ~20% PEG 400/ PEG 550 MME/ PEG 600 or PEG 1000 (Figure 4.9). Bigger sheet-shaped crystals were observed after 4 weeks of incubation in conditions also containing $Zn(OAC)_2$. These lead conditions were manually repeated at MSU with both LCP setups and sponge phase setups. The condition containing PEG 1000 was successfully reproduced and the micro crystals were harvested with a micromesh and tested at GM/CA CAT with the micro beam. These initial crystals diffracted to around 4 Å with the unattenuated X-ray beam.
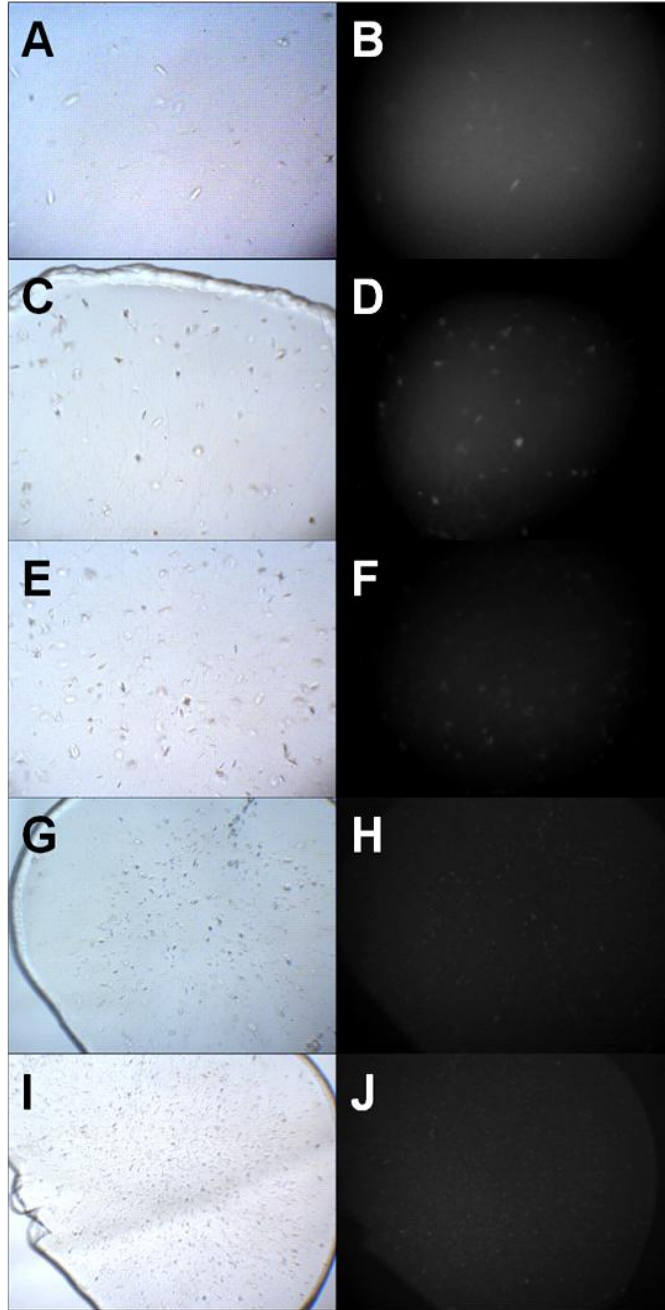
Figure 4.9. Representative pictures of *Rs*TSPO protein crystals grown in the LCP setup after 3 weeks.

*Rs*TSPO crystals grown in 100 nL+1 μL LCP setup. (A&B): 20 % PEG400, 0.1 M MES pH 6.0, 0.1 M Zn(OAC)$_2$; (C&D) 20 % PEG550 MME, 0.1 M MES pH 6.0, 0.1 M Zn(OAC)$_2$; (E&F): 20 % PEG600, 0.1 M MES pH 6.0, 0.1 M Zn(OAC)$_2$; (G&H): 20 % PEG1000, 0.1 M MES pH 6.0, 0.2 M Zn(OAC)$_2$; (I&J): crystals grown from protein-monoolein mixture incorporating 6 % cholesterol in 20 % PEG1000, 0.1 M MES pH 6.0, 0.2 M Zn(OAC)$_2$. Panels A/C/E/G/I are in brightfield and panels B/D/F/H/J are under UV.

Optimization of LCP crystallization conditions

The original crystal lead identified in the high throughput screening was extremely small and embedded in the LCP bolus. Data collection was impossible on such crystals other than to comfirm that *Rs*TSPO indeed grows 3D crystals in the LCP condition. Extensive optimization was carried out to improve the size of the crystal to allow data collection as well as to improve the quality of the crystal (Figure 4.10).

Crystal improvement   **Optimization strategies**

Crystal lead from high
throughput screening:
< 5 μm size, ~ 4 Å resolution

Addition of cholesterol in
monoolein

Slight increase of size and
resolution to ~3.5 Å

Identification of 2-propanol
as crystallization additive

Further increase the size
to ~ 20 μm and resolution
to ~ 3.0-3.3 Å

Identification of KAC/
NaAC/NH4AC as
crystallization additive

Increase the size of the
crystal in the second
dimension and resolution
to ~ 2.8 Å

Co-crystallization with
ligand PK11195, retinoic
acid and Ro-4865

Further increase the size
to ~ 30-50 μm x 10 μm
and resolution increased
to ~2.5-2.8 Å

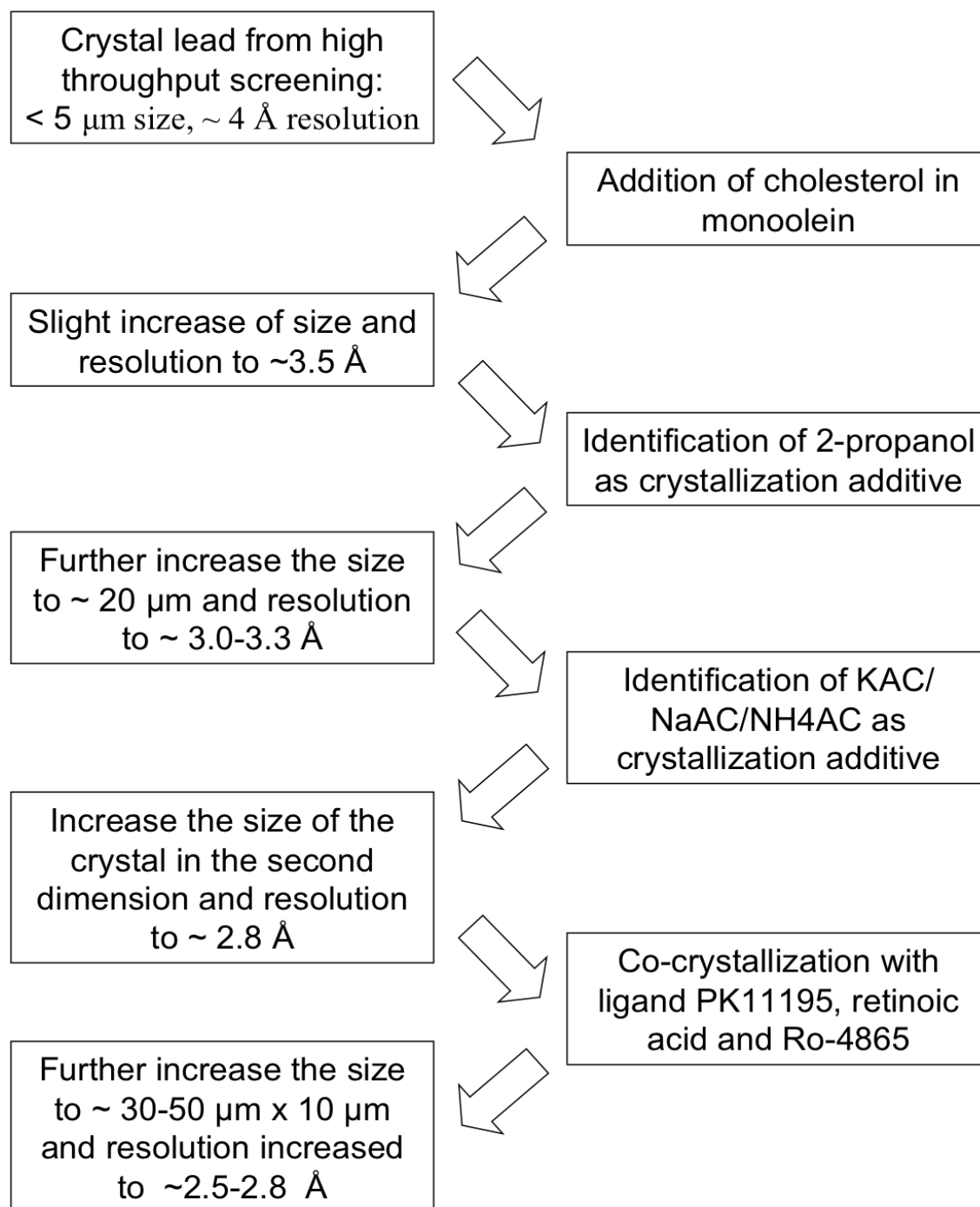**Figure 4.10. Schematic representation of optimization strategies for crystallization of** *Rs***TSPO by the LCP method.**

Addition of around 8 % cholesterol in the monoolein increased the size of the crystals to around 10-20 μm in the longest dimension. Crystals harvested on the micro-mesh can be separated when rastered with the 5 μm mini-beam. Several frames of data at 0 °, 45 ° and 90 ° were collected from a single crystal, which allowed the extraction of the unit cell parameter of these *Rs*TSPO crystals for the first time. Additional rounds of screening were carried out to identify crystallization additives such as metals, salts, and organic compounds to further improve the crystal size and quality. Acetate salts (including sodium acetate, potassium acetate and ammonium acetate) and 2-propanol improved the crystal resolution to 2.8-3.3 Å. The size of the crystals also further significantly increased, especially in the second and third dimensions, which allowed rotation and continuous data collection on these crystals. Ten to twenty degrees of data wedges could be collected on each single crystal before the crystal was destroyed by the X-ray beam. Complete datasets for structure determination were obtained by merging 20-40 wedges to achieve the required completeness and redundancy. A further improvement of the crystal quality was realized by co-crystallization of *Rs*TSPO with high affinity ligands previously identified [33]. PK11195, retinoic acid, and Ro5-4864 all improved the crystal size and resolution to some extent with PK11195 being the best. *Rs*TSPO-PK11195 complex crystals (Figure 4.11A&B) diffracted to around 2.3-2.5 Å (Figure 4.11C). The sizes of crystals were also much bigger, which allowed 30-60 degrees up to 90 degrees of data to be collected on a single crystal. The ability to obtain a complete dataset with much fewer wedges was also important in improving the data quality and critical to obtaining a better structure solution. A further major improvement that allowed full data collection on a single crystal was achieved using a mutant form of *Rs*TSPO that mimicked a human single polymorphism, A147T (A139T in *Rs*TSPO), associated with

anxiety-related diseases. Crystals diffracting to 1.8 Å resolution were obtained, which allowed structural and functional comparison with the wild-type (manuscript in preparation).
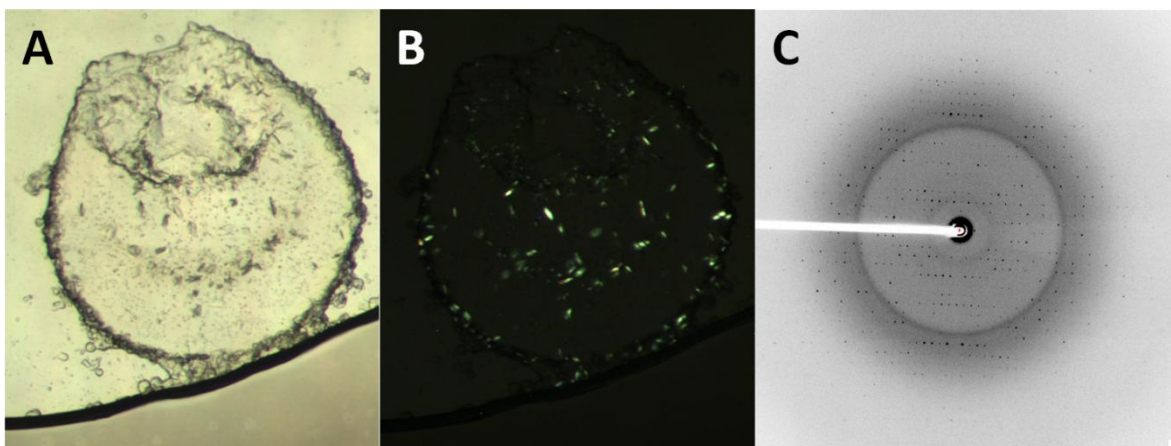
Figure 4.11. *Rs*TSPO-PK11195 crystals.
(A) Crystals imbedded in the LCP bolus under bright light; (B) Same well as in (A) under cross-polarizing light; (C) A representative diffraction image of crystals in (A) and (B).

Structure determination and refinement

Extensive attempts to solve the structure using various models of *Rs*TSPO, the EM structure of *Rs*TSPO [32], and the NMR structure of mouse TSPO [34] failed. Despite the fact that some of the *Rs*TSPO models we previously constructed [33] (in collaboration with Dr. Jens Meiler) were able to find a potential molecular replacement solution with the correct packing, no reliable structures were obtained. Concurrently, experimental phasing was performed. Selenium-methionine labeled WT crystals were obtained but were not able to solve the phase due to significant diminution of anomalous signal after merging datasets. Two suitable heavy metal derivatives of the A139T crystals were obtained (Ta and Hg). The ability to collect complete datasets on single crystals of the A139T crystal, and the fact that signals from the heavy-metal derivatives were much stronger, provided significantly better phasing power for structure determination. The structure of wild type *Rs*TSPO was solved by molecular replacement with a partially refined model of the A139T mutant.

Structure of *Rs*TSPO-WT and A139T mutant

*Rs*TSPO-A139T crystallized in 2 different space groups: C2 (at 1.8 Å) and $P2_12_12_1$ (2.4 Å) with identical overall structure except for the flexible C-terminus. The structure of the A139T mutant resolves the nearly complete polypeptide chain for monomers A (residues 1-157), B (residues 2-157), and C (residues 2-151), with no breaks in the main chain (Figure 4.12). The last residue A158 is removed with the Histag by trypsin during purification. The wild-type structure, determined at 2.5 Å resolution, resolved most of the polypeptide chain, except for disordered portions of Loop 1 (LP1). WT crystallizes in a $P2_1$ space group with two monomers in the asymmetric unit, the same as A139T in the $P2_12_12_1$ space group, while A139T in the C2 space group crystallized with three monomers in the asymmetric unit. In the latter case, the three

monomers form a dimer and a half arrangement, such that the monomer C and its symmetry mate C' form an identical dimer to the AB dimer. In all cases, *Rs*TSPO is arranged in an identical parallel dimer. WT and A139T adopt very similar overall structures. The $C\alpha$ atom superposition of the half of the molecule on the N-terminal side of the protein yields *rms* deviations less than 0.3 Å, while more deviation is observed on the C-terminal side containing LP1, which affects the access to the central binding cavity. The arrangement of α-helices in the monomer is identical in all three crystal structures: looking from the *C*-terminal side of the monomer (Fig. 4.12B), the clockwise order of the helices is TM-I, TM-II, TM-V, TM-IV, and TM-III. TM-I is kinked at residue G16 and TM5 is kinked at V130. TM2 and TM4 are curved, while TM3 is slightly curved and kinked at W87. LP1 adopts three different conformations between the A139T and the WT structures. A short helix is observed in the middle of LP1 in A139T chain A and chain B with the LP1 extending up. The short helix is partially unwound in the chain C of the A139T structure with the LP1 at an even higher up position.
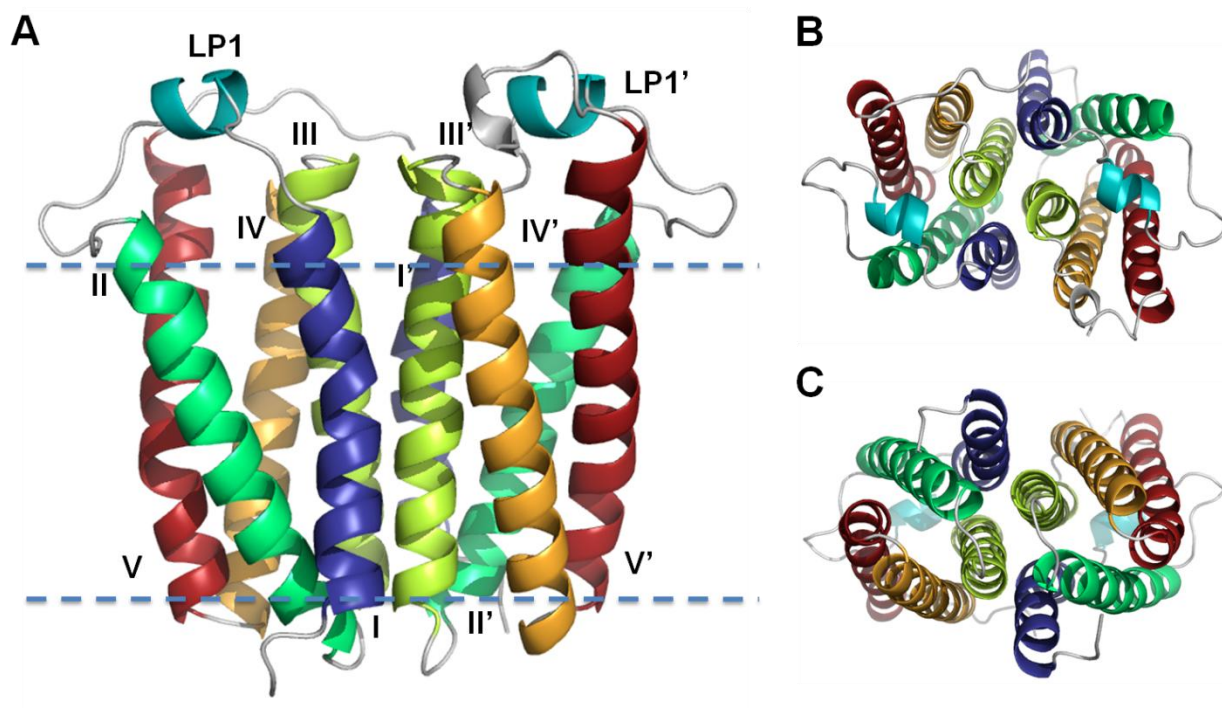
Figure 4.12. Crystal structure of RsTSPO-A139T. (A): The overall structure of the A139T dimer. Transmembrane helices are labeled as roman numerals and rainbow colored from N to C terminus; (**B**): Top view from the C-terminuls; (C): bottom view from the N-terminus.

DISCUSSION

*Rs*TSPO is unique in terms of being a 5-helix transmembrane α-helical protein as well as an outer membrane helical protein. These unique properties and the fact that it is very small and composed of almost exclusively transmembrane helices made it hard to crystallize with the traditional vapor diffusion methods. By analyzing the crystal structure of *Rs*TSPO and the systematic optimization route retrospectively, a better understanding of the successful methodologies can be obtained and potentially applied to other similar membrane proteins

Importance of promoting type I crystal packing for *Rs*TSPO with the LCP method

Despite extensive optimization of crystallization conditions in the vapor diffusion method, no good diffraction quality crystal was obtained. The lack of large soluble domains and loops to mediate crystal packing in the third dimension may be detrimental to crystallizing *Rs*TSPO by the vapor diffusion method. It was clearly shown by the crystal packing of the LCP-grown crystal (Figure 4.13) that *Rs*TSPO indeed forms type I crystals and the crystal packing interactions are almost exclusively through helical-helical interactions in the transmembrane region. In the final crystal structure of wildtype *Rs*TSPO, the only long loop (LP1) that could mediate potential crystal packing was not completely resolved and was possibly at a downward position into the transmembrane region, and thus not useful for crystal packing. Therefore, promoting the type I crystal packing was the key, and perhaps the only way, to obtain the diffraction quality crystals of *Rs*TSPO. Given that *Rs*TSPO had been previously crystallized into a 2D crystal [32], this was also a very reasonable strategy.

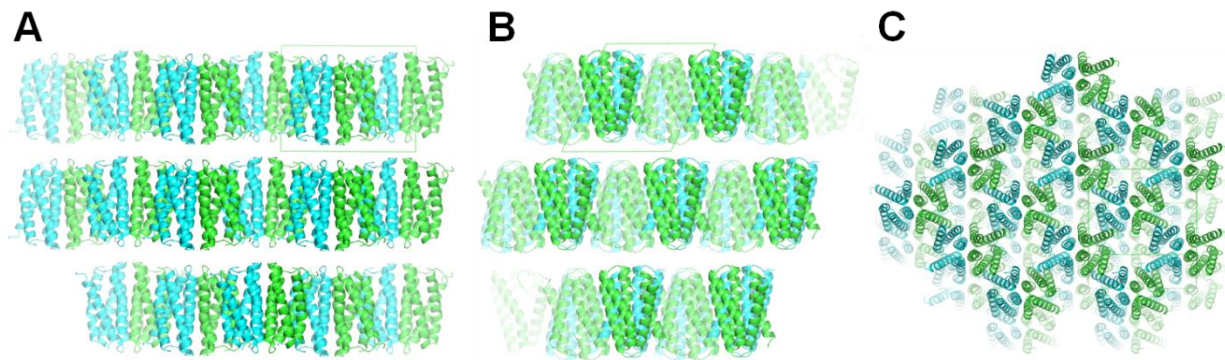**Figure 4.13 Crystal packing of wildtype *Rs*TSPO crystals grown in the LCP condition.**

(A) Viewed perpendicular to the crystallography 2-fold axis; (B) Viewed along the crystallography 2-fold axis; (C) Top view. Unit cells are shown in green boxes. Crystals were grown in the condition of 32% (w/v) PEG 1000, 100 mM $Zn(CH_3CO_2)_2$, 100 mM MES (pH 6), 100 mM $NaCH_3CO_2$, K or $NH_4CH_3CO_2$, and 6-8 % (v/v) 2-propanol.

The difference between crystal packing is illustrated in Figure 4.14. Crystal packing in the type II crystals (Figure 4.14C) relies heavily on the interaction of hydrophilic regions not covered by detergent or lipid, while the transmembrane regions are protected by detergent throughout the crystallization process and do not contribute to crystal packing. In contrast, packing of the type I crystals, as well as for the 2D crystals, is heavily dependent on the transmembrane regions as well as the lipids in between them (Figure 4.14 A&B). The hydrophilic regions may also contribute to crystal packing, as in the cases of fusion modules used in crystallization of G-protein coupled receptors [35], but this is not a requirement. In the case of the *Rs*TSPO-A139T crystals, the ability of the LP1 to form crystal contacts seems important in improving the crystal quality but transmembrane regions still form the majority of the crystal contacts. If a 2D crystal of a membrane protein can be induced to also pack in the third dimension, a type I 3D crystal can be obtained, as in the case of *Rs*TSPO, rhodopsin [1,36], and the ca_3 cytochrome oxidases [9].

Figure 4.14 Cartoon illustrations of different crystal types
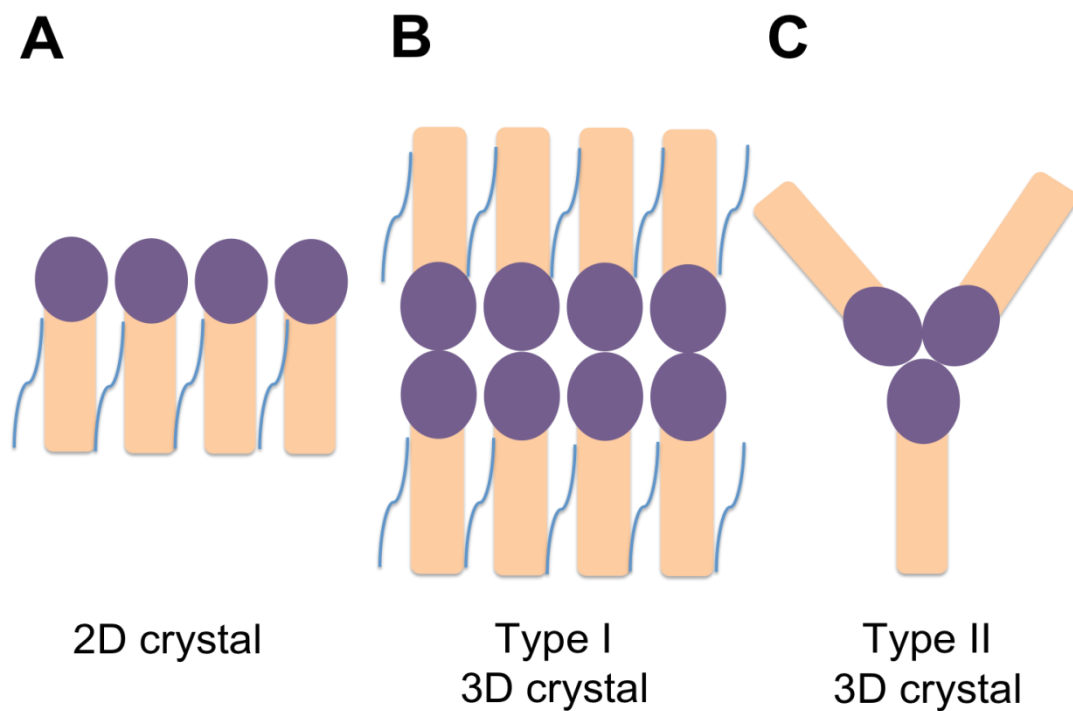
Beige rectangles represent hydrophobic transmembrane regions of a membrane protein while purple ovals represent the hydrophilic domains. Blue lines surrounding the transmembrane domains represent detergents or lipids. (A) 2D crystal; (B) Type I 3D crystal (a head to head interaction is shown but other types of interactions are also possible); (C) Type II 3D crystal.

In larger membrane proteins which have helices that are longer than the detergents and/or big hydrophilic domains, type II crystals can be obtained through the interaction of the hydrophilic domains or the transmembrane region not entirely covered by detergents. This is predominantly the case for membrane protein crystals grown in the vapor diffusion method. However, for small membrane proteins such as *Rs*TSPO, 3D crystals can most likely be obtained *via* type I crystal packing with the transmembrane domain or type II crystals with a fusion partner. The latter strategy is reasonable for crystallization purposes but the expression of a fusion protein can be challenging. *Rs*TSPO was fused with three popular fusion modules (T4 lysozyme, rubredoxin, and cytochrome $B_{562}RIL$) at various positions. All fusion constructs disrupted the expression and purification of *Rs*TSPO. As most of these fusion partners are even bigger than *Rs*TSPO itself, it is not surprising that the membrane insertion of *Rs*TSPO was severely influenced. Success of the fusion protein strategy for obtaining the GPCR structure [37] suggests that this is a very useful strategy for bigger membrane proteins, but not small membrane proteins like TSPO.

The LCP crystallization method is not only good for stabilizing membrane proteins in the lipidic environment, but it is also extremely good for promoting type I crystal packing. To date, all proteins crystallized with the LCP method formed type I crystal packing. Some of the third dimension interactions were mediated by a fusion partner, as in the cases of the GPCRs [35]. In other cases, the third dimension interaction was realized by interdigitation of the transmembrane region (PDB 2F93 [38], 4H37 [39]). Indeed, type I crystal packing promoted by the LCP is the only way that *Rs*TSPO-WT could be crystallized to diffraction quality.

Role of detergent in crystallization of *Rs*TSPO

Detergents play important roles in stabilizing membrane proteins, but unsuitable detergents

can also inhibit crystallization. In the early efforts of crystalling *Rs*TSPO by the vapor diffusion method, detergent was extensively optimized to find the detergent or detergent combination with the minimum micelle size yet also able to stabilize *Rs*TSPO during purification and crystallization. The rationale behind such optimization is to expose enough of the hydrophilic region of the membrane protein to mediate crystal packing in the type II crystal, but also to protect the most hydrophobic region of the membrane protein during the crystallization process. This strategy was successful for bigger membrane proteins [30], but finding the right balance turned out to be extremely hard for *Rs*TSPO. As a proof of concept, the combination of DM and C10E5 indeed produced the only and the best diffraction quality crystals of *Rs*TSPO by the vapor diffusion method; however, they only diffracted to 16 Å.

The detergent does not seem to play a very important role during crystallization with the LCP method as long as it can stabilize the membrane protein during purification. Once the membrane protein is incorporated into the lipidic environment, the MAG used in making the lipidic cubic phase plays a more important role. Experience with other membrane proteins shows that the length of the alkyl chain of the MAG is critical in determining the crystallizability and the crystal quality of membrane protein crystals [40,41]. In addition, experience from our lab and others shows that detergent molecules are often observed to be bound to the membrane protein in the crystal grown from the vapor diffusion method [31], but few are observed in crystals grown from the LCP method. Instead, a large amount of MAG lipid is often observed in the crystals grown from the LCP method [42], suggesting that detergent and native lipids are replaced by the LCP lipid once the membrane protein is successfully incorporated into the lipidic cubic phase.

On the other hand, detergent does play a role in regulating the phase behavior of the MAG lipid used in LCP crystallization. Studies show that increased detergent can act to induce a

sponge phase, a type of dissolved cubic phase [43,44], and some membrane proteins are in fact crystallized in the sponge phase by increasing the detergent and precipitant concentrations [45]. If a proper balance can be achieved, crystals grown from the sponge phase can reach a much bigger size compared to the regular LCP crystals. Additionally, crystal harvesting is much easier since the lipidic cubic phase is dissolved under such conditions and the bigger crystals can be easily harvested with a regular loop. In the case of *Rs*TSPO, controlling the detergent concentration was not easy because of the small size of the protein relative to the micelle of DM. Excess detergent completely disrupted the phase behavior of the monoolein and inhibited crystal growth when the protein concentration was increased in an effort to produce bigger crystals.

Common additives in vapor diffusion and LCP crystallization optimization

Additives to improve crystal quality were extensively screened with both the vapor diffusion and LCP crystallization methods. One interesting observation is that small alcohols, 2-propanol in the case of *Rs*TSPO, improved the crystal quality of *Rs*TSPO in both methods with different crystallization conditions. Similarly, 1,4-butenediol also significantly increased the crystal size of the *β2*-adrenergic receptor. Although far from conclusive, these experiences suggest that small organic molecules may play a role in regulating the phase behavior as well as the interaction of the membrane protein with lipid/detergent during crystallization.

Zinc acetate was identified in all the initial LCP hits regardless of the major precipitant. Additional acetate salts (sodium, potassium or ammonium) were identified later as additives that improved the diffraction quality of *Rs*TSPO crystals. Experience from Dr. Caffrey's group shows that a common salt can be identified to improve crystal quality in lipidic cubic phase with different types of MAGs [40,41]. These experiences show that crystallization and optimization strategies may be transferred between different systems. Analysis of common additives and

175

results from vapor diffusion experiments may help save time and resources in optimization of crystals grown by the LCP method.

Obtaining suitible heavy metal derivatives of *Rs*TSPO

Despite the fact that the LCP method is increasingly popular for obtaining crystal structures of important membrane proteins, few are novel structures. Part of the reason lies in the technical difficulties of obtaining derivatives of membrane proteins for phase determination under the LCP conditions. In the process of obtaining the phase information for *Rs*TSPO, two popular methods were tried: single-wavelength anomalous scattering (SAD), which involved incorporating selenium into the protein, and multiple isomorphous replacement-anomalous scattering (MIRAS) , which involved the addition of heavy metals. In our experience, the SAD method failed due to low signal because many non-optimal datasets from small LCP crystals needed to be merged. On the other hand, heavy metal derivatization provided better data to obtain the initial phase information. However, adding the metal without disrupting the LCP system was a technical challenge. Towards this end, we developed a novel high throughput scheme that uses a commonly available crystallization robot to deliver the heavy metal compounds onto the plates prior to the lipid/membrane protein sample in the LCP mixture. In the case of *Rs*TSPO, the ability to readily obtain a number of heavy metal derivatives was critical for solving the structure.

Insights from the *Rs*TSPO crystal structures

The crystal structures of *Rs*TSPO WT and the A139T mutant provide some new insights that facilitate the understanding of TSPO function. The tight interaction of the *Rs*TSPO dimer suggests that the dimer interface is not likely to transport substrates, in contrast to what was previously proposed (see chapter 2). Instead, our structures suggest a possible external transport

pathway likely involving binding partners, which fits with previous observations of interactions with other proteins and oligomerization of mouse TSPO and *Rs*TSPO. In addition, significant structural changes are observed between the A139T mutant and the WT in the area close to the CRAC site, confirming that this region is playing an important role in cholesterol binding. The three different conformations of LP1 observed between the WT and the mutant are consistent with a regulatory role of LP1 in ligand binding and TSPO function. Further, a binding site was identified with a bound porphyrin, but the drug ligand and cholesterol binding locations were not observed in the current structure, despite their ability to improve the crystal quality.

The structural information at atomic resolution will enable more incisive experimental and mutational approaches to fully understand TSPO function.

SUMMARY

Purification and crystallization conditions for *Rs*TSPO were systematically and extensively screened and optimized with both the vapor diffusion method and the LCP method. Analysis of the optimization strategies and results for *Rs*TSPO, in comparison with other membrane proteins, shows that crystallization of small α-helical proteins requires special attention to strategies, in particular regarding handling of detergents and selection of crystallization methods. A successful strategy for crystallization of *Rs*TSPO was presented here, providing a valuable example for crystallization of similar membrane proteins. The structures for both WT and a mutant form of TSPO were obtained, providing previously unavailable molecular insights into the controvercial function of this unusual protein.

Manuscript describing the crystal structures of *Rs*TSPO

A paper describing our new structures of WT *Rs*TSPO and the A139T mutant is in final stages of preparation to submit to *Nature* or *Science*. Due to the very restrictive policies of

Science, the data cannot be included in a thesis until after its publication. A preliminary abstract is provided in the Appendix.

APPENDIX

Crystal structures of translocator protein 18 kDa (TSPO) from *Rhodobacter sphaeroides*

Fei Li, Jian Liu, Yi Zheng, Michael Garavito, and Shelagh Ferguson-Miller
Department of Biochemistry and Molecular Biology, Michigan State University, East Lansing, Michigan 48824, USA

Transport of cholesterol into mitochondria is the first and rate limiting step of steroid hormone synthesis. Translocator protein 18 kDa (TSPO) is recognized as a key player in this process and is highly expressed in steroidogenic tissues, as well as under conditions of inflammation, metastatic cancer, Alzheimer, and Parkinson disease. A cholesterol recognition amino acid consensus sequence (CRAC) was first identified in TSPO as a general cholesterol binding motif. Various other ligands that bind to TSPO, including benzodiazepine drugs, have been implicated in regulating apoptosis and extensively studied as diagnostic imaging agents and treatment options. Conflicting data and the lack of high resolution structures has led to much controversy concerning the precise role of this conserved, developmentally-required protein. Here we present high resolution crystal structures, determined in a lipidic phase, of TSPO from *Rhodobacter sphaeroides (Rs*TSPO)*, a bacterial homolog of the mitochondrial protein. The wild-type as well as a mutant equivalent to a human single polymorphism in three forms were determined to 2.5 Å and 1.8 Å, 2.4 Å respectively. These structures belong to three different space groups and different ligand binding states, but they show the same dimer arrangement, consistent with previous results showing that *Rs*TSPO is a dimer in solution. However, our crystal structures differ significantly from a published NMR structure of the refolded monomeric mouse TSPO, suggesting that the NMR structure may represent a ligand-trapped folding intermediate. The crystal structures of *Rs*TSPO reveal ligand interaction sites and provide the basis for understanding the nature of cholesterol interactions, as well as serving as a platform for structurally-guided drug design targeting of TSPO.

REFERENCES

REFERENCES

1. Caffrey M, Cherezov V: **Crystallizing membrane proteins using lipidic mesophases**. *Nature Protocols* 2009, **4**:706-731.

2. Faham S, Bowie JU: **Bicelle crystallization: a new method for crystallizing membrane proteins yields a monomeric bacteriorhodopsin structure**. *J Mol Biol* 2002, **316**:1-6.

3. Cherezov V, Peddi A, Muthusubramaniam L, Zheng YF, Caffrey M: **A robotic system for crystallizing membrane and soluble proteins in lipidic mesophases**. *Acta Crystallogr D Biol Crystallogr* 2004, **60**:1795-1807.

4. Fischetti RF, Xu S, Yoder DW, Becker M, Nagarajan V, Sanishvili R, Hilgart MC, Stepanov S, Makarov O, Smith JL: **Mini-beam collimator enables microcrystallography experiments on standard beamlines**. *J Synchrotron Radiat* 2009, **16**:217-225.

5. Gourdon P, Andersen J, Hein K, Bublitz M, Pedersen B, Liu X, Yatime L, Nyblom M, Nielsen T, Olesen C, *et al.*: **HiLiDe-systematic approach to membrane protein crystallization in lipid and detergent**. *Crystal Growth & Design* 2011, **11**:2098-2106.

6. Yang J, Kulkarni K, Manolaridis I, Zhang Z, Dodd RB, Mas-Droux C, Barford D: **Mechanism of isoprenylcysteine carboxyl methylation from the crystal structure of the integral membrane methyltransferase ICMT**. *Mol Cell* 2011, **44**:997-1004.

7. Landau EM, Rosenbusch JP: **Lipidic cubic phases: a novel concept for the crystallization of membrane proteins**. *Proc Natl Acad Sci U S A* 1996, **93**:14532-14535.

8. Cherezov V, Yamashita E, Liu W, Zhalnina M, Cramer WA, Caffrey M: ***In meso* structure of the cobalamin transporter, BtuB, at 1.95 A resolution**. *J Mol Biol* 2006, **364**:716-734.

9. Lyons JA, Aragão D, Slattery O, Pisliakov AV, Soulimane T, Caffrey M: **Structural insights into electron transfer in *caa*3-type cytochrome oxidase**. *Nature* 2012, **487**:514-518.

10. Rasmussen SG, DeVree BT, Zou Y, Kruse AC, Chung KY, Kobilka TS, Thian FS, Chae PS, Pardon E, Calinski D, *et al.*: **Crystal structure of the β2 adrenergic receptor-Gs protein complex**. *Nature* 2011, **477**:549-555.

11. Alexandrov AI, Mileni M, Chien EY, Hanson MA, Stevens RC: **Microscale fluorescent thermal stability assay for membrane proteins**. *Structure* 2008, **16**:351-359.

12. Vedadi M, Niesen FH, Allali-Hassani A, Fedorov OY, Finerty PJ, Wasney GA, Yeung R, Arrowsmith C, Ball LJ, Berglund H, *et al.*: **Chemical screening methods to identify ligands that promote protein stability, protein crystallization, and structure determination**. *Proc Natl Acad Sci U S A* 2006, **103**:15835-15840.

13. Studier FW: **Protein production by auto-induction in high density shaking cultures**. *Protein Expr Purif* 2005, **41**:207-234.

14. Eriks LR, Mayor JA, Kaplan RS: **A strategy for identification and quantification of detergents frequently used in the purification of membrane proteins**. *Anal Biochem* 2003, **323**:234-241.

15. Urbani A, Warne T: **A colorimetric determination for glycosidic and bile salt-based detergents: applications in membrane protein research**. *Anal Biochem* 2005, **336**:117-124.

16. Schneider CA, Rasband WS, Eliceiri KW: **NIH Image to ImageJ: 25 years of image analysis**. *Nat Methods* 2012, **9**:671-675.

17. Lambert O, Levy D, Ranck JL, Leblanc G, Rigaud JL: **A new "gel-like" phase in dodecyl maltoside-lipid mixtures: implications in solubilization and reconstitution studies**. *Biophys J* 1998, **74**:918-930.

18. Newby ZER, O'Connell JD, Gruswitz F, Hays FA, Harries WEC, Harwood IM, Ho JD, Lee JK, Savage DF, Miercke LJW, *et al.*: **A general protocol for the crystallization of membrane proteins for X-ray structural investigation**. *Nature Protocols* 2009, **4**:619-637.

19. Li D, Boland C, Aragao D, Walsh K, Caffrey M: **Harvesting and cryo-cooling crystals of membrane proteins grown in lipidic mesophases for structure determination by macromolecular crystallography**. *J Vis Exp* 2012:e4001.

20. Liu W, Cherezov V: **Crystallization of membrane proteins in lipidic mesophases**. *J. Vis. Exp. (49), e2501, doi:10.3791/2501 (2011).*

21. Kabsch W: **XDS**. *Acta Crystallogr D Biol Crystallogr* 2010, **66**:125-132.

22. Winn MD, Ballard CC, Cowtan KD, Dodson EJ, Emsley P, Evans PR, Keegan RM, Krissinel EB, Leslie AG, McCoy A, *et al.*: **Overview of the CCP4 suite and current developments**. *Acta Crystallogr D Biol Crystallogr* 2011, **67**:235-242.

23. Evans P: **Scaling and assessment of data quality**. *Acta Crystallogr D Biol Crystallogr* 2006, **62**:72-82.

24. Bricogne G, Vonrhein C, Flensburg C, Schiltz M, Paciorek W: **Generation, representation and flow of phase information in structure determination: recent developments in and around SHARP 2.0**. *Acta Crystallogr D Biol Crystallogr* 2003, **59**:2023-2030.

25. Adams PD, Afonine PV, Bunkóczi G, Chen VB, Davis IW, Echols N, Headd JJ, Hung LW, Kapral GJ, Grosse-Kunstleve RW, *et al.*: **PHENIX: a comprehensive Python-based system for macromolecular structure solution**. *Acta Crystallogr D Biol Crystallogr* 2010, **66**:213-221.

26. Emsley P, Lohkamp B, Scott WG, Cowtan K: **Features and development of Coot**. *Acta Crystallogr D Biol Crystallogr* 2010, **66**:486-501.

27. Pebay-Peyroula E, Dahout-Gonzalez C, Kahn R, Trézéguet V, Lauquin GJ, Brandolin G: **Structure of mitochondrial ADP/ATP carrier in complex with carboxyatractyloside**. *Nature* 2003, **426**:39-44.

28. Schulze S, Köster S, Geldmacher U, Terwisscha van Scheltinga AC, Kühlbrandt W: **Structural basis of Na(+)-independent and cooperative substrate/product antiport in CaiT**. *Nature* 2010, **467**:233-236.

29. Perez C, Koshy C, Yildiz O, Ziegler C: **Alternating-access mechanism in conformationally asymmetric trimers of the betaine transporter BetP**. *Nature* 2012, **490**:126-130.

30. Lemieux MJ, Song J, Kim MJ, Huang Y, Villa A, Auer M, Li XD, Wang DN: **Three-dimensional crystallization of the *Escherichia coli* glycerol-3-phosphate transporter: a member of the major facilitator superfamily**. *Protein Sci* 2003, **12**:2748-2756.

31. Qin L, Hiser C, Mulichak A, Garavito RM, Ferguson-Miller S: **Identification of conserved lipid/detergent-binding sites in a high-resolution structure of the membrane protein cytochrome *c* oxidase**. *Proc Natl Acad Sci U S A* 2006, **103**:16117-16122.

32. Korkhov VM, Sachse C, Short JM, Tate CG: **Three-dimensional structure of TspO by electron cryomicroscopy of helical crystals**. *Structure* 2010, **18**:677-687.

33. Li F, Xia Y, Meiler J, Ferguson-Miller S: **Characterization and modeling of the oligomeric state and ligand binding behavior of purified Translocator Protein 18 kDa from *Rhodobacter sphaeroides***. *Biochemistry* 2013, **52**:5884-5899.

34. Jaremko L, Jaremko M, Giller K, Becker S, Zweckstetter M: **Structure of the mitochondrial translocator protein in complex with a diagnostic ligand**. *Science* 2014, **343**:1363-1366.

35. Chun E, Thompson AA, Liu W, Roth CB, Griffith MT, Katritch V, Kunken J, Xu F, Cherezov V, Hanson MA, *et al.*: **Fusion partner toolchest for the stabilization and crystallization of G protein-coupled receptors**. *Structure* 2012, **20**:967-976.

36. Fotiadis D, Liang Y, Filipek S, Saperstein DA, Engel A, Palczewski K: **The G protein-coupled receptor rhodopsin in the native membrane**. *FEBS Lett* 2004, **564**:281-288.

37. Katritch V, Cherezov V, Stevens RC: **Structure-function of the G protein-coupled receptor superfamily**. *Annu Rev Pharmacol Toxicol* 2013, **53**:531-556.

38. Moukhametzianov R, Klare JP, Efremov R, Baeken C, Göppner A, Labahn J, Engelhard M, Büldt G, Gordeliy VI: **Development of the signal in sensory rhodopsin and its transfer to the cognate transducer**. *Nature* 2006, **440**:115-119.

39. Santos JS, Asmar-Rovira GA, Han GW, Liu W, Syeda R, Cherezov V, Baker KA, Stevens RC,

Montal M: **Crystal structure of a voltage-gated K+ channel pore module in a closed state in lipid membranes**. *J Biol Chem* 2012, **287**:43063-43070.

40. Li D, Shah ST, Caffrey M: **Host lipid and temperature as important screening variables for crystallizing integral membrane proteins in lipidic mesophases. Trials with diacylglycerol kinase**. *Cryst Growth Des* 2013, **13**:2846-2857.

41. Li D, Howe N, Dukkipati A, Shah ST, Bax BD, Edge C, Bridges A, Hardwicke P, Singh OM, Giblin G, *et al.*: **Crystallizing membrane proteins in the lipidic mesophase. Experience with human prostaglandin E2 synthase 1 and an evolving strategy**. *Cryst Growth Des* 2014, **14**:2034-2047.

42. Li D, Lyons JA, Pye VE, Vogeley L, Aragão D, Kenyon CP, Shah ST, Doherty C, Aherne M, Caffrey M: **Crystal structure of the integral membrane diacylglycerol kinase**. *Nature* 2013, **497**:521-524.

43. Cherezov V, Clogston J, Papiz MZ, Caffrey M: **Room to move: crystallizing membrane proteins in swollen lipidic mesophases**. *J Mol Biol* 2006, **357**:1605-1618.

44. Wöhri AB, Johansson LC, Wadsten-Hindrichsen P, Wahlgren WY, Fischer G, Horsefield R, Katona G, Nyblom M, Oberg F, Young G, *et al.*: **A lipidic-sponge phase screen for membrane protein crystallization**. *Structure* 2008, **16**:1003-1009.

45. Waight AB, Pedersen BP, Schlessinger A, Bonomi M, Chau BH, Roe-Zurz Z, Risenmay AJ, Sali A, Stroud RM: **Structural basis for alternating access of a eukaryotic calcium/proton exchanger**. *Nature* 2013, **499**:107-110.

CHAPTER 5

Perspective and future direction on structure-function studies of TSPO

TSPO proteins have been investigated for more than 30 years, resulting in a wealth of information being available. Determination of the first high resolution crystal structure of *Rs*TSPO and the ability to purify *Rs*TSPO in the functional state opens a new door for investigation of the structure-function relationships of TSPO family proteins. Crystal structures of *Rs*TSPO, as well as the NMR structure of the mouse TSPO, provide a new opportunity to interpret previous mutagenesis data from a structure-function point of view. Additional mutagenesis experiments can also be designed with the help of the structures. On the other hand, current data and interpretation are complicated by the fact that experiments are often performed in different cell or tissue systems, which are hard for cross validation and often result in inconsistant conclusions. The successful expression, purification and crystallization of *Rs*TSPO, as well as the established tryptophan fluorescence quenching binding assay, provides a platform for testing the structure-function relationship of *Rs*TSPO. Similar protocols can also be adapted for expression, purification and charaterization of other TSPO family proteins. Much is still unknown regarding the function of this important and conserved protein family and several lines of investigation can be followed.

Crystallization of *Rs*TSPO-ligand complexes

Although ligands were added into the current crystallization experiments and improved the diffraction quality of *Rs*TSPO crystals, only partial densities of ligands were observed in potential ligand binding sites of *Rs*TSPO. Several schemes will be used to improve the incorporation of ligands into *Rs*TSPO crystals: 1) ligand concentrations will be increased to a higher level with the current method under conditions in which crystal quality will not be significantly influenced by the addition of excessive ligand and solvent DMSO; 2) *Rs*TSPO crystals will be soaked with mother liquor supplemented with high concentrations of ligand

before crystal harvesting; 3) mutants of *Rs*TSPO with higher ligand binding affinity will be designed and crystallized. Of particular interest is the cholesterol binding site, so far not revealed in our structures, mainly due to the fact that the wile-type (WT) *Rhodobacter* protein does not bind cholesterol with high affinity. The ATA/LAF (136,137,138) mutant was shown to bind both cholesterol and cholesterol hemisuccinate much more tightly than WT (Chapter 3) and well diffracting crystals are being sought. The A139T mutant, predicted to bind cholesterol less tightly, did indeed show this behavior, as well as producing our best crystals so far.

Preliminary data show that *Rs*TSPO-LAF can be purified to good homogeneity and yield similar to *Rs*TSPOWT by using CHS-supplemented buffer. Crystallization conditions will be screened and optimized with the robot to obtain diffraction quality crystals of *Rs*TSPO-LAF.

Mutagenesis of *Rs*TSPO based on the crystal structure and the co-evolution analysis

Mutants of *Rs*TSPO can be designed based on the co-evolution analysis and the crystal structure of *Rs*TSPO to achieve good protein stability, as well to test hypotheses regarding the function of TSPO *in vitro* with the established tryptophan fluorescence quenching assay. For instance, residues on helix 4 that are prediced to interact with the LAF motif can be mutated to complement the loss of stability of *Rs*TSPO-LAF; residues at the dimer interface can be mutated to test the function of the dimer; residues involved in the potential ligand binding site can be mutated to study the ligand binding mechanism as well as to test the influence of ligand binding *in vitro*.

Characterization of the oligomeric state of *Rs*TSPO and the stoichiometry of the endogenous ligand by mass spectrometry

Oligomerization of TSPO proteins have been reported but the interactions that maintain the oligomer are not yet identified and its functional significance remains to be further investigated.

All our crystals so far show the same dimer form, but whether the solution form is the same, and whether higher order associations exist, remains to be investigated. A collaboration has been established with Dr. Brandon Ruotolo and Dr. Philip Andrews at the University of Michigan to further characterize the oligomerization of purified *Rs*TSPO with the ion-mobility mass spectrometry (IM-MS) and cross-linking methodology. Preliminary data show that *Rs*TSPO monomer and dimer species are identified in the mass spectrum and purified *Rs*TSPO was cross-linked by the amine cross-linker DC4. Optimization of cross-linking experiments combined with mutagenesis would allow us to identify residues critical for oligomerization. Further investigation with IM-MS would also allow for identification of bound lipids and ligands co-purified with *Rs*TSPO in low abundance.

Expression, purification and crystallization of human TSPO

Despite the high sequence identity that *Rs*TSPO shares with human TSPO, considerable differences exist between *Rs*TSPO and human TSPO, in particular at the loop 1 region where a role was proposed in ligand binding. In addition, given the much higher affinity to drug ligands, the chance of observing a bound ligand with the human TSPO is better. High resolution crystal structures of the human TSPO with ligands bound will undoubtedly provide more direct information for understanding of the regulation of TSPO by ligands and for facilitating drug development targeting TSPO. The successful expression, purification and crystallization of *Rs*TSPO provides a good guide for other TSPO family proteins, including the human TSPO.

Human TSPO has been successfully expressed in *E. coli* with the current purification procedure but was co-purified with GroEL. Further optimization of purification will be needed to purify the human protein from *E. coli*. Meanwhile, preliminary data show that human TSPO can be expressed and purified to good yield and homogeneity for crystallization with the *sf9* insect

cell expression system (personal communication from Dr. Yi Zheng). The expression in

Rhodobacter is also a possibility, since *R. sphaeroides* can successfully express many membrane

proteins and a preliminary result shows that human TSPO was expressed in *Rhodobacter*.